

Faculdade de Engenharia da Universidade do Porto



**Energy Storage in Batteries - Dynamic System
Modelling and Response**

Carlos Rafael Ribeiro Fernandes

Dissertation submitted in partial fulfilment of the requirements for the Degree of
Master of Science in Electrical and Computers Engineering

Supervisor: Prof. Doctor Helder Filipe Duarte Leite
Co-Supervisor: Doctor Ismael Tiago Sá Miranda

January 2019

Resumo

A integração de recursos renováveis tem contribuído para o aumento dos requisitos de flexibilidade nos sistemas elétricos de energia. Paralelamente a este constante aumento de introdução de produção dispersa, tem-se assistido à criação de novas soluções para colmatar a variabilidade da produção renovável, nomeadamente sistemas de armazenamento de energia. Por conseguinte, surgem dificuldades em coordenar ambas as tecnologias para redes tão vastas, sendo expectável que estas limitações sejam ultrapassadas através da transformação das redes atuais em micro-redes, equipadas com sistemas inteligentes de comunicação, permitindo uma flexibilização de recursos e uma coordenação otimizada.

Uma das características distintivas das micro-redes é a capacidade de poderem operar interligadas com a rede de distribuição local, ou de forma isolada, isto é, desligadas da rede. A operação das micro-redes em rede isolada consiste num modo de operação sensível e requer a implementação de estratégias de controlo específicas para o correto funcionamento do sistema, nomeadamente ao nível das proteções. A presente dissertação apresenta o funcionamento de uma micro-rede, com foco na análise do seu comportamento em cenários de falha, nomeadamente curto-circuitos simétricos e assimétricos.

A metodologia é aplicada a três casos de estudo distintos, suportados por uma simulação computacional, referentes à ligação de uma micro-rede às redes de distribuição de média e baixa tensão, bem como o seu funcionamento em modo isolado. Estes estudos permitem avaliar a contribuição dos diversos elementos do sistema para a corrente de curto-circuito e a adequabilidade dos sistemas de proteção do sistema, podendo haver a necessidade de adaptabilidade das proteções existentes.

Abstract

The integration of renewable resources has contributed to increase flexibility requirements in electric power systems. Parallel to this constant increase in the introduction of dispersed production, new solutions have been created to cope with the variability of renewable production, namely energy storage systems. As a result, there are difficulties in coordinating both technologies for such complex and active networks. It is foreseeable that these limitations may be tackled by the adoption of microgrids, with multiple distributed energy resources and equipped with intelligent communication systems, allowing resource flexibility and optimized coordination.

One of the distinguishing characteristics of microgrids is the ability to operate interconnected with the local distribution network, or isolated, meaning, disconnected from the main network. The operation of isolated microgrids is a sensitive mode of operation and requires the implementation of specific control strategies for the correct functioning of the system, namely at the level of protection systems. The present dissertation presents the operation of a microgrid, focusing on the analysis of its behaviour in fault scenarios, namely symmetrical and asymmetrical short-circuits.

The methodology is applied to three different case studies, supported by a computational simulation, concerning the connection of a microgrid to the medium voltage and low voltage distribution networks, as well as its operation in isolated mode. These studies allow the evaluation of the contribution of the various elements of the system to the short-circuit current and the suitability of the system protection systems that may require the adaptability of existing protections.

Acknowledgements

I would like to thank my thesis supervisor Professor Dr. Helder Leite of the Electrical and Computer Engineering Department at University of Porto, for accepting me under his supervision and allowing me the opportunity to work in such an interesting and challenging subject. Also, I would like to express my gratitude to my co-supervisor Dr. Ismael Miranda for his expertise, patience and wisdom. He was always a sustainer of this work. I am grateful for their support and guidance.

To Efacec for giving me the opportunity to integrate the Energy Storage department and providing me all the support and tools to accomplish this work. I also want to address an acknowledgment to all the department members, the engineers Alberto Bernardo, João Monteiro, José Fonseca, Marta Ribeiro and Pedro Félix for valuable discussions and insights and for the useful cooperation during all the time. I would also thank to my colleagues Afonso Lopes, Konstantinos Kotsalos, and Nuno Costa that I have met during this journey and for their important contributions. For all the support and good moments inside and outside Efacec, thank you for always helping me through every challenge.

Furthermore, a special tribute to my family and friends, who always support me unconditionally and encourage me through every situation. Thank you for everything.

To Ana, thank you for being by my side, no matter what.

Table of Contents

Chapter 1	Introduction.....	1
1.1.	Overview.....	1
1.2.	Motivation	1
1.3.	Thesis Scope and Objectives	2
1.4.	Publications	2
1.5.	Dissertation’s Structure.....	3
Chapter 2	Integration of Energy Storage Systems in Electric Power Systems	5
2.1.	The Relevance of Energy Storage within the Smart Grid Concept	5
2.2.	The Particular Case of Microgrids	6
2.3.	Energy Storage Systems.....	8
2.3.1.	Energy Storage System Characteristics and Applications.....	8
2.3.2.	Energy Storage Technologies and Characteristics.....	9
2.3.2.1.	Mechanical Energy Storage.....	10
2.3.2.2.	Thermal Energy Storage	10
2.3.2.3.	Electrical Energy Storage.....	11
2.3.2.4.	Electrochemical Energy Storage.....	11
2.4.	The Relevance of Protection Systems in the Context of Microgrids with Energy Storage .	12
2.5.	Chapter Summary	13
Chapter 3	Fault Analysis in a Microgrid Context	15
3.1.	Power Converter Interface	16
3.1.1.	Low Voltage Fault Ride-Through in Distribution Networks	17
3.2.	Per-Unit System	18
3.2.1.	Loads Model.....	20
3.2.2.	Generators Model	21
3.2.3.	Lines and Cables Model	22
3.2.4.	Transformers Model	23
3.2.5.	Power Converters Model.....	23
3.3.	Short-circuit Analysis of Inverter-Based DER.....	24
3.3.1.	Short-Circuit Behaviour	25
3.3.2.	Symmetrical Fault	29
3.3.2.1.	General Calculation Methodology.....	29

3.3.2.2.	Systematic Methodology for Computational Calculation.....	30
3.3.3.	Unsymmetrical Fault	33
3.3.3.1.	Application of symmetrical components.....	33
3.3.3.2.	Short-circuit impedances of electrical equipment.....	35
3.3.3.3.	Systematic Methodology for Computational Calculation.....	41
3.4.	Chapter Summary	48
Chapter 4	Applications of Short-circuit Analysis	49
4.1.	Short-Circuit Calculation	49
4.1.1.	Short-Circuit Current Contribution during Balanced Faults	50
4.1.1.1.	Low Voltage Grid Connection	50
4.1.1.2.	Medium Voltage Grid Connection	54
4.1.1.3.	Islanded mode of operation	57
4.1.2.	Analysis of Short-Circuit Current during Unbalanced Faults	59
4.1.2.1.	Microgrid connected to the Low Voltage Grid	60
4.1.2.2.	Microgrid connected to the Medium Voltage Grid	63
4.1.2.3.	Islanded mode of operation	65
4.2.	<i>MATLAB/Simulink</i> Simulation Platform	66
4.3.	Chapter Summary	67
Chapter 5	The Democrat Case Study	69
5.1.	Microgrid Data and Model Assumptions	70
5.2.	Microgrid Description.....	71
5.3.	Microgrid Fault Analysis.....	75
5.3.1.	Case 1: Microgrid Connected to the Low Voltage Grid.....	75
5.3.1.1.	Three-Phase Short-Circuit	77
5.3.1.2.	Line-to-Line Short-Circuit	79
5.3.1.3.	Line-to-Ground Short-Circuit	81
5.3.1.4.	Line-to-Line Short-Circuit with Ground Connection	83
5.3.2.	Case 2: Microgrid Connected to the Medium Voltage Grid	86
5.3.2.1.	Three-Phase Short-Circuit	86
5.3.2.2.	Line-to-Line Short-Circuit	89
5.3.2.3.	Line-to-Ground Short-Circuit	90
5.3.2.4.	Line-to-Line Short-Circuit with Ground Connection	92
5.3.3.	Case 3: Microgrid Connected to an Islanded Grid.....	94
5.3.3.1.	Three-Phase Short-Circuit	96
5.3.3.2.	Line-to-Line Short-Circuit	98
5.3.3.3.	Line-to-Ground Short-Circuit	100
5.3.3.4.	Line-to-Line Short-Circuit with Ground Connection	102
5.4.	Chapter Summary	104
Chapter 6	Conclusions and Future Work.....	105
6.1.	Conclusions.....	105
6.2.	Future Work.....	106
References.....		109

List of figures

Figure 1- Low Voltage Ride-Through [54].	18
Figure 2-Network Equivalent.	19
Figure 3-Model of a load.	21
Figure 4-Per-unit load impedance.	21
Figure 5- Per-unit generator model.	22
Figure 6-Two port representation of a transmission line.	22
Figure 7- Short transmission line representation.	22
Figure 8- Equivalent π representation of a long line.	23
Figure 9- Per-unit transformer model.	23
Figure 10- Per-unit converter model.	24
Figure 11- Symmetrical AC wave.	25
Figure 12- Asymmetrical AC wave.	25
Figure 13- Asymmetrical and Symmetrical AC currents.	27
Figure 14- "Near the generator" short-circuit.	28
Figure 15- "Far from generator" short-circuit.	29
Figure 16- Symmetrical short-circuit.	29
Figure 17- Thevenin Diagram.	30
Figure 18-Fault in node k.	31
Figure 19-Short-circuit current in node k.	32
Figure 20- Symmetrical fault at bus 1.	53
Figure 21- (a) Positive and negative-sequence systems; (b) Zero-sequence system.	60
Figure 22- (a) Positive and negative-sequence systems; (b) Zero-sequence system.	63
Figure 23- (a) Positive and negative-sequence systems; (b) Zero-sequence system.	65
Figure 24- Battery Rack.	71
Figure 25- Power Inverter.	72
Figure 26- Power Transformer	73
Figure 27- Electric Vehicle Charger	73
Figure 28- Diesel Generator	74
Figure 29- Circuit Breaker	74
Figure 30-Simulink Model of a Low Voltage Microgrid.	75

Figure 54 - Current waveforms in the LV utility grid and in the inverter, respectively.....	77
Figure 55 - Utility grid RMS voltage waveform.....	77
Figure 56 - Active and reactive power waveforms.....	78
Figure 57 - Utility grid voltage waveforms for symmetrical short-circuit-Case1.....	78
Figure 58 - Utility grid current waveforms for symmetrical short-circuit -Case1.....	78
Figure 59- RMS Values of the Short-Circuit Current for symmetrical short-circuit - Case1.....	79
Figure 60- Inverter voltage waveforms for symmetrical short-circuit-Case1.....	79
Figure 61- Inverter Current Waveforms for symmetrical short-circuit-Case1.....	79
Figure 62- Active and reactive power waveforms for symmetrical short-circuit-Case1.....	80
Figure 63- Utility grid voltage waveforms for line-to-line short-circuit -Case1.....	80
Figure 64- Utility grid current waveforms for line-to-line short-circuit - Case1.....	81
Figure 65- Inverter voltage waveforms for line-to-line short-circuit - Case1.....	81
Figure 66- Inverter current waveforms for line-to-line short-circuit - Case1.....	81
Figure 67- Active and reactive power of the load for line-to-line short-circuit - Case1.....	82
Figure 68- Utility grid voltage waveforms for line-to-ground short-circuit - Case1.....	82
Figure 69- Utility grid current waveforms for line-to-ground short-circuit - Case1.....	83
Figure 70- Inverter voltage waveforms for line-to-ground short-circuit - Case1.....	83
Figure 71- Inverter current waveforms for line-to-ground short-circuit - Case1.....	83
Figure 72- Active and reactive power of the load for line-to-ground short-circuit - Case1.....	84
Figure 73- Utility grid voltage waveforms for line-to-line-to-ground short-circuit - Case1.....	84
Figure 74- Utility grid current waveforms for line-to-line-to-ground short-circuit - Case1.....	85
Figure 75- Inverter voltage waveforms for line-to-line-to-ground short-circuit - Case1.....	85
Figure 76- Inverter current waveforms for line-to-line-to-ground short-circuit - Case1.....	85
Figure 77- Active and reactive power waveforms of the load for line-to-line-to-ground short-circuit - Case 1.....	86
Figure 78- Simulink model of a Low Voltage Microgrid Connected to the Medium Voltage Utility Grid.....	87
Figure 79- Fault Location voltage waveforms for symmetrical short-circuit- Case2.....	87
Figure 80- Fault location current waveforms for symmetrical short-circuit- Case2.....	88
Figure 81- RMS values of the short-circuit current for symmetrical short-circuit- Case2.....	88
Figure 82- Inverter voltage and current waveforms for symmetrical short-circuit, respectively - Case 2.....	89
Figure 83- Active and reactive power waveforms for symmetrical short-circuit- Case1.....	89
Figure 84- Fault Location voltage waveforms for line-to-line short-circuit - Case2.....	90
Figure 85- Fault location current waveforms for line-to-line short-circuit - Case2.....	90
Figure 86- Inverter current waveforms for line-to-line short-circuit - Case2.....	91
Figure 87- Active and reactive power of the load for line-to-line short-circuit - Case2.....	91
Figure 88- Fault Location voltage waveforms for line-to-ground short-circuit - Case2.....	91
Figure 89- Fault location current waveforms for line-to-ground short-circuit - Case2.....	92
Figure 90- Active and reactive power of the load for line-to-ground short-circuit - Case2.....	92

Figure 91- Fault location voltage waveforms for line-to-line-to-ground short-circuit - Case2.....	93
Figure 92- Fault Location current waveforms for line-to-line-to-ground short-circuit - Case2.....	93
Figure 93- Active and reactive power waveforms of the load for line-to-line-to-ground short-circuit - Case2.....	94
Figure 94- Islanded Microgrid.....	95
Figure 95- Microgrid voltage waveforms- Case 3.....	95
Figure 96- Current waveforms of the Generator and Inverter, respectively- Case 3.....	96
Figure 97- Active and Reactive Power waveforms of the EV Charger and Load bank, respectively- Case 3.....	97
Figure 98- Fault Location voltage waveforms for symmetrical short-circuit- Case3.....	97
Figure 99- Fault location current waveforms for symmetrical short-circuit- Case3.....	98
Figure 100- RMS values of the short-circuit current for symmetrical short-circuit- Case3.....	98
Figure 101- Inverter current waveforms for symmetrical short-circuit- Case 3.....	98
Figure 102- Active and Reactive Power waveforms of the EV Charger and Load bank for symmetrical short-circuit, respectively- Case 3.....	99
Figure 103- Fault Location voltage waveforms for line-to-line short-circuit - Case3.....	99
Figure 104- Fault location current waveforms for line-to-line short-circuit - Case3.....	100
Figure 105- Inverter current waveforms for line-to-line short-circuit - Case3.....	100
Figure 106- Active and Reactive Power waveforms of the EV Charger and Load bank for a line-to-line short-circuit, respectively- Case 3.....	100
Figure 107- Fault Location voltage waveforms for line-to-ground short-circuit - Case3.....	101
Figure 108- Fault location current waveforms for line-to-ground short-circuit - Case3.....	101
Figure 109- Inverter current waveforms for line-to-ground short-circuit - Case3.....	101
Figure 110- Diesel generator current waveforms for line-to-ground short-circuit - Case3.....	102
Figure 111- Current waveforms and respective phase shifts for the inverter and generator.....	102
Figure 112- Active and reactive power of the EV charger and load bank for line-to-ground short-circuit - Case3.....	103
Figure 113- Fault location voltage waveforms for line-to-line-to-ground short-circuit - Case3.....	103
Figure 114- Fault Location current waveforms for line-to-line-to-ground short-circuit - Case3.....	104
Figure 115- Active and reactive power waveforms of the load bank and EV charger for line-to-line-to-ground short-circuit - Case3.....	104

List of Tables

Table 1- Initial voltage values (c parameter).	19
Table 2- Zero-sequence representation of transformers.	37
Table 3- Synchronous machine reactances (in p.u. of rated MVA).	40
Table 4- Low Voltage system parameters.	51
Table 5- Low Voltage cable impedance.	53
Table 6- Medium voltage system parameters.	55
Table 7- Medium Voltage Cable impedances.	56
Table 8- Islanded microgrid system parameters	58
Table 9- Equivalent impedances.	61
Table 10- Equivalent impedances.	61
Table 11- Positive and negative-sequence equivalent impedances.	64
Table 12- Zero-sequence equivalent impedances.	64
Table 13- Current magnitude	64
Table 14- Positive and negative-sequence equivalent impedances.	65
Table 15- Zero-sequence equivalent impedances.	65
Table 16- Current magnitude	66
Table 17- BESS parameters	71
Table 18- Inverter Parameters	72
Table 19- Load Bank Parameters.	72
Table 20- Transformer Parameters.....	73
Table 21- EV Charger Parameters	73
Table 22- Generator Parameters	74
Table 23- Circuit-Breaker Parameters.	74
Table 24- Short-Circuit Currents- Case 1.....	85
Table 25- Short-Circuit Currents - Case 2.	93
Table 26-Short-Circuit Currents - Case 3.....	104

Acronyms and Symbols

AC	Alternating Current
BESS	Battery Energy Storage System
CBDG	Converter-Based Distributed Generation
DC	Direct Current
DER	Distributed Energy Resources
DG	Distributed Generation
DSO	Distribution System Operator
EPS	Electric Power System
ES	Energy Storage
ESS	Energy Storage System
FRT	Fault Ride-Through
LV	Low Voltage
LVRT	Low Voltage Ride-Through
MG	Microgrid
MV	Medium Voltage
PCC	Point of Common Coupling
PV	Photovoltaic
RES	Renewable Energy Source
RMS	Root Mean Square
SC	Short-circuit
SG	Smart Grid
TSO	Transmission System Operator
VSC	Voltage Source Converter

Chapter 1

Introduction

1.1. Overview

This work proposes a dynamic analysis of the behaviour of Battery Energy Storage Systems (BESS) for different modes of operation and fault scenarios in the context of a Microgrid (MG) integration. This chapter presents a brief description of the addressed problem, motivation, objectives and scope of the study. In addition, it summarizes the methodology used for this research and the dissertation structure.

1.2. Motivation

Energy Storage (ES) began to be thought due to industrialization and the need to increase the installed capacity in the energy networks. This subject became deeper when, at the beginning of the 20th century, it was implemented the first stationary ES. Initially, it consisted in storing energy in lead-acid accumulators to feed residential and industrial loads when the power stations were turned off, by connecting it directly to the grid [1]. However, the energy-to-weight ratio was very low and more flexible alternatives were, in fact, needed.

In 1929, pumped hydroelectric storage arose, which consisted of pumping water upstream and, when the demand exceeded the production, the water stored in the reservoirs would be released by the turbines, producing electricity. However, with the massive introduction of residential loads in the network, this type of storage became insufficient, but the main problem with this technology was that it had a very low response time to energy variations, and energy demand has become higher [2]. In the past few years, the interest in ES has grown due to the need of managing energy prices regarding self-consumption, as well as investments on network expansion and the integration of Renewable Energy Sources (RESs). Mostly, ES until today is done through pumped hydroelectric [3], although a large increase on ES based on battery bank has been achieved in last years. Increased peak electricity demand coupled with investment in renewable-based generating units has resulted in challenges such as transmission congestions, reversed power flows in distribution grids and even load shedding in some power systems.

On the other hand, deployment of Energy Storage Systems (ESSs) has been regarded as a viable solution for the effective exploitation of renewable resources.

One of the main features of the electric energy system is the ability to generate large amounts of energy in a short period of time, although energy consumption fluctuates

throughout the day. It is, therefore, important to develop technologies that allow effective storage so that the mismatch between demand and supply by the source is null or minimum, so there is no need to resort to fossil fuels to cover the periods when there is no renewable production. These production breaks are due to the variability of renewable sources, namely solar and wind [4], which constitute the largest share of renewable production.

ES can, hence, fill this gap by maintaining relatively constant power supply values, facilitating the work of the system operators [5].

1.3. Thesis Scope and Objectives

As renewable penetration increases, power intermittence in the power system is more frequent and severe. Thus, much attention has been focused on the development of ES technologies to properly accommodate the inherent characteristics of RES generation, which can also contribute to grid the system stability in case of disturbances.

The introduction of Distributed Energy Resources (DER) offers many benefits but at the same time presents some limitations that will be addressed in the next chapters. It is therefore evident the importance of the development of storage technologies and consequent implementation in Low Voltage (LV) distribution networks. However, due to their variable and distributed nature, the increasing integration of DER into LV networks has raised some challenges, mainly technical, for the correct functioning of LV distribution networks. The main challenge is the Electric Power System (EPS) coordination in different scenarios and modes of operation since DER can operate connected to the distribution network or in an islanded mode.

This work intends to model and simulate the dynamic behaviour of MGs with the integration of BESS in specific scenarios of operation, performing an objective analysis during fault situations. Such scenarios aim to study its behaviour during their connection to Medium Voltage (MV) and LV distribution networks, as well as their behaviour in islanded mode. This modelling is intended to recreate a real MG. It was assumed that the storage systems were available during the islanded mode operation and the transition was due to an upper system disconnection, through the action of the protection system. Moreover, it is intended to verify the performance of the protection systems applied to a real MG.

1.4. Publications

During the course of this dissertation it was submitted an abstract paper titled: "Fault Analysis in a Microgrid Context: The DEMOCRAT Project" for the IEEE conference: 2nd International Conference on Smart Energy Systems and Technologies, Porto, Portugal, September 2019. This abstract is still awaiting acceptance.

1.5. Dissertation's Structure

The Dissertation is structured in six chapters, reflecting the methodological steps followed.

- Chapter 1 covers the study of the problem by referring its interest. A contextualization to the topic is addressed in this work, whose detailed description is presented in subsequent chapters.
- Chapter 2 discusses the drivers behind the development of the Smart Grid (SG) and MG concepts, its social, economic and quality-related advantages and the current challenges imposed by its implementation. This chapter focuses on the description of the most revealing general characteristics of ESSs, presents a concise information about the different ES technologies and the importance of the protection systems for interconnected and in islanded power systems.
- Chapter 3 describes the electrical model of the network being studied, with a detailed description of the distribution network parameters, storage system, loads and other system components. Presents a description of the behaviour of the systems during different types of fault, as well as some considerations for calculating Short-Circuit (SC) currents.
- Chapter 4 applies the SC concepts presented in the previous chapter to symmetrical and asymmetrical faults for three different network configurations. It also presents the simulation platform used and the foundations of the planning framework for integrating BESSs in distribution networks of both islanded and interconnected power systems.
- Chapter 5 presents the results for the simulated case studies, the assessment and validation of the developed methodology described in the previous chapter.
- Chapter 6 highlights the main findings of this dissertation and points out some lines for future works.

4 Introduction

Chapter 2

Integration of Energy Storage Systems in Electric Power Systems

The high concern with environmental problems and the scarcity of fossil fuels has promoted the development of measures to reverse the indiscriminate increase of fossil fuels consumption, to reduce the emission of green-house gases and, therefore, to encourage the use of Renewable Energy Sources (RESs). Thus, today it is seen a great development of the areas related to renewable energies and, namely, in the field of Energy Storage (ES) and inherent technological solutions.

The increase in global energy demand means that it could be challenging to meet consumption using only conventional energy production, leading to the integration of alternative resources capable of satisfying demand in the near future, while reducing its environmental impact [6]. Reducing greenhouse gas emissions is seen as one of society's main challenges to achieving a more sustainable supply [7], with a focus on the integration of clean energy sources into electricity generation [8].

Although the production of electricity from RES represents a promising solution to respond to this challenge, on the other hand, their high dependence on weather conditions brings variability and uncertainty to their production. Due to the variable nature of renewables, the generated power profile may not be able to match the load requirement, and thus, their remuneration may be penalized by deviations from the production forecast at each hour of the day. In this scenario, storage systems associated with Distributed Energy Resources (DER) can play a role in minimizing economic penalties [4]. In addition, by reducing uncertainty in renewable production, they value technically and economically the energy that is produced by these sources, contributing to the benefits of greater integration of these sources in the electrical systems.

2.1. The Relevance of Energy Storage within the Smart Grid Concept

Smart Grid (SG) can be defined as self-sufficient systems, which allows integration of any type and any scale generation sources to the grid that reduces the workforce targeting sustainable, reliable, safe and quality electricity to all consumers [9]. A fundamental aspect

6 Integration of Energy Storage Systems in Electric Power Systems

of operating an electric power network is its operation at a frequency and voltage within very strict values (e.g. 50 Hz, and 1 p.u.) to guarantee energy quality. These parameters may fluctuate slightly as long as they remain within the range of values that ensures the proper functioning of the loads. A large variation in these parameters can trigger a situation of instability in the power grid and may ultimately cause it to collapse with a systemic failure.

The deployment of Energy Storage Systems (ESSs) contributes to maximizing energy efficiency of a distribution network, and overall network performance can be enhanced by their optimal placement, sizing, and operation.

ESSs are frequently used in large-scale applications such as power generation, distribution and transmission networks, DER, renewable energy, and local industrial and commercial facilities [1]. The application of ESSs in distribution networks can benefit the supplier, the customer, and the Distribution System Operator (DSO) as well as the Transmission System Operator (TSO) and the generation operator (conventional and DER) [10] in numerous ways (e.g. managing peak loads and reducing import energy requirements).

Currently, in order to cope with the variability of RES production, the electrical system is equipped with plants with a rapid response capacity, namely thermal, combined cycle gas and large hydroelectric power plants [11], which, together with the interconnections, regulate the variations of power injection in the distribution networks. Nevertheless, although power plants of the electrical system can potentially solve systemic stability problems, their scope is not efficient in solving local problems at the distribution networks level. It is therefore fundamental to change the current paradigm so that more efficient management of the Electric Power Systems (EPS) can be fostered [12].

The objectives for attaining desirable enhancements such as energy savings, distribution cost reduction, optimal demand management, and power quality management or improvement in a distribution network through the implementation of ESSs requires a wide range of equipment and functionalities, as well as different technologies such as IT and communications, control technologies and ES [13].

2.2. The Particular Case of Microgrids

The distribution network is evolving from a traditionally radial system to a multi-terminal grid with flexible energy distribution [13].

During the last decades, the EPS has progressed on the basis of a traditional hierarchical structure considering three different levels: production, transmission and distribution. Historically, this passive distribution network structure relies on the concept of delivering bulk energy from the transmission network to consumers at lower voltages [12].

The planning model of the conventional ESS allows the energy transport in large scale with reduced losses in the lines and its unidirectional power flow simplifies the model of operation of the energy distribution network. In addition, the large electric power production units contribute significantly to the stability of the system [12]. However, most large power plants such as coal-based thermal power plants are characterized by low-efficiency levels, ranging from 28% to 35% [14]. One of the main characteristics of the conventional paradigm of the EPS is the great distance that separates the production of the consumption that implies the construction of vast and expensive transmission networks, being that the growth of these distances causes the increase of energy losses in the lines. In a hierarchical system, the

existence of regulatory or structural problems can create difficulties in investing in new production facilities or in transmission networks [14]. The resulting impact proves to be negative in terms of the security of the overall system supply, since any problem in an upper hierarchical part can affect numerous elements of the lower hierarchical part.

Recently, and particularly since the early 1990's [14], power systems are facing a substantial growth on the interest of connecting generation plants to the distribution network, usually denominated as Distributed Generation (DG) contributing to the DER concept, assuming an important role in the new organizational paradigm of electric energy production and consumption, facing challenges and significant changes in the EPS operation as networks behave as active networks contrary to the previous paradigm in which the networks were passive.

The emergence of the concept of distributed production simultaneously with the development and improvement of some already existing concepts such as storage devices and controllable loads that together with generation technologies comprise DER. With the arrival of liberalized markets and environmental challenges, it required that the industry responsible for electricity supply reinvent the way the EPS is thought [13]. This new paradigm is seen as the way to ensure that tomorrow's power grids can meet the needs of future consumers. In this way, the production management started to be done in a decentralized way, aiming to equip existing networks with the means to coordinate the diverse assets reaching high safety standards and low-cost supply efficiency, thus contributing to a more sustainable system with lower environmental impacts.

A Microgrid (MG) can be generally defined as a small-scale power network plus its loads and several DER connected to it, together with the appropriate management and control functionalities supported by a communication infrastructure [14]. It has a distinguishing characteristic that is the ability to be operated as a coordinated entity, both in interconnected or islanded mode. The emergence of the MG imposes further challenges to the system operation from security and reliability to economics.

In recent years, there have been several technical impacts resulting from the massive introduction of DG in the Low Voltage (LV) networks without any type of associated control, affecting the network's voltage and frequency. Thus, ESS can play a vital role to compensate these disturbances and seem to be a crucial part of SGs in the future [15]. This effect is notorious in the more external busbars of the network since the voltage values may exceed the technical limits defined, due to the resulting bidirectional power flow [16].

Active management of the distribution network with the inclusion of ancillary monitoring and control systems is seen as a key element in achieving cost-effective solutions and maximizing the benefits of dispersed generation [17]. MGs, when operated efficiently and intelligently, introduce great benefits to the overall system, in particular the flexibility they bring to the system because they can be operated autonomously when disconnected from the network [17] or interconnected to the main network. In this way, adequate management of distribution networks, particularly in the context of MGs, will make it possible to minimize consumption from the upstream network at peak periods, reduce the need for investments in reinforcement or new electrical infrastructures and, therefore, defer or even avoid investment costs [11]. Taking advantage of and maximizing the value of generation near the places of consumption and the existence of flexible resources are leveraged gains of efficiency that translate into an EPS with lower environmental impacts and transversal benefits also for the final consumer.

ES technologies play a major role in the SG concept and in a scenario where there is a massification of DG in LV distribution networks [14]. From the consumer point of view, through the use of this type of technologies, more attractive conditions for self-consumption emerge, storing surplus energy during periods of greater renewable production for injection in the network in periods of higher consumption, reducing the monetary value of the energy bill [13]. Regarding the operation of LV distribution networks with a high presence of small power DG, the storage devices may have different applications such as peak shaving, with the objective of improving the operation of these networks [18], in a SG context.

2.3. Energy Storage Systems

As there is a growing increase in the integration of renewable solar and wind energy in the EPS, there is an interest in resources that increase the network flexibility. Compensations in the energy production phase create some challenges, since, with increasing energy production from renewable sources during periods of lower load, it is necessary to store the surplus energy. In fact, ES translates the transformation of this energy into different types with the particularity to be used in the future for various purposes. The implementation of ES can be made in the five main subsystems of the EPS: production, transmission, substations, distribution and final consumers [15]. Thus, in the same way as SGs are essential to increase the deployment of ESS, these also achieves the objectives of an efficient and smart network.

2.3.1. Energy Storage System Characteristics and Applications

ES in LV distribution networks can play an important role in supporting control and balancing strategies. At the distribution network level, it also contributes to the voltage and frequency control and to mitigate the network power congestion. At the consumer level, contributes to the optimization of the electricity costs through smart metering and the possibility of avoiding high-cost investments to expand network components such as transformers and/or lines.

The use of ESS in the network has benefits, namely greater reliability with less undesirable interruptions, a greater efficiency due to lower values of losses [8], an effective levelling of consumption, reducing congestion rates based on the installation of storage systems in distribution substations, among others.

The main applications for ESSs are:

- Energy Time-shifting: electric energy is stored in periods of lower demand and are subsequently used or sold in peak periods, minimising the demand charges [3]. This requires a considerable storage capacity and moderate response times [19].
- Transmission and distribution investment deferral: in addition to the conventional options for network capacity expansion, operators can use storage devices to improve dispatch operations and even reduce network congestion [14]. The integration of ESS avoids the capacity reinforcement of a distribution grid by tackling load growth, derived from the integration of electrical vehicles, and peak demand, therefore avoiding constrained grid assets [3].
- Grid regulation: this application includes frequency and voltage area regulation which have an added value in islanded power systems where a very fast response from BESSs can be crucial to maintain the security of supply and avoid load shedding [3]. This is related to supply and demand, making possible the network frequency control, while the voltage provides support for reactance control at a more local level [20].
- Power quality: this application counteracts the network disturbances in order to maintain and guarantee a power supply [19]. The power level needs to be compatible with the consumption of the final consumer [21].
- Power reliability: this application guarantees the bridging power during a power outage. It can be applied in uninterrupted power application, such as uninterruptable power supply [19] or industrial processes, data centres or healthcare facilities, although with less impact than the others. The requirements have as a concern the alignment between the electrical power and the final consumer's load (usually up to tens of MW).

2.3.2. Energy Storage Technologies and Characteristics

As the grid evolves in the coming years and incorporates new generation resources and consumption patterns, various combinations of capacity, power, reliability, and cost-effectiveness in storage technologies might prove useful. Due to the inability of DER to deliver power in coordination with network and consumption requirements [14], a new technological solution was adopted that combines the DER and ES. Many areas of resource use have long utilized storage to manage supply and demand, from food preservation technologies, silos, and warehouses to dams for water reservoirs [22]. In the literature, ESSs have a wide variety of potential options to respond to these demands, including mechanical, chemical, thermal, electrical and electrochemical technologies [22]. Each of these four categories is in commercial use today and presents a possible solution at grid-scale in the future.

2.3.2.1. Mechanical Energy Storage

The working principle of this technology is to utilize kinetic energy and potential energy for storage. The largest grid-scale ES technology is pumped hydropower storage (“pumped hydro”), representing nearly 99% of global installed electrical storage capacity [13]. Pumped hydro uses excess electricity generated during off-peak times to pump water from a lower reservoir (charging) to a higher reservoir. When required, the water flows back to the lower reservoir, producing electricity after powering a turbine with a generator to cover temporary peaks in demand from consumers or unplanned outages at other power plants. While pumped hydro is a highly useful, cost-effective, and proven technology, its further expansion has been limited by its geographical requirements, environmental concerns, and high capital costs [22].

Compressed air energy storage is similar to pumped hydro although relies on pressurizing air, pumping it into underground geological formations. The air is later released to drive turbines when there is a demand peak. In the limited commercial applications of CAES to date, stored air is released and mixed with natural gas to generate electricity [22].

Flywheels store rotational energy in an accelerated rotor and use excess energy to drive the motion of a wheel suspended on bearings or magnets. This suspension allows the rotational body to keep a constant speed. If the flywheel’s rotational speed is reduced electricity may be extracted from the system by a transmission device. Flywheels have been in use since 1970 [13] in various forms due to their simplicity, reliability, and responsiveness. They are most commonly used today for industrial and commercial applications which require high discharge power, although a few grid-scale installations have been built.

2.3.2.2. Thermal Energy Storage

Thermal storage technologies store available heat in an insulated reservoir for residential or industrial applications, such as space heating and cooling, being deployed to overcome the mismatch between thermal energy demand and supply [15]. The capacity of a storage system is defined by the specific heat capacity and the mass of the medium used. Currently, thermal storage technologies are subdivided into three main groups: latent heat, sensible heat and thermo-chemical sorption (absorption and adsorption) [23].

Thermal salts, which are the most used latent heat storage media, [13] are commonly associated with concentrating solar power plants. This technology uses phase change materials as a media, and this particular case utilizes the excess energy to heat a molten salt solution. The energy in this solution can be turned into electricity by heating steam, which drives a conventional turbine. Due to the inefficiency of the energy transfer, thermal conductivity is a key instrument in latent heat system [15].

Sensible heat storage leads to temperature changes in the process and the thermal energy is stored solely through a change of temperature of the storage medium.

Sorption storage systems work as thermo-chemical heat pumps. Its physical process is characterised by the accumulation and take-up of one material by means of a second material. The accumulation of a material on a surface is called adsorption. In the case of the accumulation in the liquid phase, the process is called absorption, being both exothermal processes [23].

The wide-scale adoption of thermal batteries could act as a peak shaving [22], reducing peak demand while increasing the overall efficiency of energy systems, although these sorts of solutions are rarely considered in the same category as other ES technologies.

2.3.2.3. Electrical Energy Storage

Electrical storage refers to an electrostatic storage process of converting electrical energy into a form that can be stored for converting back to electrical energy when required [24]. These systems comprise a small range of technologies, namely double-layer capacitors and superconducting magnetic energy storage [13].

Double-layer capacitors fill the gap between classical capacitors and general batteries. They are an extremely high-power storage system based on electrostatic effects that occur between two carbon electrodes with high specific surface areas per volume. The electrodes are immersed in an electrolyte, and it is used a separator between the electrodes [25]. The two main features are the extremely high capacitance values, of the order of many thousand farads, and the possibility of very fast charges and discharges due to extraordinarily low inner resistance which are features not available with conventional batteries. [13].

In superconducting magnetic energy storage systems, the energy is stored in the magnetic field created by the flow of direct current in a superconducting coil [13]. The main advantages for this technology are the very quick response since the requested power is available almost instantaneously and the high overall round-trip efficiency.

2.3.2.4. Electrochemical Energy Storage

Electrochemical storage technologies are commonly known as batteries. These power sources convert chemical into electrical energy and are proven options for most distribution network applications due to their long lifetime and good efficiency [10]. The most familiar storage technology in the contemporary ES market is the Li-ion battery [26]. Its lithium compound electrode and electrolyte structure recall similar alkaline batteries that have been used to power consumer electronics for decades. The key difference is that Li-ion batteries are lighter and significantly more energy-dense than their alkaline counterparts. [27] Lead-acid batteries are also familiar. They consist of two lead electrodes submerged in a liquid sulfuric acid electrolyte.

Early grid-scale applications composed of stacked lead-acid cells were plagued by safety issues. Recent improvements to this 150-year-old technology include incorporating a gel or solid absorbed glass mat electrolyte instead of the standard liquid to improve safety, and the addition of ultracapacitors to improve performance. Nickel-based batteries are similar to lithium-based batteries in their construction, but the use of nickel allows for different charging properties which suit distinct applications. Nickel-cadmium and the newer, less toxic, nickel metal hydride batteries provide improved energy and power compared to lead-acid batteries and operate in a wider variety of temperature conditions and levels of discharge, but they have not been used much in grid-scale projects [22]. Electrochemical flow batteries, a relatively recent invention, dispense with the electrode and electrolyte system in favour of two circulating electrolyte fluids which exchange electrons directly across a shared membrane. These batteries are well-suited to grid-scale storage due to their relatively low energy density and power output. While some power is required for the operation of mechanical components,

the battery itself has a low self-discharge rate, extended life cycles, rapid response times [24] and can increase scale simply by adding electrolyte volume.

Liquid metal batteries combine the capacity and discharge of electrochemical cells with the stability of thermal salts [28]. These batteries replace the traditional solid metal electrode structure and electrolyte solution with metallic liquid electrodes and electrolytes to create a more stable and higher energy density electrical cell. [29]. Similar to Li-ion batteries, liquid metal cells can be stacked into systems to provide various amounts of ES and high on-demand power supply while total system heat generation can be prodigious, because the liquid metal reforms for each reaction, liquid metal batteries could significantly improve upon many of the reliability and safety concerns of standard electrochemical batteries.

2.4. The Relevance of Protection Systems in the Context of Microgrids with Energy Storage

The environmental goals and liberalization of energy markets have led to a huge increase of DER in the electrical power system, which includes not only DG but also ES and responsive loads. The power system architecture, incorporating DER, is changing from a hierarchical power supply to small-scale power grids [12]. Thus, the concept of MGs is significantly growing, boosting the idea of a sustainable growth and providing more flexibility, reliability and control [30]. This relevance is due to some distinctive features namely the capability of operating autonomously, providing voltage and frequency regulation, although its stability relies in ES and generation availability [17]; having a single Point of Common Coupling (PCC), regarding the MG as a controllable entity [31].

A MG can operate in two steady state modes, grid-connected or island, in the event of an upstream fault or a scheduled event, and in two transient modes of operation [32], islanding or resynchronization. In grid-connected mode, the terminal voltage and frequency of the DER are generally near their nominal values. Hence, in this mode, the units deliver their nominal active and reactive power [31] and the main grid will provide high fault currents to activate fault protection devices such as fuses or circuit breakers. However, in an islanded MG, since it is dominated by power electronic interfaces and the DG are mainly inverter based [30], the fault current is limited. Hence, since there may not be enough fault currents supply, the conventional overcurrent protection devices may not sense the fault and will not operate and so, MGs with the ability to operate both in the grid connected and islanded modes require more sophisticated protection schemes for a successful operation [33].

During transient modes, voltage and frequency disturbances occur, which must be rapidly mitigated so that the system maintains its stability and the synchronous devices with the network do not collapse [34]. The transition must be instantaneously detected by the DERs which must be switched to a voltage control mode, acting as a grid forming unit or automatic voltage regulators [12, 35] in order to guarantee constant voltage for local sensitive loads.

Thus, the grid synchronization, which commutes from islanded MG to grid-connected, or vice-versa is a critical procedure of the entire operation [36]. According to the literature [34], an effective solution for MG protection is an adaptive protection system since the commonly used differential and bidirectional relays cannot give reliable protection. For a MG with inverter interfaced DER, the protection scheme cannot differentiate between fault current and an overload current. Adaptive protections are capable of readjusting the relay settings automatically when in a transient mode.

In a scenario of large integration of DG, a simultaneous miss operation of the interconnection relays may provoke serious system operation problems. In fact, if a Short-Circuit (SC) takes place in the transmission network and its effects on voltage are propagated downstream to the distribution level, it may provoke the decoupling of a large amount of DG [12]. Since they are tripped, a sudden increase in power flows coming from upstream, takes place in this network area, such that it may provoke cascading operation of overcurrent relays in distribution and transmission branches, because of overload situations. Furthermore, the voltage profiles in the area where the DG was disconnected can be seriously affected and turn into a voltage collapse phenomenon.

To ensure the uninterrupted operation of its critical loads, the MG must be capable of operating in both the grid-connected mode and the islanded mode and offer a smooth and seamless transition between these two modes. ES and protection systems are, therefore, a key element in the MG concept, enabling these two modes of operation. Furthermore, the storage voltage controller should help to smooth the islanding and resynchronisation of the MG to the main grid and the fast operation of protection systems improves the ability to maintain synchronism, which is crucial to the system stability [34].

2.5. Chapter Summary

MGs will be key to the "smart" energy use for communities, industries and residential buildings. The use of ES is an important part of the energy supply chain, as well as the maintenance of the energy source. Associated with these concepts, it is imperative to consider the protection systems for their effective operation and applicability.

- Section 2.1. of this chapter presents the SG concept and the importance of the integration of ESSs, presenting its technical and economic value for distribution networks management.
- Section 2.2. presents the MG concept, its operating characteristics and the benefits of its integration in EPSs.
- In Section 2.3. are presented many ES technological options. Each technology has its own operating mode, involving different materials and processes. These aspects define the typical characteristics of each technology, as well as its application potential and constraints. Although a wide range of storage solutions were addressed, the study presented in the following sections was restricted to lithium-ion battery systems, since these are more cost-effective.
- Section 2.4. discusses the relevance of protection systems. It is also detailed the MG behaviour in fault scenarios and different modes of operation.

Chapter 3

Fault Analysis in a Microgrid Context

Low Voltage (LV) distribution electrical networks have a typical radial topology, while Medium Voltage (MV) distribution networks may have both ring and radial topology [37]. The radial configuration allows the end customers to be supplied with reliable and high-quality energy from multiple distribution transformers and different supply paths. Due to its large size and number of connected dispersed elements, it is necessary for the network to hold many protections so as to locate and isolate faults with minimum disruption to the rest of the network and to efficiently protect the electrical power networks from faults, such as Short-Circuits (SCs). The protection system is also required to safeguard users and to prevent or reduce damage to the network components and critical loads [38].

The protection system operates on the principle that when a fault occurs, the resulting current is usually significantly higher than that experienced under normal operating conditions. This allows an upper threshold to be set and when the current rises above this threshold, it indicates that there is a fault in the system and the corresponding faulted shortest section should be turned off. The fault current can be of varying magnitude depending on the location of the fault, which can lead to different fault levels [39] at different parts of the network.

As far as fault current injection is concerned, converter-based resources present very different characteristics to its synchronous counterparts and unlike a synchronous generator, which can supply an instantaneous injection of fault current upon fault inception, this characteristic is not replicated in converter based plant [40] as will be exposed in the following section. Thus, the fault current plays a major role in the safety of three-phase systems based on power converters, because, due of its limitation, it may not act effectively the protections.

Fault analysis in three-phase systems is, therefore, one of the essential exercises in the design and determination of the Electric Power Systems (EPSs) protection, particularly in cases such as microgrids (MGs) that can have multiple operation modes.

This chapter will describe the relevance of power converters for fault analysis in a MG context, the fundamentals of three-phase system representation and the properties of the calculation tools. It will also explain the fundamentals of the calculation of different SC types, with an approach that facilitates the use of spreadsheets for simple cases and applications for large systems.

3.1. Power Converter Interface

Worldwide, electric power grids are transforming toward varied levels of modernization. Drivers for such transformations include the need for enhanced reliability and power quality to serve loads; accommodation of projected growth in demand levels; and integration of cleaner sources of electricity generation and Energy Storage (ES).

Distributed Energy Resources (DER) have been introduced in EPSs, located close to the load and interconnected with the electrical distribution system.

These units typically comprise fossil-fuel, renewable resources electric vehicles and ES technologies, and are becoming increasingly common in distribution networks, presenting several challenges, inherent in their use, for protection systems. The introduction of these resources, and in the event of an incident (e.g., fault), will increase the amount of available current and therefore influence protective devices requirements in the distribution system [41].

There are considerable differences in the performance under fault conditions among the three basic types of DER: synchronous machines, induction machines, and inverter-based sources. The last, consisting mainly of solar Photovoltaics (PV), wind turbines, fuel cells, microturbines and BESS require inverters to interface with the utility grid [42].

Power systems have originally been planned with synchronous generators and then the integration of Converter-Based Distributed Generation (CBDG) have created challenges in circuit breaker ratings, protection operating times and even system synchronization. Unlike the synchronous or induction machines, which have torque, the systems based on power converters do not have a rotating mass component, not having the ability to efficiently contribute to the inertia of the system and to feed the fault current [40], which have a significant impact on the behaviour and characteristics of the transmission system.

A unique feature of inverter-based DER is the power electronics interface. Power electronics have the ability to control fault current contributions from DER systems regarding the design of the converter's control system and the protection of switching devices from excessive currents during faulty conditions [43]. This adjustability can thereby optimize the system protection coordination issues by controlling fault current levels.

Typically, CBDG are designed to act as ideal current sources or Voltage Source Converters (VSCs) [44]. Several inverter-based fault current contribution research documents contain a widely used criterion derived from experience, of one to two times an inverter's full load current for a few cycles [43, 45, 46, 47]. Therefore, are provided minimal fault current contributions and have a small effect on overcurrent protection and coordination strategies for fuse and circuit breakers [41].

Power converters for renewable energy integration present a higher complexity when compared with those used in industrial or stand-alone systems because there is a need to efficiently manage power flow and stay synchronized with the grid [48]. This power electronic connection also increases the appliance of the sources when they have to work without the grid (island mode) [49].

Thus, intermittent nature of renewable resources, makes power electronics crucial for voltage, frequency and power output characteristics regulation, increasing its interest in its interface to the power grid [48]. With the inclusion of CBDG units, as these have power fluctuations due to their renewable character, a problem arises regarding the inertia of the

system and, consequently, to voltage control, power balance fluctuations and frequency regulation [41].

During an incident, a rapid system response is required so that the voltage and frequency values are kept within the narrow band, ensuring stability and continuity of service. With the decrease in system inertia, during a fault, the frequency of the network varies more abruptly. The interface of the converters associated to the renewable generation is made through voltage and current control schemes and frequency adaptive synchronization, with very restricted operating bands [50]. When a fault occurs, the limits can be exceeded and may lead to the disconnection of the DER and this phenomenon can lead to a chain reaction, leading to the blackout of the system. Recently, adaptive protection mechanisms to the LV distribution system have been implemented, namely Fault Ride-Through (FRT) requirements for power converters [51].

3.1.1. Low Voltage Fault Ride-Through in Distribution Networks

Grid stability and security of supply are two important aspects for energy supply. In order to avoid power outages, it is necessary that power generating plants should have control capabilities and protection mechanisms [51].

The occurrence and removal of SC faults by protection systems will often result in a momentary voltage sag experienced across the entire power system. A long, persistent, severe fault or the inability for generation to ride-through a fault could result in the disconnection of large amounts of generation and possibly system collapse. The FRT ability of generation to remain connected through disturbances on the power system is therefore critical to power system security [52].

These requirements can be fulfilled by conventional power plants. In the meantime, however, the share of Renewable Energy Sources (RESs) in the total electricity generation has become so significant that these must contribute to the grid stability too [41, 49]. Therefore, the Transmission System Operators (TSOs) have established the so-called grid codes with certain critical values and control characteristics that the generating plants have to fulfil. The grid codes referred to the distribution networks focus on protection requirements, quality of supply, power factor and earthing requirements [53].

An important part of these requirements is the so-called Low Voltage Ride-Through (LVRT) capability of generating plants. LVRT brought some changes in the design and control of generating machines, although this concept is not always applicable to installations connected to the distribution network [45]. It gives guidelines to define a lower voltage limit during which the generating plants must support the grid, avoiding outages [46].

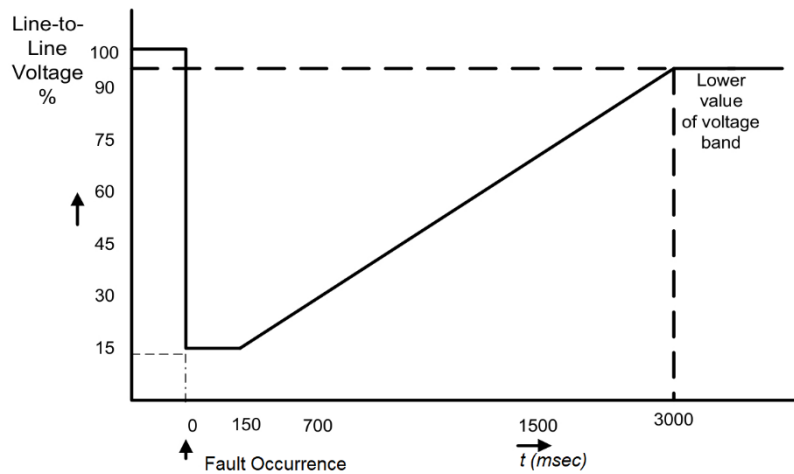


Figure 1- Low Voltage Ride-Through [54].

Short-term voltage dips may occur, for example, when large loads are connected to the grid or as a result of grid faults like SCs. Renewable generating plants such as wind turbines were allowed to disconnect from the grid during a fault when the voltage drop exceeded 10-20% the rated value [54]. If too many generating plants disconnect at the same time the entire network could collapse, a scenario which is also known as “blackout”. For this reason, the LVRT requirement has been established which is meant to guarantee that the generating plants stay connected to the grid [51]. Additionally, many grid codes demand that the grid should be supported during voltage drops to as low as 5% of nominal voltage [54].

Generating plants can support the grid by feeding reactive current into the network and so raise the voltage. Immediately after the fault clearance, the active power output must be increased again to the value prior to the occurrence of the fault within a specified period of time. The public distribution system is regulated in Europe by EN 50160 [55], which gives the main voltage parameters and their permissible deviation ranges at the customer’s Point of Common Coupling (PCC) in public LV and MV electricity distribution systems, under normal operating conditions [50]. These requirements which at the beginning were only applied to wind farms [45], now also have to be fulfilled by Photovoltaic (PV) systems and, most recently, by combined heat and power plants. The PV inverter recognizes the voltage drop and feeds a reactive current of approximately 100% of the nominal voltage into the system for the duration of the fault in order to support the grid [50]. After fault clearance, the active power output is increased to the value prior to the occurrence of the fault and the DER may provide post-fault voltage support [41].

3.2. Per-Unit System

Fault current in power networks is a key factor for calculating the ratings of interrupting and sensing protection devices. Analysis of the SC capacity and the pre-fault calculations are necessary for selecting the circuit breakers, the protective relays as well as their settings [39].

It is, therefore, necessary to define calculation methodologies to obtain fault currents. The most common method of performing SC calculation is the "impedance method" according to the IEC 60909 standard, which is used to efficiently calculate the SC currents at a given point, in case of balanced or unbalanced SCs, in LV three-phase AC systems, operating at a nominal frequency of 50 Hz or 60 Hz [56]. This method consists of the sum of all resistances and reactances upstream of the fault, which requires knowledge of all the characteristics of the network components. The calculation of the current comes from the complex generalisation of Ohm's Law [57]:

$$I_k'' = \frac{c \cdot U_{nk}}{\sqrt{3} \cdot \sum_{i=1}^n (Z_i)} \quad (3.1)$$

Where

I_k'' - fault current;
 U_{nk} - nominal voltage;
 Z_i - fault impedance.

The general principle of the application of the previous equation is based on the Thevenin theorem, which states that a linear electrical network, seen from the defect node, can be replaced by an open circuit equivalent voltage source and an equivalent impedance [39]. Depending on the magnitude of the SC, i.e. minimum or maximum, and where it occurs, i.e. LV, Medium Voltage (MV) or high voltage grids, a coefficient c is defined to obtain a more efficient approximation. These values are shown in the following table:

Table 1- Initial voltage values (c parameter).

	Maximum I_k''	Minimum I_k''
Low Voltage (<1kV)	1,0	0,95
Medium Voltage (<35kV)	1,1	1,0
High Voltage (>35kV)	1,1	1,0

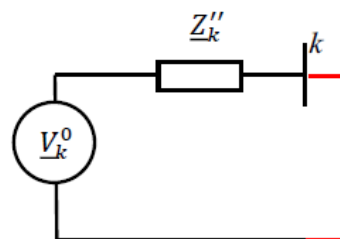


Figure 2-Network Equivalent.

Power systems contain many elements that need to be included in this calculation, considered as impedances. Thus, a standard notation system is used for the simplification of complex systems. In per-unit notation, the physical quantity is expressed as a fraction of the reference value [58]. This reference value depends on the characteristics of the element to be simplified and the base chosen.

$$\text{per-unit value} = \frac{\text{actual value}}{\text{base value}} \quad (3.2)$$

Normally, per-unit impedances of network equipment are always declared at their base values. In case there are components with different bases, it is possible to transform different per-unit equipment impedances at different bases to a common selected base according to the following equation [39]:

$$Z_{New} = Z_{Old} * \left(\frac{S_{New}}{S_{Old}}\right) * \left(\frac{V_{Old}}{V_{New}}\right)^2 \quad (3.3)$$

Where

Z_{New} - impedance on new selected base;

Z_{Old} - impedance on given old base;

S_{New} and V_{New} - new selected base power and voltage;

S_{Old} and V_{Old} - old given base power and voltage.

Base impedance of any section of system can be calculated by

$$Z_{Base\Omega} = \frac{V_{Base}^2}{S_{Base}} \quad (3.4)$$

Where

$Z_{Base\Omega}$ - base impedance (Ω);

V_{Base} - base voltage (V);

S_{Base} - selected base power (VA).

To convert actual impedance to per-unit impedance, the following equation can be utilised

$$Z_{p.u.} = Z_{\Omega} * \frac{S_{Base}}{V_{Base}^2} \quad (3.5)$$

Where

$Z_{p.u.}$ - per-unit impedance;

Z_{Ω} - given impedance (Ω).

3.2.1. Loads Model

In some SC models, the load impedance can be neglected, because it is very high compared to the impedances of the remaining system components. In this case, errors are obtained on the order of 5%. In most SC studies, only the active part of the loads is neglected, and for those cases where only the reactive part is considered, the errors obtained are less than 1%. Therefore, it can be assumed as an accurate approximation.

Loads, when passive, may be represented by constant impedances while reactive loads, e.g. induction motors, require a more detailed representation because they may contribute to feed the sub-transient SC period [59].

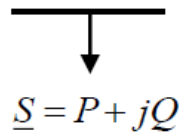


Figure 3-Model of a load.

The load conversion to per-unit model is based on the equation 3.5.

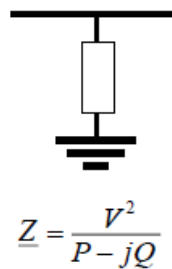


Figure 4-Per-unit load impedance.

3.2.2. Generators Model

A generator is an electrical machine that transforms mechanical or kinetic energy into electrical energy and can be modelled as synchronous or asynchronous machines. Usually winding resistance is despised, being considered only the reactance.

The asynchronous generator usually operates as a motor, but at the initial instants of the SC it works as a generator. During the SC it no longer receives the reactive energy from the network, which is required for the excitation, rapidly decreasing the magnetic flux, contributing to the SC only during the sub-transient period.

The synchronous generator has its operation at the network nominal frequency and for its modelling, it is considered a steady state regime in each period, e.g. sub-transient, transient and symmetrical. For the modelling, depending on the type of circuit-breaker, the sub-transient reactance is used for fast acting circuit breakers and transient reactance for slow acting circuit breakers, while for asynchronous machines, only the sub-transient reactance is considered [59].

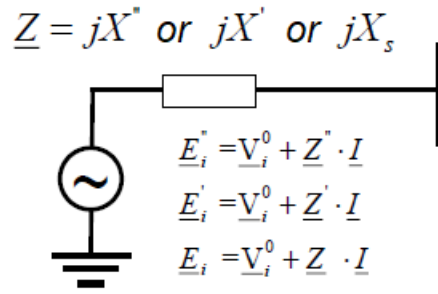


Figure 5- Per-unit generator model.

3.2.3. Lines and Cables Model

Power transmission cable systems are the backbone of electrical energy supply [60]. The interconnected lines facilitate the bulk transport of electrical energy from a generating site to a substation or a customer.

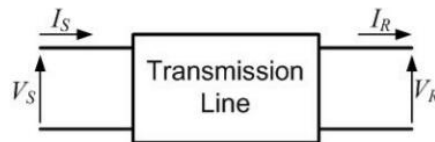


Figure 6-Two port representation of a transmission line.

Through the length of the lines, the systems can be subdivided into short and long, and their representation models, estimated. In the short-line approximation, the shunt capacitance is almost negligible and then the total impedance of the line is $\underline{Z} = R + jX$.

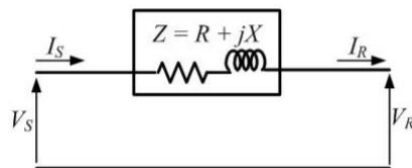


Figure 7- Short transmission line representation.

As in the power flow studies, the longest lines are modelled according to the pi model. In this model is considered a lumped series impedance and two shunt admittance Y_{sh} , placed at the two ends [61]. The value of these admittances is equal to half the admittance value of the line, Y .

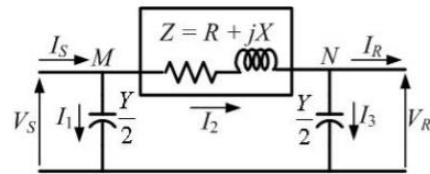


Figure 8- Equivalent π representation of a long line.

In MV, high voltage or very high voltage overhead lines, as the reactance value is substantially higher than the resistance value, the parameters R and Y_{sh} can be neglected. In contrast, in LV networks, the cables resistance is much higher than the reactance and therefore the X can be neglected. Usually, the smaller the reactance, higher the Short-Circuit Current (SCC) will be [59].

3.2.4. Transformers Model

When it comes to stabilising the power grid, it is necessary to adopt solutions that efficiently control the voltage levels and guarantee a stable operation. The transformer will enable low-loss and extremely efficient power transmission over long distances and are a key component due to its reliable operation that is crucial to ensuring a stable and resilient power supply [62].

In power transformers there are longitudinal components which are the leakage reactance component X_f and a small resistance which can be neglected. The transverse components are the resistances associated with the iron losses and magnetization reactance which is very high in most of the transformers [63]. This statement allows transformers to be represented by a simple reactance.

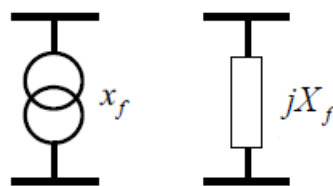


Figure 9- Per-unit transformer model.

When there is a fault in the power grid, it is necessary to consider the transformer winding configuration in case the fault is asymmetrical, as shall be seen in subsection 3.3.3.2.

3.2.5. Power Converters Model

DER are mainly connected to the power system through DC/AC or AC/DC/AC converters [64], depending on the type of renewable source. Although there exist numerous alternative technologies, e.g. current source converters and Voltage Source Converters (VSCs), most of the CBDG units, use a VSC [49, 50].

Sources interfaced to the network via a DC/AC grid-side converter present identical characteristic with respect to their expected SCC contribution, regardless of the primary energy source. For the representation of such sources, the provisions of IEC 60909 standard for reversible static converter-fed drives could be applied, treating these sources as asynchronous machines [45, 56].

According to [65], the behaviour of converters during a SC can be divided into two periods, the transient period and the steady-state period. In terms of performance of the MG protection systems, the transient period is the most important since it corresponds to the first cycles of the SCC, where it is higher.

Due to the power electronics associated with the converters and the current-limiting controller that prevents the semiconductors from damage, the SCC contribution for three-phase faults is limited to its rated current or slightly above its rated current [66]. On the other hand, it inhibits the inverter to inject a larger current output to trigger the overcurrent protection devices [67].

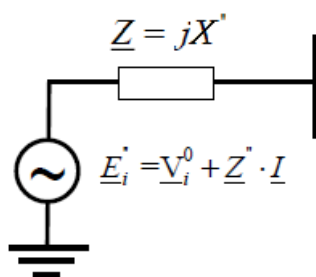


Figure 10- Per-unit converter model.

3.3. Short-circuit Analysis of Inverter-Based DER

A SC generally corresponds to a fault that causes undesired ground contact or between phases, introducing in the electrical circuit an impedance much smaller than normal. This generally leads to high currents that could lead to equipment damage or even failure besides putting people in danger. It is important to calculate the maximum that these currents can achieve to size the cutting power of the equipment and calibrate the protective timing [59]; and the minimum, to confirm the lower limits of protection operation, namely, that they act in a useful way even in a fault situation, in which the currents are far from the maximum.

The SC considered generally as more powerful is the symmetrical three-phase SC [68]. This refers to the released power, not necessarily in terms of phase current since there are cases where a line-to-ground SC may lead to a higher current than the three-phase symmetrical SC. That is one reason why it is not enough to calculate the currents in the latter case. On the other hand, in terms of frequency of occurrence, the single-phase, or line-to-ground SC is, by far, the most common.

3.3.1. Short-Circuit Behaviour

When SC fault occurs in the distribution network, the current fault would flow towards the fault point. This current, which is normally substantially higher than the load currents verified under normal conditions [39], if it lasts too long, causes the conductors to heat up and may result in transient over voltages that may endanger the equipment insulation in other parts of the system and possible irreversible deterioration of the equipment due to electrodynamic stresses [69] between phases of the conducting elements, namely busbars, windings, etc.

The fault current, commonly known as SCC is defined as the maximum possible value of current that may occur at a particular location in the distribution system assuming that no fault related influences are acting to reduce the fault current. It is related to the capacity and size of the power sources, e.g. generators, motors and the utility grid, supplying the system and is typically independent of the circuit current load and structure [70].

The main factors determining the magnitude and duration of the SCCs are the type of fault, existing fault current sources, and the impedances between the sources and the point of the SC [69]. The characteristics, locations, and sizes of the fault current sources connected to the distribution system at the time the SC occurs have an influence on both the initial magnitude and the wave shape of the fault current. Depending on these factors, the fault current can be classified as symmetrical or asymmetrical. A symmetrical current presents the shape of an AC current around the zero axis, with symmetry of positive and negative peak values.



Figure 11- Symmetrical AC wave.

The asymmetrical current, due to the resistances and reactances of the system, namely the $\frac{R}{X}$ coefficient [59, 71], presents a waveform with an asymmetry around the zero axis, comprising a DC component and an AC component.

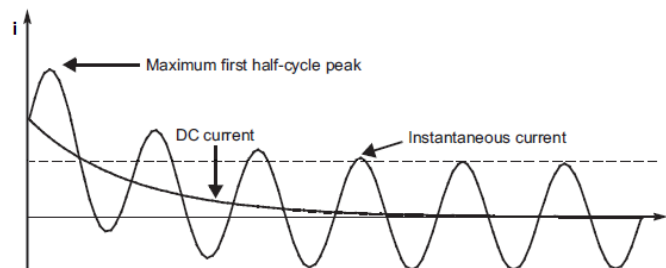


Figure 12- Asymmetrical AC wave.

The total SCC available in a distribution system is usually supplied from a number of sources, which can be grouped into three main categories. The first is the utility transmission system supplying the facility, which acts like a large, remote generator. The second includes “local” generators either in the plant or nearby in the utility. The third source category is synchronous

and induction motors, which are located in many plants and facilities. All these are rotating machines; those of the second and third categories have machine currents that decay significantly with time due to reduction of flux in the machine during a SC [69].

For a SC at its terminals, the induction motor symmetrical current disappears entirely after one to ten cycles while the current of a synchronous motor is maintained at a lower initial value by its energized field. Networks having a greater proportion of induction motors to synchronous motors will have quicker decays of AC SCC components. The fault current magnitude during the first few cycles is further increased by the DC fault current component (Figure 10). This component also decays with time, increasing the difference in SCC magnitude between the first cycle after the SC occurs and a few cycles later. The total SCC that has steady-state AC, decaying AC, and decaying DC current components can be expressed as shown in the following equation.

$$I_{sc} = I_{dc\ decay} + I_{ac\ decay} + I_{ac\ steady\ state} \quad (3.6)$$

With

$$I_{dc\ decay} = (I_{ac\ steady\ state}) \sin(\alpha - \phi) e^{\frac{R\omega t}{X}} \quad (3.7)$$

$$I_{ac\ decay} = \sqrt{2}I_s \sin(\omega t + \alpha - \phi) e^{-kt} \quad (3.8)$$

$$I_{ac\ steady\ state} = \sqrt{2}I_s \sin(\omega t + \alpha - \phi) \quad (3.9)$$

Where

I_{dc} is the decaying symmetrical Root Mean Square (RMS) current magnitude;

ϕ is the angle of the applied voltage in radians when the fault occurs;

ω is the angular frequency;

I_s is the symmetrical steady-state RMS current magnitude;

k is a variable depending upon the mix and size of rotational loads;

t refers to time, in seconds.

The ratio of the system reactance and resistance indicates the rate of decay of any DC offset in SCC. The greater the fault point X/R ratio, the longer will be the asymmetrical fault current decay time. For a specific X/R ratio, the angle of the applied voltage at the time of SC initiation determines the degree of fault current asymmetry that will exist for that X/R ratio [68].

If a SC occurs at the peak of the voltage waveform, the SCC will start at zero and trace a sine wave that will be symmetrical around the zero axis over time. In this case, there is no DC component [59]. If the fault occurs at any point between a voltage zero and a voltage crest, the current will be asymmetrical to some degrees depending upon the point at which the SC occurs on the applied voltage waveform. If a SC occurs at a zero-voltage point, the current will start at zero but cannot follow a sine wave symmetrically around the zero axis because in an

inductive circuit the current must lag the applied voltage by 90° [69]. This is the most critical situation because the DC component is maximum and there is the possible doubling of the peak current comparing to the initial symmetrical SCC [59].

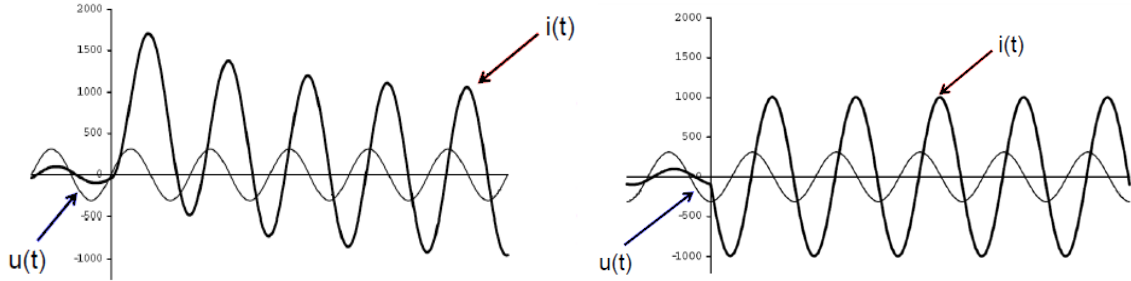


Figure 13- Asymmetrical and Symmetrical AC currents.

Three periods relating to the time variation of the fundamental component of the SCC are then defined [59]:

- Sub-transient period: it is the initial period during which the SCC value rapidly decreases;
- Transient period: following period, corresponding to a slower decrease of the SCC, until the permanent value of that current is reached;
- Permanent period: period in which the SCC has its steady value. Typically, this period is not reached, since the total insulation time of the fault is much lower.

At the time of the SC, alternating current generators, synchronous and induction motors and utility ties will supply current, being the predominant sources of SCCs.

The transient conditions prevailing, while the SCC develops, differ depending on the distance between the fault location and the generator. This distance is not necessarily physical but means that the generator impedances are less than the impedance of the elements between the generator and the fault location [71].

A SC is considered to be "near generator" when the magnitude of the symmetrical AC component of the prospective fault current decays with time. The symmetrical alternating component of the SCC decreases from the symmetrical SCC to the permanent SCC and the aperiodic DC component decays from an initial value to zero [56]. This decrease is due to the variation in time of the synchronous machine's reactance and their influence on the variation of the impedance seen from the defect site. A fault close to a generator is affected by the sub-transient, transient and permanent periods as shown in the following equation [72]:

$$I_{sc}(t) = E\sqrt{2} \left[\left(\frac{1}{X_d''} - \frac{1}{X_d'} \right) e^{-t/t_d''} + \left(\frac{1}{X_d'} - \frac{1}{X_d} \right) e^{-t/t_d'} + \frac{1}{X_d} \right] \sin(\omega t) + \frac{E\sqrt{2}}{X_d''} e^{-t/t_a} \quad (3.10)$$

Where

E is the phase-to-neutral RMS voltage at the generator terminals (V);

X_d'' is the generator direct-axis sub-transient reactance (Ω);

X_d' is the generator direct-axis transient reactance (Ω);

X_d is the generator synchronous reactance (Ω);

t''_d is the generator sub-transient time constant (s);

t'_d is the generator transient time constant (s);

t_a is the aperiodic time constant (s).

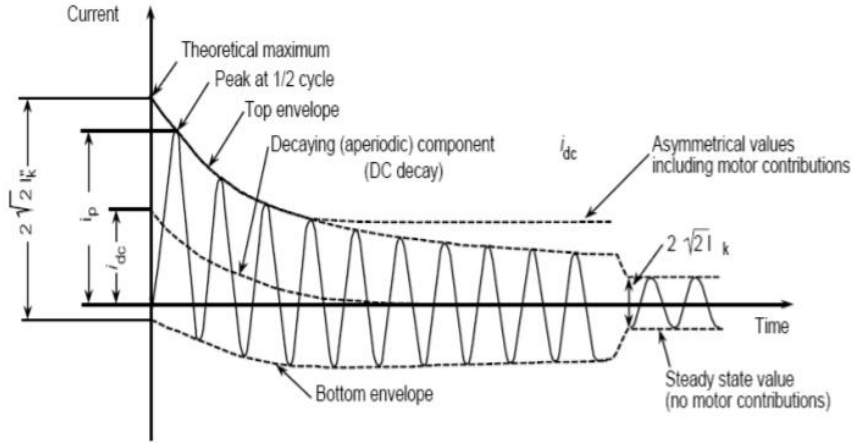


Figure 14- "Near the generator" short-circuit.

A SC is considered to be "far from generator" when the magnitude of the symmetrical AC component of the prospective fault remains essentially constant with time. This is due to the small relative weight that the synchronous machines have in the equivalent impedance value. In this case, the effect of the generator sub-transient behaviour is ignored and since there is no AC decrement for this type of SC, the steady-state fault current is nearly equal in magnitude to the initial fault current [56]. The SCC comprises only the steady-state AC, and decaying DC current components as shown in the following equation [72]:

$$I_{sc}(t) = \frac{E\sqrt{2}}{Z_{fault}} \left[\sin\left(\omega t + \frac{\pi}{2}\right) - e^{-\frac{R\omega t}{X}} \right] \quad (3.11)$$

Where

E is the RMS voltage of the circuit (V);

Z_{fault} is the fault impedance (Ω);

$\frac{R}{X}$ is the resistance and reactance ratio at the point of fault (Ω).

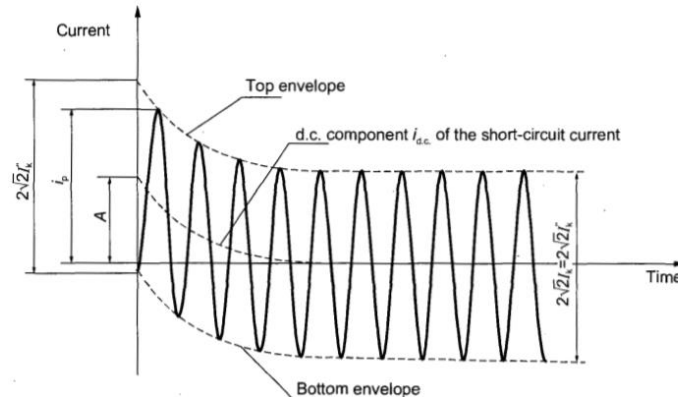


Figure 15- "Far from generator" short-circuit.

3.3.2. Symmetrical Fault

In a three-phase power system, the type of faults that can occur are classified by the combination of conductors or buses that are faulted together through an impedance. Symmetrical SCs consist in a three-phase fault where three conductors are physically held together with zero impedance between them.

For a balanced symmetrical system, the fault current magnitude is balanced equally within the three phases. While this type of fault does not occur frequently, its results are used for protective device selection, because this fault type generally yields the maximum SCC values [69].

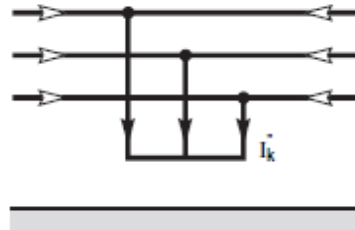


Figure 16- Symmetrical short-circuit.

3.3.2.1. General Calculation Methodology

To determine the precise magnitude of a SCC, after the inception of a fault is a rather complex calculation. In order to calculate with a reasonable degree of accuracy, the SCC that can be expected to flow in a system, it is necessary to find an equivalent circuit for each system element. For three phase balanced circuits simplification, it is common to adopt the single-phase equivalent circuit [69] according to the impedance method mentioned in the previous section.

In order to apply the single-line scheme and to perform a per-phase analysis, it is necessary to consider some calculation assumptions. In this way, it is assumed that the network is

symmetric, being constituted by balanced components; voltage sources generate three-phase symmetrical electromotive force systems; the defect is symmetrical; the system components are represented by elements with constant parameters; a fault impedance Z_{fault} is introduced between the SC node and the circuit reference [59].

The symmetrical SCs analysis will therefore be carried out by steady-state and symmetrical study of a linear circuit, using the laws for the analysis of these circuits. The Thevenin Theorem allows to establish for an electrical network, seen from any node i , an equivalent scheme represented by an equivalent impedance seen from node i when all the sources of voltage and current are cancelled and replaced by their respective internal impedance, in series with a voltage source equal to the pre-fault voltage and the fault impedance. The initial symmetrical SCC is thus calculated according to:

$$I_k'' = \frac{V_k^0}{Z_{kk}'' + Z_{fault}} \quad (3.12)$$

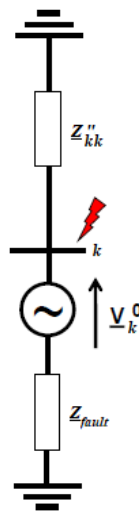


Figure 17- Thevenin Diagram.

3.3.2.2. Systematic Methodology for Computational Calculation

For a general EPS with n nodes, where k is the node where it is intended to simulate the occurrence of a symmetrical three-phase SC, due to its size and complexity, a calculation methodology based on vector and matrix calculation is used. In this way, vectors of dimension n , referring to the values of the nodal voltages are defined:

$$[V^0] = \begin{bmatrix} V_1^0 \\ \vdots \\ V_k^0 \\ \vdots \\ V_n^0 \end{bmatrix} \quad [V^T] = \begin{bmatrix} V_1^T \\ \vdots \\ V_k^T \\ \vdots \\ V_n^T \end{bmatrix}$$

The previous vectors refer to pre-defect nodal voltages, obtained by solving a power flow problem for the operating conditions of the system before the occurrence of the defect, and

to the nodal voltage variations vector. For this purpose, it is considered the single-line diagram of the network with the models of the various components related to SC studies, namely their internal impedances.

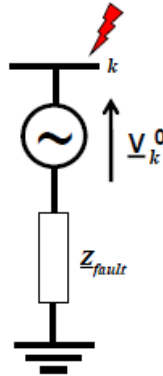


Figure 18-Fault in node k.

Post-fault nodal voltages are obtained through the sum of the pre-fault nodal voltage and the nodal voltage variation vectors.

$$[V^f] = [V^0] + [V^T] \quad (3.13)$$

The calculation of the variation of the nodal voltages is done through the impedance matrix of the single-line diagram of the Thevenin network.

$$\begin{bmatrix} V_1^T \\ \vdots \\ V_k^T \\ \vdots \\ V_n^T \end{bmatrix} = \begin{bmatrix} Z_{11} & \dots & Z_{1k} & \dots & Z_{1n} \\ \vdots & \ddots & \vdots & \ddots & \vdots \\ Z_{k1} & \dots & Z_{kk} & \dots & Z_{kn} \\ \vdots & \ddots & \vdots & \ddots & \vdots \\ Z_{n1} & \dots & Z_{nk} & \dots & Z_{nn} \end{bmatrix} \begin{bmatrix} 0 \\ \vdots \\ -I_k'' \\ \vdots \\ 0 \end{bmatrix} \quad (3.14)$$

The elements of the main diagonal represent the of Thevenin equivalent impedance upstream of the respective node while the elements outside the main diagonal represent the transfer impedance of the node, relating the effect of the injected current and voltage.

$$\underline{V}_k^T = -\underline{I}_k'' \cdot \underline{Z}_{kk} \quad (3.15)$$

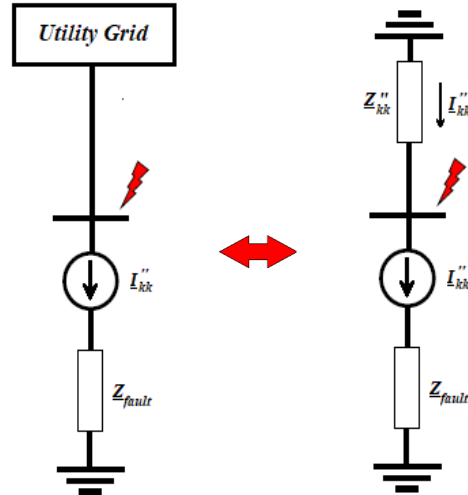


Figure 19-Short-circuit current in node k.

According to the previous equation, the post-defect voltages vector can be represented by:

$$\begin{bmatrix} V_1^f \\ \vdots \\ V_k^f \\ \vdots \\ V_n^f \end{bmatrix} = \begin{bmatrix} V_1^0 \\ \vdots \\ V_k^0 \\ \vdots \\ V_n^0 \end{bmatrix} + \begin{bmatrix} V_1^T \\ \vdots \\ V_k^T \\ \vdots \\ V_n^T \end{bmatrix} = \begin{bmatrix} V_1^0 \\ \vdots \\ V_k^0 \\ \vdots \\ V_n^0 \end{bmatrix} + \begin{bmatrix} \dots & Z_{1k} & \dots \\ \vdots & \vdots & \vdots \\ \dots & Z_{kk} & \dots \\ \vdots & \vdots & \vdots \\ \dots & Z_{nk} & \dots \end{bmatrix} \begin{bmatrix} 0 \\ \vdots \\ -I_k'' \\ \vdots \\ 0 \end{bmatrix} = \begin{bmatrix} V_1^0 - Z_{1k} \cdot I_k'' \\ \vdots \\ V_k^0 - Z_{kk} \cdot I_k'' \\ \vdots \\ V_n^0 - Z_{nk} \cdot I_k'' \end{bmatrix} \quad (3.16)$$

For the post-fault currents circulating in the network branches, i.e. from bus i to bus j :

$$I_{ij}^f = \frac{V_i^f - V_j^0}{Z_{ij}} + V_j^f \cdot \frac{Y_{sh,ij}}{2} \quad (3.17)$$

The currents supplied to the SC by the generators coupled to the grid are given by:

$$I_g^f = I_g^0 + I_g^T = I_g^0 + \frac{V_j^0 - V_j^f}{jX_g''} \quad (3.18)$$

The presented systematic methodology for computational calculation of symmetrical SCs can be divided into 3 distinct stages. The first stage corresponds to the conditions of pre-fault operation in which the power flow problem is solved, obtaining the initial conditions of the system.

The second stage corresponds to the variations caused by the fault in which are established the single-line Thevenin equivalent scheme according to per-unit system, the nodal impedances matrix and calculated the fault current, described in equation 3.12.

The third stage corresponds to the post-defect operation conditions in which are calculated the node voltage, the current in the branches, as described in equation 3.17 and the contributions of generators and network equivalents, described in equation 3.18.

3.3.3. Unsymmetrical Fault

In contrast to symmetrical SCs, an unsymmetrical fault breaks the underlying assumptions used in three-phase power, invalidating the single-phase equivalent circuit condition method for calculating SCC [56]. Usually, electrical power systems are assumed to be balanced, allowing an easier study. However, when an unsymmetrical fault occurs, there is a contact between a line and the ground, between lines or even between lines and the ground, unbalancing the three-phase lines which leads to unequal currents with unequal phase shifts in a three-phase system. Consequently, it is impossible to directly use tools such as the one-line diagram, where only one phase is considered. However, due to the linearity of power systems, it is usual to consider the resulting voltages and currents as a superposition of symmetrical components, to which three-phase analysis can be applied.

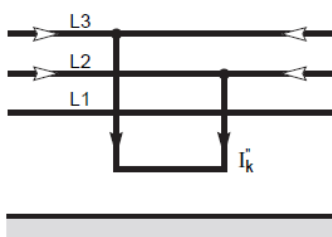


Figure 20- Line-to-line short-circuit.

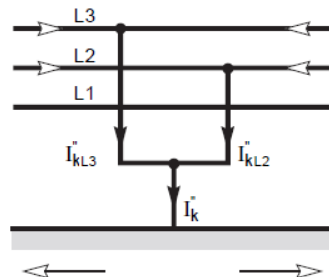


Figure 21- Line-to-line-to-ground short-circuit.

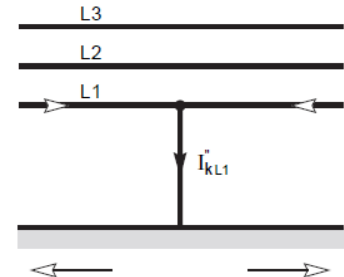


Figure 22- Line-to-ground short-circuit.

3.3.3.1. Application of symmetrical components

This powerful mathematical instrument proposed by Charles Fortescue in 1918 [68] allows an asymmetric n -phasor system to be decomposed into $n-1$ symmetric n -phasor systems with different phase sequences and a zero-sequence n -phasors system [73]. For an asymmetric system with three current and voltage phasors, it is then possible to represent the unbalanced phase components by their decomposition into a sum of three symmetric three-phase systems, called symmetrical components.

The symmetrical components are divided into: positive-sequence, negative-sequence, and zero-sequence. In a three-phase system, one set of three equal magnitude vectors displaced from each other by 120 degrees in the same sequence as the original set of unsymmetrical vectors is called the positive-sequence component. A second set of three equal magnitudes vectors displaced from each other by 120 degrees in the reverse sequence as the original set of unsymmetrical vectors is called the negative-sequence component. A third set of three equal magnitude vectors displaced from each other by 0 degrees is called the zero-sequence component.

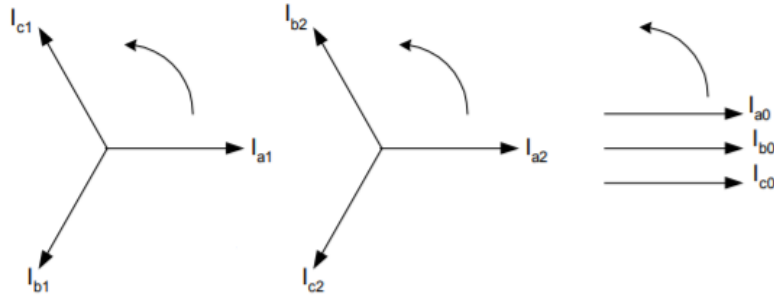


Figure 23- Representation of the positive (1), negative (2) and zero-sequence (0) systems.

When using symmetrical components, it is convenient to define an operator “ α ” such that:

$$\alpha = 1 \angle 120^\circ = e^{j\frac{2\pi}{3}} = -0.5 + j\frac{\sqrt{3}}{2} \quad (3.19)$$

Taking the line conductor a as reference, the currents I_a , I_b and I_c are given by:

$$I_a = I_{a(1)} + I_{a(2)} + I_{a(0)} \quad (3.20)$$

$$I_b = I_{b(1)} + I_{b(2)} + I_{b(0)} = \alpha^2 I_{a(1)} + \alpha I_{a(2)} + I_{a(0)} \quad (3.21)$$

$$I_c = I_{c(1)} + I_{c(2)} + I_{c(0)} = \alpha I_{a(1)} + \alpha^2 I_{a(2)} + I_{a(0)} \quad (3.22)$$

The transformation of symmetrical components into values per phase can therefore be obtained

$$\begin{bmatrix} I_a \\ I_b \\ I_c \end{bmatrix} = \begin{bmatrix} 1 & 1 & 1 \\ \alpha^2 & \alpha & 1 \\ \alpha & \alpha^2 & 1 \end{bmatrix} \begin{bmatrix} I_{a(1)} \\ I_{a(2)} \\ I_{a(0)} \end{bmatrix} \quad (3.23)$$

The Fortescue Matrix is then defined as the matrix that allows the transformation of symmetrical components into values per phase.

$$\begin{bmatrix} I_a \\ I_b \\ I_c \end{bmatrix} = [T] \begin{bmatrix} I_{a(1)} \\ I_{a(2)} \\ I_{a(0)} \end{bmatrix} \quad (3.24)$$

Where

$$[T] = \begin{bmatrix} 1 & 1 & 1 \\ \alpha^2 & \alpha & 1 \\ \alpha & \alpha^2 & 1 \end{bmatrix} \quad (3.25)$$

The equations above can be rewritten to allow the determination of the symmetrical components associated with an unbalanced system

$$\begin{bmatrix} I_a \\ I_b \\ I_c \end{bmatrix} = [T] \begin{bmatrix} I_{a(1)} \\ I_{a(2)} \\ I_{a(0)} \end{bmatrix} \quad (\Rightarrow) \quad \begin{bmatrix} I_{a(1)} \\ I_{a(2)} \\ I_{a(0)} \end{bmatrix} = [T]^{-1} \begin{bmatrix} I_a \\ I_b \\ I_c \end{bmatrix} \quad (3.26)$$

Where

$$[T]^{-1} = \frac{1}{3} \begin{bmatrix} 1 & \alpha & \alpha^2 \\ 1 & \alpha^2 & \alpha \\ 1 & 1 & 1 \end{bmatrix} \quad (3.27)$$

There is thus a unique transformation between values per phase of an unbalanced system and its symmetrical components. The above equations also show that the zero-sequence component is different from zero only if the sum of the values per phase is not null. As the sum of the line voltages in a three-phase system is always zero, the zero-sequence voltage component is never present in the system line voltages, regardless of the degree of its unbalance.

As referred previously, electrical power systems are usually balanced. However, unbalanced SC/fault conditions typically result in equally unbalanced voltages and currents. If the voltages and currents in a system can be related by constant impedances, the system is said linear, and the superposition principle can be applied. In this way, the system voltages, subject to an unbalanced current system, can be obtained considering the isolated response of each symmetrical components.

The impedance of elements in a symmetrical electrical system may be resolved into positive, negative, and zero-sequence components. In a balanced three-phase system, only positive-sequence impedances are required, and only positive-sequence voltage drops, and current flows result from the analysis [69]. In systems where the phase impedances are not equal or where unbalanced faults are simulated using symmetrical networks, positive, negative, and perhaps zero-sequence voltage drops, and current flows will result.

The elements of the electrical energy system of interest for this analysis are synchronous and asynchronous machines (generators and motors) and power converters that contribute to supply SCCs; transformers, lines and loads. It is then necessary to evaluate how each component of the system depends on its winding connection and the relationships that can be established with the symmetrical components.

3.3.3.2. Short-circuit impedances of electrical equipment

The analysis of an unsymmetrical fault on a symmetrical system consists of finding the symmetrical components of the unbalanced currents which are flowing. The positive and negative-sequences of linear, symmetrical, static circuits are identical because the impedance of such circuits is independent, or phase order provided the applied voltages are balanced [74]. The impedance of such circuits to zero-sequence currents may differ from the impedance to positive and negative-sequence currents. In general, the impedances of static elements are the same in positive and negative-sequences but may differ in the zero-sequence. In the case of rotating machines, all three sequence impedances might be different [56].

The study of impedance to negative and zero-sequence current becomes complex when a complete analysis is attempted for many different kinds of circuits. Only the more elementary

cases and those which will be encountered in the analysis will be considered. Positive-sequence impedances do not need detailed explanation because they have been discussed previously.

Three-phase Loads

For symmetrical three-phase static loads consisting of lumped constants or loads which can be analysed as having lumped constants, the impedances to current of positive, negative and zero-sequences are the same because each phase is isolated from, and independent of, other phases. If the load is delta-connected or star-connected with an ungrounded neutral, no path exists for the flow of zero-sequence current. If there is an impedance Z_n in the connection between neutral and ground, an impedance of $3Z_n$ is placed in series with the zero-sequence impedance of the load since $3I_{\alpha(0)}$ flows in the neutral impedance.

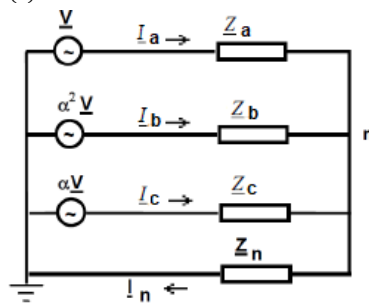


Figure 24- Star connected shunt impedance with neutral.

Three-phase Transformers

A three-phase power transformer is a passive, non-rotating machine. Therefore, the leakage impedance does not vary with the order that the phases are applied. In this way, the positive and negative-sequence impedances have the same value. However, the transformer complicates the analysis of asymmetrical SCs, because its zero-sequence impedance depends on the type of windings and the connection of neutral points to ground [75]. The measurement of this impedance is carried out by means of a classic SC test, applying an electromotive force to the three phases on the side where the measurement is to be carried out, the other winding being short-circuited [68]. An example of the zero-sequence impedance estimation for a transformer with star-to-star connection with neutral ground connection is presented below.

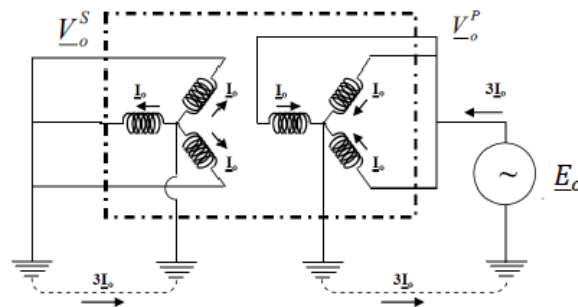


Figure 25- Short-circuit test for a star-to-star connected transformer.

In this scheme, the currents, both in the primary and secondary windings, have free path to close the circuit. Thus, the impedance that is seen on either side of the transformer is the machine leakage impedance [74].

$$\underline{E}_0 = \underline{V}_0^P + jX^P I_0 \quad (3.28)$$

$$\underline{V}_0^S = jX^S I_0 \quad (3.29)$$



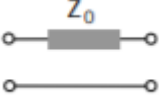
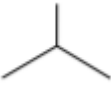
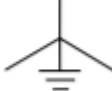
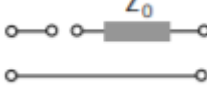

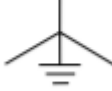


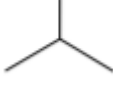
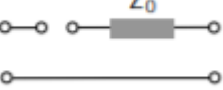
Since in the per-unit system, primary voltages \underline{V}_0^P and secondary \underline{V}_0^S are equal

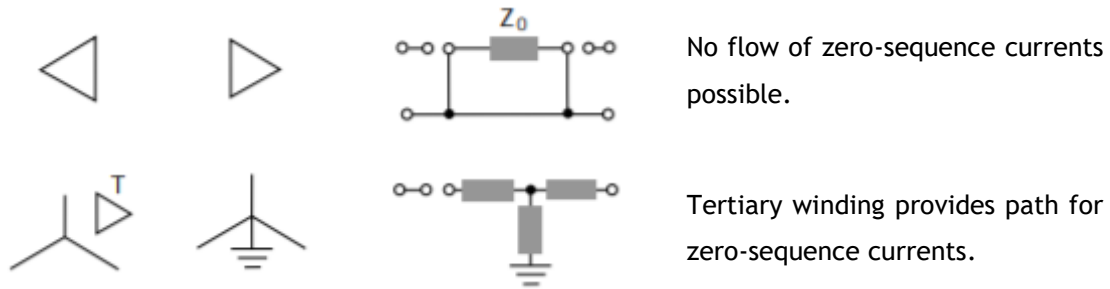
$$\underline{V}_0^P = \underline{V}_0^S \quad (3.30)$$

$$\underline{E}_0 = (jX^P + jX^S)I_0 = (jX_l)I_0 \quad (3.31)$$

As current I_0 is only limited by the leakage impedance X_l , if it is equal to the nominal value, the voltage will be numerically equal to the zero-sequence impedance $Z_{(0)}$, which in turn is equal to transformer leakage impedance. Depending on the type of windings, it may not be possible to ground the neutral point of one of the windings; In this case, the circuit with the test generator will not be closed and the current will be zero, meaning that the zero-sequence impedance has an infinite value. In other words, the zero-sequence circuit, viewed from that side of the transformer, is an open-circuit. The different zero-sequence transformer representations for various winding arrangements are listed on the following table [75].

Table 2- Zero-sequence representation of transformers.

Connections of windings		Representation per phase	Comments
Primary	Secondary		
			Zero-sequence currents free to flow in both primary and secondary circuits.
			No path for zero-sequence currents in primary circuits.
			Single-phase currents can circulate in the delta but not outside it.
			No flow of zero-sequence currents possible.



Lines and Cables

Lines and cables are bilateral static elements composed of identical conductors with identical characteristic impedances and with a symmetrical geometric arrangement such that the mutual impedances are also all equal.

For the construction of a convincing model it is necessary to take into account that the current in any phase will induce the other phases and the neutral conductor, due to the electromagnetic coupling [68]. Recalling this, the Kirchhoff equations for the phases *a*, *b* and *c* can be written, considering the series and induced voltage drops in both phase and the neutral conductors.

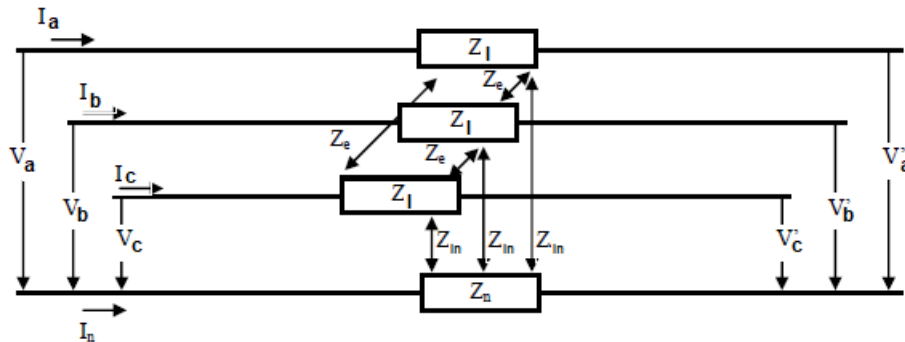


Figure 26-Asymmetrical currents in a symmetrical three-phase line with neutral conductor.

$$V_a = Z_l I_a + Z_e I_b + Z_e I_c + Z_{ln} I_n + V_a' - (Z_n I_n + Z_{an} I_a + Z_{an} I_b + Z_{an} I_c) \tag{3.32}$$

$$V_b = Z_l I_b + Z_e I_a + Z_e I_c + Z_{ln} I_n + V_b' - (Z_n I_n + Z_{ln} I_a + Z_{an} I_b + Z_{an} I_c) \tag{3.33}$$

$$V_c = Z_l I_c + Z_e I_a + Z_e I_b + Z_{ln} I_n + V_c' - (Z_n I_n + Z_{ln} I_a + Z_{an} I_b + Z_{an} I_c) \tag{3.34}$$

Recalling that

$$I_n = -(I_a + I_b + I_c) \tag{3.35}$$

And assuming that

$$Z_c = Z_l + Z_n - 2Z_{ln} \tag{3.36}$$

$$Z_m = Z_e + Z_n - 2Z_{ln} \tag{3.37}$$

Where

Z_c is the characteristic impedance;

Z_l is the leakage impedance;

Z_{ln} is the line-to-neutral impedance;

Z_m is the mutual impedance;

Z_e is the electromagnetic impedance;

The symmetric matrix equation can be written in the three phases, equivalent to the characteristic and mutual impedances of a three-phase system with neutral

$$\begin{bmatrix} V_a - V_a' \\ V_a - V_a' \\ V_a - V_a' \end{bmatrix} = \begin{bmatrix} Z_c & Z_m & Z_m \\ Z_m & Z_c & Z_m \\ Z_m & Z_m & Z_c \end{bmatrix} \begin{bmatrix} I_a \\ I_b \\ I_c \end{bmatrix} \quad (3.38)$$

The transformation to symmetrical components can be applied, obtaining the model of the decoupled line in three symmetrical components

$$\begin{bmatrix} V_a - V_a' \\ V_a - V_a' \\ V_a - V_a' \end{bmatrix} = \begin{bmatrix} Z_{(1)} & 0 & 0 \\ 0 & Z_{(2)} & 0 \\ 0 & 0 & Z_{(0)} \end{bmatrix} \begin{bmatrix} I_{a(1)} \\ I_{a(2)} \\ I_{a(0)} \end{bmatrix} = \begin{bmatrix} Z_{(1)} I_{a(1)} \\ Z_{(2)} I_{a(2)} \\ Z_{(0)} I_{a(0)} \end{bmatrix} \quad (3.39)$$

The positive and negative-sequence impedances are the normal balanced values. The zero-sequence impedance depends upon the nature of the return path through the earth if no fourth wire is provided. In the absence of detailed information, the following rough guide to the value of $Z_{(0)}$ may be used. For a single-circuit line $Z_{(0)}/Z_{(1)}$ should be assumed as 3.5 with no earth wire and $Z_{(0)}/Z_{(1)}$ assumed as 2 with one earth wire [75].

Generators

In the SC calculation model, the generator impedances are considered to be purely reactive (resistance is neglected). As mentioned before, the contribution of a synchronous machine to a SC is divided into three fundamental periods, as a result of sudden changes in current due to the change in magnetic fluxes.

Constructively, generators are designed to create electromotive forces in positive-sequence. Therefore, to determine the positive-sequence impedance of an alternator, it is enough to excite the machine to 100% of its nominal electromotive force and to SC its terminals. The SCCs will only correspond to the positive-sequence circuit [68]. Observing the current values in one phase will allow the calculation of the positive-sequence impedance. This impedance is given by

$$Z_{(1)} = X_{(1)} = \frac{1}{|I_{steadystate}|} \text{ p.u.} \tag{3.40}$$

The negative-sequence impedance can be calculated by applying an inverse electromotive force to the generator by short-circuiting the inductor circuit. Measuring the currents flowing to the test machine, the impedance can be obtained

$$Z_{(2)} = X_{(2)} = \frac{E_{(2)}}{|I_{steadystate}|} (\Omega) \tag{3.41}$$

Since zero-sequence current means identical current in each phase winding, a convenient method of measuring zero-sequence impedance is to connect the three-phase windings in series and to apply a single-phase voltage, short-circuiting the inductor circuit.

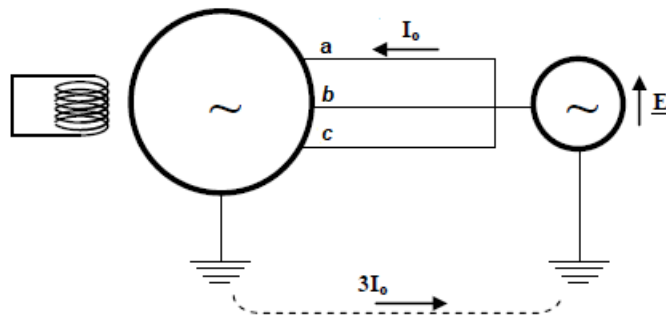


Figure 27- Assembly to obtain the zero-sequence impedance.

By measuring the currents flowing to the machine under test

$$Z_{(0)} = X_{(0)} = \frac{E}{I_{a(0)}} (\Omega) \tag{3.42}$$

Typically, the per-unit system values of generator and motor impedances are shown in the following table. As in the case of lines and cables, these values are used in the absence of detailed information.

Table 3- Synchronous machine reactances (in p.u. of rated MVA).

Reactances	Synchronous motors		Synchronous condenser	Hydro generators	Thermal generators
	High-speed	Low-speed			
X_d	0.80	1.10	1.60	1.00	1.15
X'_d	0.30	0.35	0.40	0.30	0.15
X''_d	0.18	0.20	0.25	0.20	0.10
$X_{(2)}$	0.19	0.35	0.25	0.20	0.13
$X_{(0)}$	0.05	0.07	0.08	0.07	0.04

Power Converters

Finally, reversible static converters are considered for three-phase systems similar as asynchronous motors. In case of a fault, the DC system only contributes to an AC SC when the converter operates as an inverter, if the grid-control protection does not operate [69]. Thus, it continues to conduct current from the DC motor acting as a source to the AC SC.

The induction motor impedance based on its reactive current injection is given by

$$Z_{motor} = X_{motor} = \frac{1}{I_{LR}/L_{rM}} \cdot \frac{V_{rM}}{\sqrt{3}I_{rM}} p.u. \quad (3.43)$$

Where

I_{LR}/L_{rM} is the ratio of the locked-rotor to the rated current of the machine;

V_{rM} is the rated voltage of the machine.

According to IEC 60909 standard, the I_{LR}/L_{rM} ratio for reversible static converters is equal to 3, V_{rM} corresponds to the rated voltage of the converter and I_{rM} corresponds to the rated current [56]. Then

$$Z_{converter} = X_{converter} = \frac{1}{3} \cdot \frac{V_{converter}}{\sqrt{3}I_{converter}} p.u \quad (3.44)$$

If there is no information about the converter or if relevant data is omitted, the circuit component that represents the DC machine contributing through an inverting converter in the equivalent circuit for an AC SC calculation, is considered as an equivalent locked rotor current of 0.33 ($X'' = 33\%$), based on the AC three-phase apparent power input of the converter transformer, or at rated DC machine load and an equivalent X/R ratio of 10 if there is no transformer [69].

3.3.3.3. Systematic Methodology for Computational Calculation

Recognizing the extremely important role of the application of systems transformation to symmetrical components and the need to reduce complexity of electrical systems, a methodology was defined, to calculate asymmetrical SCCs. The strategy involves decomposing the original circuit into three symmetric systems by aggregating the respective impedances and decomposing the voltages and currents, solving each circuit in the domain of symmetrical components.

In this methodology, the Thevenin theorem is applied to each of the positive, negative and zero-sequence circuits. Thus, the Thevenin equivalent of each of these circuits, viewed from a system node, is composed of a series open circuit voltage source with an equivalent impedance, which is given by the principal diagonal value of the nodal impedance matrix of the respective network. Due to the diversity of transformer zero-sequence circuit models, it will be possible to be considered only a subsystem, since transformers may present an infinite impedance in the zero-sequence circuit.

The open-circuit voltage source refers to the pre-defect voltage, \underline{V}^f , assuming that the system in this condition was operating normally, and therefore, the existing voltages and

currents are only non-zero in their positive-sequence component, considering the electromotive forces of the generators.

As in the case of symmetrical faults, the pre-fault operating point is taken for each positive, negative and zero-sequence network, as given by

$$\underline{V}^f = \underline{Z} \cdot \underline{I}^f \tag{3.45}$$

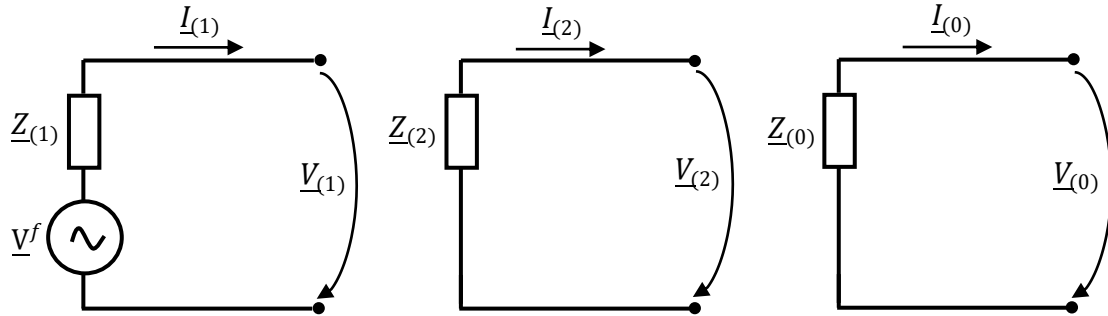


Figure 28-Thévenin equivalent in the positive, negative and zero-sequences.

According to the previous schemes, equation 3.36 can be written in matrix form for a system with n nodes and a fault in node k

$$\begin{bmatrix} \underline{V}_{1(1)} \\ \vdots \\ \underline{V}_{k(1)} \\ \vdots \\ \underline{V}_{n(1)} \end{bmatrix} = \begin{bmatrix} \underline{V}_1^f \\ \vdots \\ \underline{V}_k^f \\ \vdots \\ \underline{V}_n^f \end{bmatrix} + \begin{bmatrix} \underline{Z}_{1k(1)} \\ \vdots \\ \underline{Z}_{kk(1)} \\ \vdots \\ \underline{Z}_{nk(1)} \end{bmatrix} [-\underline{I}_{(1)}] \quad \begin{bmatrix} \underline{V}_{(2)} \\ \vdots \\ \underline{V}_{k(2)} \\ \vdots \\ \underline{V}_{n(2)} \end{bmatrix} = \begin{bmatrix} \underline{Z}_{1k(2)} \\ \vdots \\ \underline{Z}_{kk(2)} \\ \vdots \\ \underline{Z}_{nk(2)} \end{bmatrix} [-\underline{I}_{(2)}] \quad \begin{bmatrix} \underline{V}_{(0)} \\ \vdots \\ \underline{V}_{k(0)} \\ \vdots \\ \underline{V}_{n(0)} \end{bmatrix} = \begin{bmatrix} \underline{Z}_{1k(0)} \\ \vdots \\ \underline{Z}_{kk(0)} \\ \vdots \\ \underline{Z}_{nk(0)} \end{bmatrix} [-\underline{I}_{(0)}] \tag{3.46}$$

After the positive, negative and zero-sequence voltages and currents are known, the voltages and currents in each phase and in each node can be calculated through the Fortescue matrix, shown in equation 3.18. This methodology can be applied to several types of SCs, as shown below.

Line-to-ground short-circuit

It corresponds to an abrupt structural change in the three-phase EPS, characterized by the establishment of an electrical contact between a phase and the ground, through a circuit of low impedance. This type of fault is the most common representing about 80% of occurrences [71] and is the least disturbing to the system. The line-to-ground fault current magnitude is determined by the method in which the system is grounded, and the impedance of the ground return circuit is the path of the fault current [69]. Calculation of the exact line-to-ground fault current magnitudes requires special calculating techniques using symmetrical components.

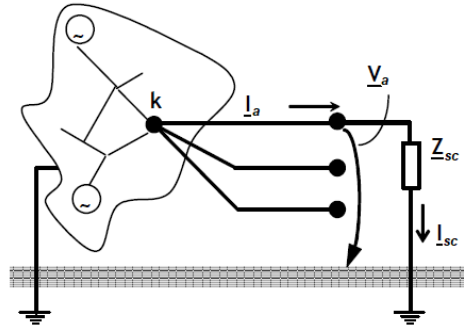


Figure 29- Line-to-ground fault.

For this type of fault, the contact of a phase (phase *a*) with the ground is considered, and the vector of the currents in the system are given by

$$\begin{bmatrix} I_a \\ I_b \\ I_c \end{bmatrix} = \begin{bmatrix} I_{sc} \\ 0 \\ 0 \end{bmatrix} \quad (3.47)$$

Converting to symmetrical components

$$\begin{bmatrix} I_{a(1)} \\ I_{a(2)} \\ I_{a(0)} \end{bmatrix} = [T]^{-1} \begin{bmatrix} I_a \\ I_b \\ I_c \end{bmatrix} = \frac{1}{3} \begin{bmatrix} 1 & \alpha & \alpha^2 \\ 1 & \alpha^2 & \alpha \\ 1 & 1 & 1 \end{bmatrix} \begin{bmatrix} I_{sc} \\ 0 \\ 0 \end{bmatrix} = \begin{bmatrix} \frac{1}{3} I_{sc} \\ \frac{1}{3} I_{sc} \\ \frac{1}{3} I_{sc} \end{bmatrix} \quad (3.48)$$

Which means that the positive, negative and zero-sequence components of the current are the same. Considering that $\underline{V}^f = \underline{Z}_{sc} \cdot I_{sc} = 3 \cdot \underline{Z}_{sc} \cdot I_{a(0)}$ and $\underline{V}^f = \underline{V}_{k(1)} + \underline{V}_{k(2)} + \underline{V}_{k(0)}$, the following equation is obtained

$$3 \cdot \underline{Z}_{sc} \cdot I_{a(0)} = \underline{V}^f - (\underline{Z}_{kk(1)} + \underline{Z}_{kk(2)} + \underline{Z}_{kk(0)}) \cdot I_{a(0)} \quad (3.49)$$

(=)

$$I_{a(1)} = I_{a(2)} = I_{a(0)} = \frac{\underline{V}^f}{\underline{Z}_{kk(1)} + \underline{Z}_{kk(2)} + \underline{Z}_{kk(0)} + 3 \cdot \underline{Z}_{sc}}$$

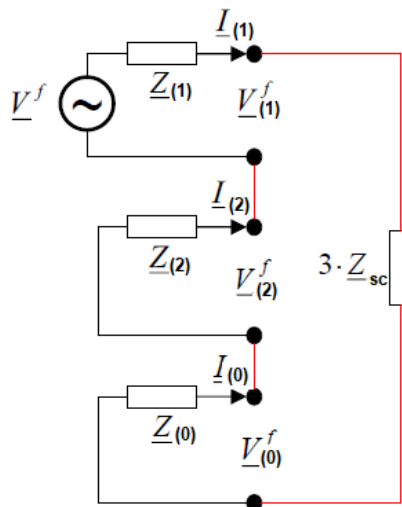


Figure 30- Thevenin equivalent impedances seen from the defect node.

The SCC is then given by

$$I_{sc} = \frac{3 \cdot V^f}{Z_{kk(1)} + Z_{kk(2)} + Z_{kk(0)} + 3 \cdot Z_{sc}} \quad (3.50)$$

In a line-to-ground fault, the current in the faulted phase is high and very low or nearly zero in the remaining two. In contrast, the voltage at the fault node in the corresponding phase, is low depending on the fault impedance, while the voltage at the same phase, at the remaining nodes, increases with the distance to the fault node. In the two phases not affected by the fault, the voltage will be close to the nominal per-unit value, and an overvoltage can occur comparing to the pre-defect values and tends to decrease with the distance to the defect node.

Typically, due to the transformer winding connections and the type of neutral connection, the zero-sequence equivalent circuit has a different topology than the positive and negative-sequence equivalent circuit.

Line-to-line short-circuit

Bolted line-to line faults occur when there is a conductive path between two different lines caused by an impedance, physical contact or by ionization of air, representing about 15% of total occurrences [71]. Since it is an unbalanced fault, it is necessary to apply the system transformation to symmetrical components for the calculation of the SCC. In the case of this type of SC, it is possible to simplify the system by cancelling the zero-sequence component, because there is no contact with the ground, applying only the positive and negative-sequence components, as will be shown later.

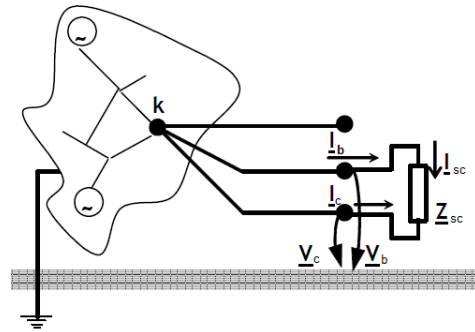


Figure 31- Line-to-line-fault.

For the system represented by the previous figure, the fault occurs between phases *b* and *c*. The vector of the currents is given by

$$\begin{bmatrix} I_a \\ I_b \\ I_c \end{bmatrix} = \begin{bmatrix} 0 \\ I_b \\ -I_b \end{bmatrix} = \begin{bmatrix} 0 \\ I_{sc} \\ -I_{sc} \end{bmatrix} \quad (3.51)$$

Applying the transformation to symmetrical components

$$\begin{bmatrix} I_{(1)} \\ I_{(2)} \\ I_{(0)} \end{bmatrix} = [T]^{-1} \begin{bmatrix} I_a \\ I_b \\ I_c \end{bmatrix} = \frac{1}{3} \begin{bmatrix} 1 & \alpha & \alpha^2 \\ 1 & \alpha^2 & \alpha \\ 1 & 1 & 1 \end{bmatrix} \begin{bmatrix} 0 \\ I_b \\ -I_b \end{bmatrix} = \begin{bmatrix} \frac{1}{3}(\alpha - \alpha^2)I_b \\ \frac{1}{3}(\alpha^2 - \alpha)I_b \\ 0 \end{bmatrix} \quad (3.52)$$

Considering that $\underline{V}_b - \underline{V}_c = \underline{Z}_{sc} \cdot \underline{I}_{sc} = \underline{Z}_{sc} \cdot \underline{I}_b$, $\underline{V}_b = \alpha^2 \underline{V}_{k(1)} + \alpha \underline{V}_{k(2)} + \underline{V}_{k(0)}$ and $\underline{V}_c = \alpha \underline{V}_{k(1)} + \alpha^2 \underline{V}_{k(2)} + \underline{V}_{k(0)}$, expressing the current of phase b in its symmetrical components, the following equation is obtained

$$(\alpha^2 - \alpha) \underline{V}_{k(1)} + (\alpha - \alpha^2) \underline{V}_{k(2)} = \underline{Z}_{sc} (\alpha^2 \underline{I}_{(1)} + \alpha \underline{I}_{(2)}) \quad (3.53)$$

Since $\underline{I}_{(1)} = -\underline{I}_{(2)}$

$$(\alpha^2 - \alpha) \underline{V}_{k(1)} + (\alpha - \alpha^2) \underline{V}_{k(2)} = \underline{Z}_{sc} (\alpha^2 - \alpha) \underline{I}_{(1)} \quad (3.54)$$

Substituting the voltage variables for the expression derived from the Thevenin equivalents

$$\underline{I}_{(1)} = -\underline{I}_{(2)} = \frac{\underline{V}^f}{\underline{Z}_{kk(1)} + \underline{Z}_{kk(2)} + \underline{Z}_{sc}}, \quad \underline{I}_{(0)} = 0 \quad (3.55)$$

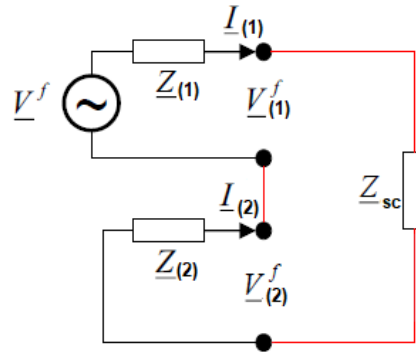


Figure 32- Thevenin equivalent impedances seen from the defect node.

The SCC is then given by

$$\underline{I}_{sc} = \alpha^2 \underline{I}_{(1)} + \alpha \underline{I}_{(2)} = (\alpha^2 - \alpha) \underline{I}_{(1)} \quad (3.56)$$

Applying the result obtained to the matrix of currents per phase

$$\begin{bmatrix} \underline{I}_a \\ \underline{I}_b \\ \underline{I}_c \end{bmatrix} = \begin{bmatrix} 0 \\ (\alpha^2 - \alpha) \underline{I}_{(1)} \\ -(\alpha^2 - \alpha) \underline{I}_{(1)} \end{bmatrix} = \begin{bmatrix} 0 \\ \frac{-j\sqrt{3} \underline{V}^f}{\underline{Z}_{kk(1)} + \underline{Z}_{kk(2)} + \underline{Z}_{sc}} \\ \frac{j\sqrt{3} \underline{V}^f}{\underline{Z}_{kk(1)} + \underline{Z}_{kk(2)} + \underline{Z}_{sc}} \end{bmatrix} \quad (3.57)$$

In a phase-to-phase SC, the current magnitude in the two faulted phases is high and zero in the healthy phase. The voltages of the faulted phases are approximately equal to half of their nominal value whereas in the phase where the SC does not occur, the voltage will be approximately nominal in the per-unit system.

As mentioned, there are no zero-sequence currents because the circuit is not closed by the ground or by the return conductor. This factor does not affect the values of the SCC due to the lack of grounding connection, but some transformer winding connections may have relevant impacts.

Line-to-line short-circuit with ground connection

Line-to-line-to-ground faults are typically line-to-ground faults that have escalated to include a second phase conductor. In this unbalanced fault, the magnitudes of double line-to-ground fault currents are usually greater than those of line-to-line faults but are less than those of three-phase faults [69].

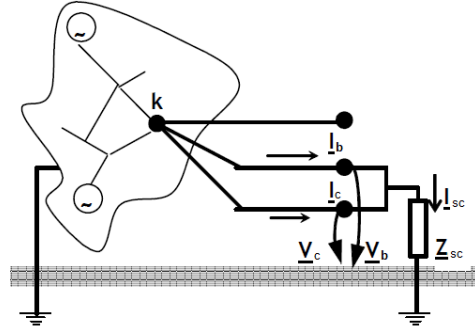


Figure 33- Double line-to-ground short-circuit.

The system under analysis presents the occurrence of a defect between phases *b* and *c*. In this case, the fault conditions are

$$\begin{bmatrix} I_a \\ I_b \\ I_c \end{bmatrix} = \begin{bmatrix} 0 \\ I_b \\ I_c \end{bmatrix} \quad (3.58)$$

It is then possible to obtain the characteristics of the symmetrical components of the SCC

$$\begin{bmatrix} I_{(1)} \\ I_{(2)} \\ I_{(0)} \end{bmatrix} = [T]^{-1} \begin{bmatrix} I_a \\ I_b \\ I_c \end{bmatrix} = \frac{1}{3} \begin{bmatrix} 1 & \alpha & \alpha^2 \\ 1 & \alpha^2 & \alpha \\ 1 & 1 & 1 \end{bmatrix} \begin{bmatrix} 0 \\ I_b \\ I_c \end{bmatrix} = \begin{bmatrix} \frac{1}{3}(\alpha I_b + \alpha^2 I_c) \\ \frac{1}{3}(\alpha^2 I_b + \alpha I_c) \\ \frac{1}{3}(I_b + I_c) \end{bmatrix} \quad (3.59)$$

Regarding the values per phase of the post-defect voltage

$$\begin{bmatrix} V_a \\ V_b \\ V_c \end{bmatrix} = \begin{bmatrix} V_a \\ (I_b + I_c)Z_{sc} \\ (I_b + I_c)Z_{sc} \end{bmatrix} \quad (3.60)$$

Transforming into symmetrical components

$$\begin{bmatrix} V_{(1)} \\ V_{(2)} \\ V_{(0)} \end{bmatrix} = \frac{1}{3} \begin{bmatrix} 1 & \alpha & \alpha^2 \\ 1 & \alpha^2 & \alpha \\ 1 & 1 & 1 \end{bmatrix} \begin{bmatrix} V_a \\ (I_b + I_c)Z_{sc} \\ (I_b + I_c)Z_{sc} \end{bmatrix} = \frac{1}{3} \begin{bmatrix} V_a - 3I_{(0)}Z_{sc} \\ V_a - 3I_{(0)}Z_{sc} \\ V_a + 6I_{(0)}Z_{sc} \end{bmatrix} \quad (3.61)$$

Observing the vector of the symmetrical components of the post-defect voltage at the node where the SC occurs, it is concluded that $V_{(1)} = V_{(2)}$ and $V_{(1)} - V_{(0)} = -3I_{(0)}Z_{sc}$.

From the previous equations following scheme can be obtained, that allows to define the symmetrical components of the current.

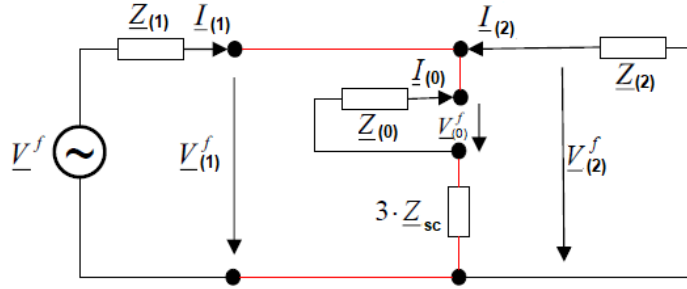


Figure 34- Thevenin equivalent impedances seen from the defect node.

The positive, negative and zero-sequence components of the current are then

$$\underline{I}_{(1)} = \frac{\underline{V}^f}{\underline{Z}_{kk(1)} + ((\underline{Z}_{kk(0)} + 3 \cdot \underline{Z}_{sc}) // \underline{Z}_{kk(2)})} \quad (3.62)$$

(=)

$$\underline{I}_{(1)} = \frac{(\underline{Z}_{kk(2)} + \underline{Z}_{kk(0)} + 3 \cdot \underline{Z}_{sc}) \cdot \underline{V}^f}{\underline{Z}_{kk(1)} \cdot \underline{Z}_{kk(2)} + \underline{Z}_{kk(1)} \cdot (\underline{Z}_{kk(0)} + 3 \cdot \underline{Z}_{sc}) + \underline{Z}_{kk(2)} \cdot (\underline{Z}_{kk(0)} + 3 \cdot \underline{Z}_{sc})}$$

$$\underline{I}_{(2)} = -\frac{(\underline{Z}_{kk(0)} + 3 \cdot \underline{Z}_{sc})}{\underline{Z}_{kk(2)} + \underline{Z}_{kk(0)} + 3 \cdot \underline{Z}_{sc}} \cdot \underline{I}_{(1)} \quad (3.63)$$

(=)

$$\underline{I}_{(2)} = -\frac{(\underline{Z}_{kk(0)} + 3 \cdot \underline{Z}_{sc}) \cdot \underline{V}^f}{\underline{Z}_{kk(1)} \cdot \underline{Z}_{kk(2)} + \underline{Z}_{kk(1)} \cdot (\underline{Z}_{kk(0)} + 3 \cdot \underline{Z}_{sc}) + \underline{Z}_{kk(2)} \cdot (\underline{Z}_{kk(0)} + 3 \cdot \underline{Z}_{sc})}$$

$$\underline{I}_{(0)} = -\frac{\underline{Z}_{kk(2)}}{\underline{Z}_{kk(2)} + \underline{Z}_{kk(0)} + 3 \cdot \underline{Z}_{sc}} \cdot \underline{I}_{(1)} \quad (3.64)$$

(=)

$$\underline{I}_{(0)} = -\frac{\underline{Z}_{kk(2)} \cdot \underline{V}^f}{\underline{Z}_{kk(1)} \cdot \underline{Z}_{kk(2)} + \underline{Z}_{kk(1)} \cdot (\underline{Z}_{kk(0)} + 3 \cdot \underline{Z}_{sc}) + \underline{Z}_{kk(2)} \cdot (\underline{Z}_{kk(0)} + 3 \cdot \underline{Z}_{sc})}$$

From the above equations, it is possible to calculate the SCC

$$\underline{I}_{sc} = \underline{I}_{(1)} + \underline{I}_{(2)} \quad (=) \quad \underline{I}_{sc} = 3 \cdot \underline{I}_{(0)} \quad (3.65)$$

3.4. Chapter Summary

The SC study is of fundamental importance in the power systems analysis, since it is possible to obtain values related to the system variables when a fault occurs, namely voltage, current, power and even power factor. Currently there is a wide set of techniques to perform the study of electrical faults. Combining circuit theory with mathematical methods, it is possible to identify and analyse the state of the system after the occurrence of a fault. The presented SC model makes approximations aiming at a system linearization, using the symmetrical components method, which consists of obtaining, from an unsymmetrical system, three decoupled systems called positive, negative and zero-sequences.

- Section 3.1. presents the relevance of CBDG for the MG operation and fault analysis.
- Section 3.2. of this chapter presents the methodology for calculating the SC current, the standard notation system for converting the elements of the system to the same base, and finally the model of each element.
- Section 3.3. exposes in detail the main characteristics of the SC current, the types of faults that typically occur in an EPS, and the associated calculation methodologies.

Chapter 4

Applications of Short-circuit Analysis

Numerical calculation of Short-Circuits (SCs) in the network is extremely important in the planning, design and operation of facilities and networks, in order to anticipate the consequences of the simulated faults. This knowledge makes it possible to take the necessary measures to minimize damaging electrical equipment and efficiently protect people, with the least possible disturbance in the system. This includes not only the placement and regulation of devices that promote the interruption of defective circuits, but also ensure that all components of the network covered by the fault currents can withstand their effects while they persist.

4.1. Short-Circuit Calculation

The SC studies are essential for the correct sizing of the various components of the Electric Power System (EPS) regarding the dynamic and thermal stresses of the SC currents. On the other hand, they are crucial, both for the definition of the cutting power of the protective devices, and for the design and regulation of the protections.

Setting the assumptions for calculating SCCs, the methodologies presented in the previous chapter are applied to a Microgrid (MG) consisting of an inverter-based Battery Energy Storage System (BESS), a load, a synchronous generator, an electric vehicle charging station and the respective connections to medium and Low Voltage (LV) distribution networks, being that their connection is mutually exclusive. It is considered that the system was stable and the voltage in the buses of the system is its nominal value. The following figure represents a MG related to the Democrat project that will be detailed later.

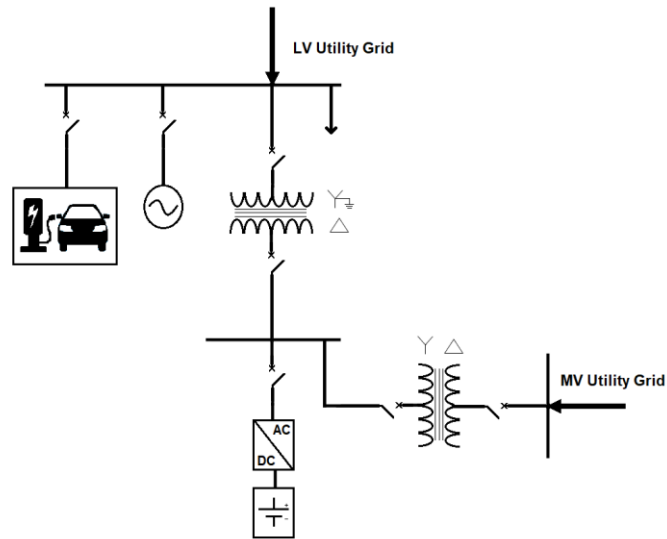


Figure 35- Microgrid diagram.

4.1.1. Short-Circuit Current Contribution during Balanced Faults

The symmetrical SC analysis shall be based on the methodology presented in subsection 3.3.2. and applied to the system shown in the previous figure. Three different operating modes will therefore be exposed: connection of the system to the Medium Voltage (MV) distribution network, connection of the system to the LV distribution network and operation in isolated mode.

4.1.1.1. Low Voltage Grid Connection

The analysis of this type of connection will consider only the storage system, the LV utility grid connection transformer, the load bank and utility grid, as shown in the following figure.

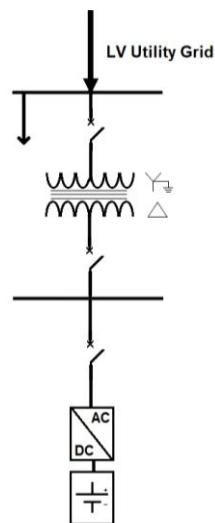


Figure 36- Low voltage grid-connected microgrid.

In order to carry out the SC analysis, it is necessary to know the characteristics of the MG elements. For this purpose, the following parameters are considered

Table 4- Low Voltage system parameters.

Element	Parameters			
	Voltage(V)	Apparent Power (VA)	Power factor	Rated Current (A)
Utility Grid	400	20×10^6	–	–
Load Bank	400	25×10^4	0.8	–
Power Transformer	400/315	25×10^4	–	–
Inverter	315	25×10^4	–	458
Battery Storage System	$736^{(DC)}$	21.8×10^4	1	$296^{(DC)}$

Taking into account what has been presented in subsection 3.2, it is necessary to transform all elements of the system into an equivalent linear model, considering them as impedances.

Utility Grid

The LV network is considered as a large generator whose characteristic $X/R = 0.9$. Assuming the value for the base power, $S_{Base} = 25 \times 10^4 VA$ and according to equations 3.2 and 3.4

$$S_{Utility p.u.} = \frac{S_{Utility}}{S_{Base}} = \frac{20 \times 10^6}{25 \times 10^4} = 80 p.u. \quad (4.1)$$

$$Z_{Utility p.u.} = \frac{V_{Utility p.u.}^2}{S_{Utility p.u.}} = \frac{1}{80} = 0,0125 p.u \quad (4.2)$$

Considering the characteristic X/R

$$Z_{Utility p.u.} = \sqrt{R^2 + X^2} \quad (4.3)$$

$$Z_{Utility p.u.} = 9.2912 \times 10^{-3} + j8.362 \times 10^{-3} p.u.$$

Load Bank

The load is modelled according to equation 3.5

$$Z_{Load Bank p.u.} = \frac{V_{Load Bank}^2}{P_{Load Bank} - jQ_{Load Bank}} = 0.512 + j0.384 p.u. \quad (4.4)$$

Power Transformer

Considering that the transformer has a leakage reactance equal to the characteristic impedance, $Z_{transf} = X_f = 4.2\%$, it is only necessary to convert it to the corresponding base. The transformer is then modelled by equation 3.3. As the system and transformer bases are the same

$$Z_{transf_{p.u.}} = X_f = j0.042 \text{ p.u.} \quad (4.5)$$

Battery Energy Storage System

For the MG under study, the batteries behave as a current source, injecting into the bus to which they are connected. Considering the efficiency of the inverter can be calculated the current injected into the network by the storage system.

$$P_{DC} - P_{Inverter\ losses} = P_{AC} \quad (4.6)$$

(=)

$$P_{DC} - (1 - \eta) \cdot P_{DC} = V_{AC} \cdot I_{AC} \quad (4.7)$$

Considering the efficiency of the converter of 98.4%

$$21.8 \times 10^4 - (1 - 0.984) \times 21.8 \times 10^4 = \sqrt{3} \times 315 \times I_{AC} \quad (4.8)$$

(=)

$$I_{AC} = 392.17 \text{ A}$$

Inverter

The modelling of the inverter, as mentioned in the previous chapter, is based on the nominal voltage and the current that it provides to the network to which it is connected. Since the supplied current is the output current of the battery system, the inverter impedance model is obtained from equation 3.41, previously presented and, therefore

$$Z_{inverter_{p.u.}} = X_{inverter} = \frac{1}{3} \cdot \frac{V_{converter}}{\sqrt{3}I_{AC}} = j0,155 \text{ p.u} \quad (4.9)$$

For the correct operation of the inverter, a filter was considered, having an equivalent impedance of

$$Z_{filter_{p.u.}} = 0.112 + j0,109 \text{ p.u} \quad (4.10)$$

In this way, the impedance of the inverter also includes the impedance of the filter.

Lines and Cables

For the interconnection of the elements described above, it is considered some electrical connecting cables, whose impedances are specified in the following table

Table 5- Low Voltage cable impedance.

Connector	From	To	Impedance (p.u.)
Cable 1	Utility Grid	Power Transformer	$0.0131 + j0,0071$
Cable 2	Power Transformer	Load Bank	$0.0065 + j0,0035$
Cable 3	Power Transformer	Inverter	$0.0024 + j0,0019$

Knowing the equivalent impedances of all elements of the system can then be applied the methodology for calculation of symmetrical SCs, previously presented. Thus, considering a fault in the furthest bus from the storage system, the magnitude of the SCC can be analysed using the following scheme

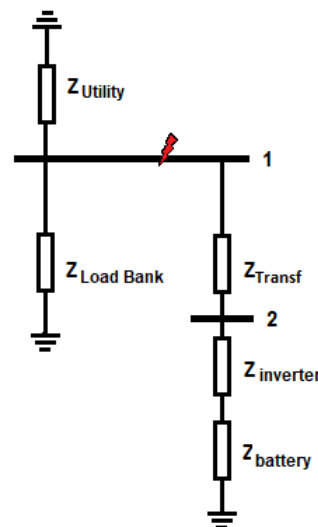


Figure 20- Symmetrical fault at bus 1.

By the application of the Thevenin theorem, the initial symmetrical SCC is calculated according to equation 3.1. since it is possible to represent the system as an equivalent impedance seen from node 1 in series with a voltage source equal to the pre-fault voltage and the fault impedance, and in this case, it is considered as null. It is also considered that the system was in stability and, thus, assume the pre-defect conditions $\underline{V}^0 = 1 \text{ p.u.}$ and $I_{12}^0 = 0$.

Thus,

$$I_1'' = \frac{V_1^0}{Z_{11}'' + Z_{fault}} = \frac{1}{Z_{11}''} \quad (4.11)$$

Where $Z_{11}'' = Z_{Utility\ p.u.} // Z_{Load\ Bank\ p.u.} // (Z_{transf\ p.u.} + Z_{battery+inverter\ p.u.})$

The SCC for the system is then

$$I_1'' = \frac{1}{Z_{11}''} = \frac{1}{1.981 \times 10^{-2} + j1.466 \times 10^{-2}} = 32.621 - j24.138 \text{ p.u.} \quad (4.12)$$

In order to calculate the magnitude of the SCC, it is necessary to define a base for the circuit current

$$I_{Base\ 400V} = \frac{S_{Base}}{\sqrt{3} \cdot V_{Base}} = \frac{25 \times 10^4}{\sqrt{3} \times 400} = 360.844 \text{ A} \quad (4.13)$$

The SCC for the example described above is given by

$$I_{short-circuit} = |I_1''| \cdot I_{Base\ 400V} = 14645 \text{ A} \quad (4.14)$$

4.1.1.2. Medium Voltage Grid Connection

The analysis of this type of connection will consider only the storage system, the MV utility grid connection transformers and the load bus, load bank and utility grid, as shown in the following figure.

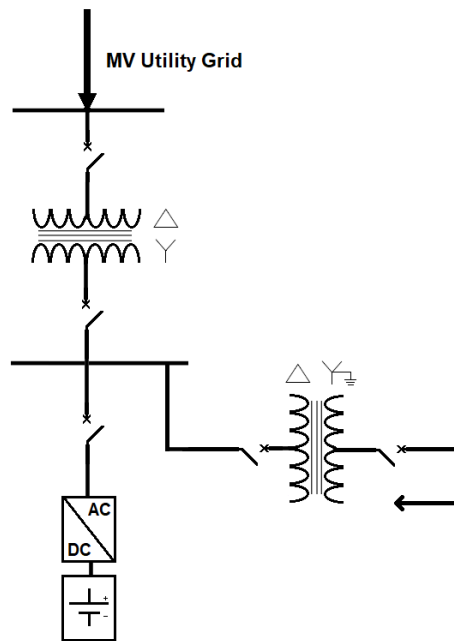


Figure 38- Medium voltage grid-connected microgrid.

Proceeding in the same way as the previous case, it is necessary to know the characteristics of the elements of the MG. For this, the following parameters were defined

Table 6- Medium voltage system parameters.

Element	Parameters			
	Voltage(V)	Apparent Power (VA)	Power factor	Rated Current (A)
Utility Grid	400	100×10^6	–	–
Load Bank	400	25×10^4	0.8	–
MV Power Transformer	15000/315	25×10^4	–	–
LV Power Transformer	400/315	25×10^4	–	–
Inverter	315	25×10^4	–	458
Battery Storage System	$736^{(DC)}$	21.8×10^4	1	$296^{(DC)}$

It is then necessary to transform all elements of the system into an equivalent linear model, considering them as impedances.

Utility Grid

The MV network is considered as a remote generator whose characteristic $X/R = 5$. Assuming the value for the base power, $S_{Base} = 25 \times 10^4 \text{ VA}$ and according to equations 3.2 and 3.4

$$S_{Utility_{p.u.}} = \frac{S_{Utility}}{S_{Base}} = \frac{100 \times 10^6}{25 \times 10^4} = 400 \text{ p.u.} \quad (4.15)$$

$$Z_{Utility_{p.u.}} = \frac{V_{Utility_{p.u.}}^2}{S_{Utility_{p.u.}}} = \frac{1}{400} = 2.5 \times 10^{-3} \text{ p.u} \quad (4.16)$$

Considering the characteristic X/R

$$Z_{Utility_{p.u.}} = \sqrt{R^2 + X^2} \quad (4.17)$$

$$Z_{Utility_{p.u.}} = 4.903 \times 10^{-4} + j2.451 \times 10^{-3} \text{ p.u}$$

Power Transformers

Considering that the transformer connected to the MV network has a leakage reactance equal to the characteristic impedance, $Z_{transf} = X_f = 4\%$, it is only necessary to adapt it to the corresponding base. The transformer is then modelled by

$$Z_{MVtransf_{p.u.}} = X_f = j0.04 \text{ p.u.} \quad (4.18)$$

Lines and Cables

For the interconnection of the elements described above, it is considered some electrical connecting cables, whose impedances are specified in the following table.

Table 7- Medium Voltage Cable impedances.

Connector	From	To	Impedance (p.u.)
Cable 1	Utility Grid	Power Transformer	$0.000013 + j0,0000014$
Cable 2	Power Transformer	Inverter	$0.0024 + j0,0019$
Cable 3	Power Transformer	Load Bank	$0.0065 + j0,0035$

Since the equivalent impedances of the other elements have been calculated in the previous case, the symmetrical SC calculation methodology presented previously can be applied. Thus, considering a fault in the point of coupling of the storage system to the distribution network, the magnitude of the SCC can be analysed using the following scheme

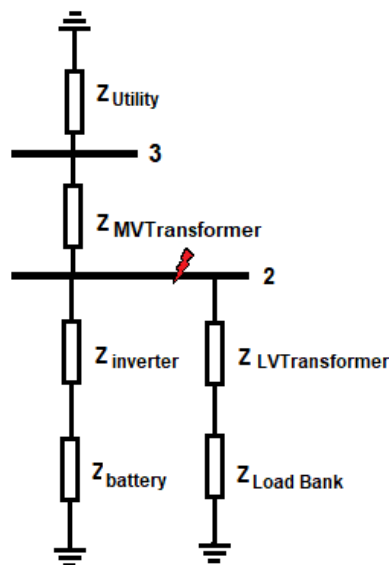


Figure 39- Symmetrical fault at bus 2.

By the application of the Thevenin theorem, the initial symmetrical SCC is calculated according to Equation 3.7 since it is possible to represent the system as an equivalent impedance seen from node 2 in series with a voltage source equal to the pre-fault voltage and the fault impedance, being that in this case, this is considered as null.

As in the previous case, it is considered that the system was in stability and, therefore, assume the pre-defect conditions $\underline{V}^0 = 1 \text{ p.u.}$ e $\underline{I}_{32}^0 = 0$. Thus

$$\underline{I}_2'' = \frac{\underline{V}_2^0}{\underline{Z}_{22}'' + \underline{Z}_{fault}} = \frac{1}{\underline{Z}_{22}''} \quad (4.19)$$

Where

$$\underline{Z}_{22}'' = (Z_{Utility\ p.u.} + Z_{MV\ transf\ p.u.}) // [(Z_{LV\ transf\ p.u.} + Z_{Load\ Bank\ p.u.}) // (Z_{battery+inverter\ p.u.})] \quad (4.20)$$

The SCC for the system in question is then

$$I_2'' = \frac{1}{\underline{Z}_{22}''} = \frac{1}{3.601 \times 10^{-3} + j3.578 \times 10^{-2}} = 2.785 - j27.670 \text{ p.u.} \quad (4.21)$$

In order to calculate the magnitude of the SCC, it is necessary to define a base for the circuit current. Since the fault occurs on the 315V bus, the base current is given by

$$I_{Base\ 315V} = \frac{S_{Base}}{\sqrt{3} \cdot V_{Base}} = \frac{25 \times 10^4}{\sqrt{3} \times 315} = 458.214 \text{ A} \quad (4.22)$$

The SCC for the example described above is given by

$$I_{short-circuit} = |I_2''| * I_{Base\ 315V} = 12743 \text{ A} \quad (4.23)$$

4.1.1.3. Islanded mode of operation

Finally, the operation of the MG in isolated mode shall be considered, taking into account only the storage system, the diesel generator, the electric vehicle charger, the load-side busbar transformer and the load bank, as shown in the following figure.

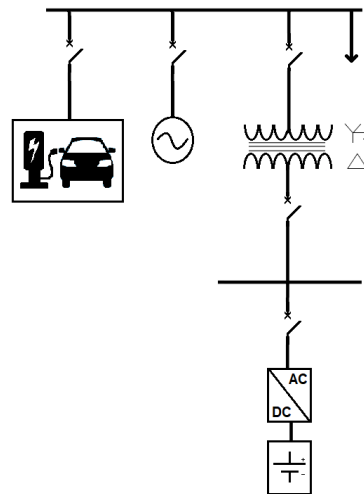


Figure 40- Islanded microgrid.

Proceeding in the same way as in the previous cases, it is necessary to know the characteristics of the elements of the MG. For this, the following parameters were defined

Table 8- Islanded microgrid system parameters

Element	Parameters			
	Voltage(V)	Apparent Power (VA)	Power factor	Rated Current (A)
Load Bank	400	25×10^4	0.8	–
Electric Vehicle Charger	400	50×10^3	0.98	73
Diesel Generator	400	30×10^4	0.8	–
LV Power transformer	400/315	25×10^4	–	–
Inverter	315	25×10^4	–	458
Battery Storage System	736 ^(DC)	21.8×10^4	1	296 ^(DC)

It is then necessary to transform all elements of the system into an equivalent linear model, considering them as impedances.

Electric Vehicle Charger

The electric vehicle charger, for fault analysis, is considered as a load. Assuming the value for the base power, $S_{Base} = 25 \times 10^4$ VA and according to equation 3.4

$$Z_{EV\ charger\ p.u.} = \frac{V_{EV\ charger}^2}{S_{EV\ charger}} = \frac{400^2}{49 \times 10^3 - j9.95 \times 10^3} = 3.136 + j0.637\ p.u. \quad (4.24)$$

Diesel Generator

Considering that the generator has a leakage reactance equal to the characteristic impedance, $Z_{Generator} = X'_f = 12\%$, it is only necessary to convert it to the corresponding base. The transformer is then modelled by

$$Z_{Generator\ p.u.} = X'_f \cdot \frac{S_{Base}}{S_{Generator}} = 0.12 \times \frac{25 \times 10^4}{30 \times 10^4} = j0.1\ p.u. \quad (4.25)$$

Having been calculated the equivalent impedances of the other elements in the previous cases, the symmetrical SC calculation methodology presented previously can be applied. Thus, considering a fault in the 400V bus, the magnitude of the SCC can be analysed using the following scheme

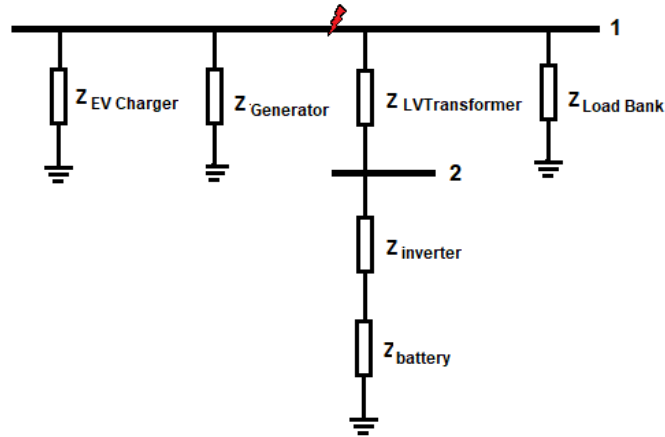


Figure 41- Symmetrical fault at bus 1.

By the application of the Thevenin theorem, the initial symmetrical SCC is calculated according to equation 3.7 since it is possible to represent the system as an equivalent impedance seen from node 2 in series with a voltage source equal to the pre-fault voltage and the fault impedance.

As in the previous cases, it is considered that the system was in stability and, therefore, assume the pre-defect conditions $\underline{V}^0 = 1 \text{ p.u.}$ and $\underline{I}_{12}^0 = 0$. Thus,

$$\underline{I}_1'' = \frac{\underline{V}_2^0}{\underline{Z}_{11}'' + \underline{Z}_{fault}} = \frac{1}{\underline{Z}_{11}''} \quad (4.26)$$

Where

$$\underline{Z}_{11}'' = \left(\underline{Z}_{battery+inverter \text{ p.u.}} + \underline{Z}_{LVtransf \text{ p.u.}} \right) // \underline{Z}_{Generator \text{ p.u.}} // \underline{Z}_{EV \text{ charger p.u.}} // \underline{Z}_{Load \text{ Bank p.u.}} \quad (4.27)$$

The SCC for the system in question is then

$$\underline{I}_1'' = \frac{1}{\underline{Z}_{11}''} = \frac{1}{1.308 \times 10^{-2} + j6.958 \times 10^{-2}} = 2.610 - j13.881 \text{ p.u.} \quad (4.28)$$

The SCC for the example described above is given by

$$I_{short-circuit} = |\underline{I}_1''| * I_{Base} = 5096 \text{ A} \quad (4.29)$$

4.1.2. Analysis of Short-Circuit Current during Unbalanced Faults

In this subsection the analysis of asymmetrical SCs based on the methodology described in subsection 3.3.3 will be presented and applied to the same MG. Different operation modes will also be exposed by connecting the system to the MV distribution network, connecting the system to the LV distribution network and operating in isolated mode.

4.1.2.1. Microgrid connected to the Low Voltage Grid

The study of asymmetrical short-circuits requires a more detailed study of the system since it is necessary to take into account the symmetrical components of the system. In this way, each system will be represented into its positive, negative and zero-sequences. Due to the small size of the MG under analysis, for the construction of the matrix of the nodal impedances, the matrix of the admittances will be used instead of the algorithm of direct construction due to its complexity.

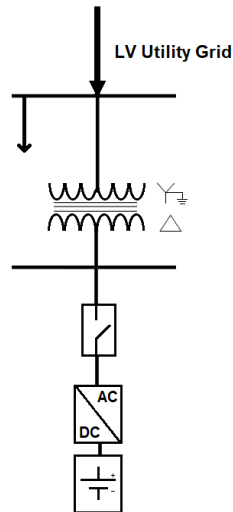


Figure 42-Low voltage microgrid.

Considering the diagram of the previous figure, it can be decomposed into its positive, negative and zero-sequence components, with the first two having the same configuration. The scheme in the zero-sequence component is influenced by the configuration of the transformer windings.

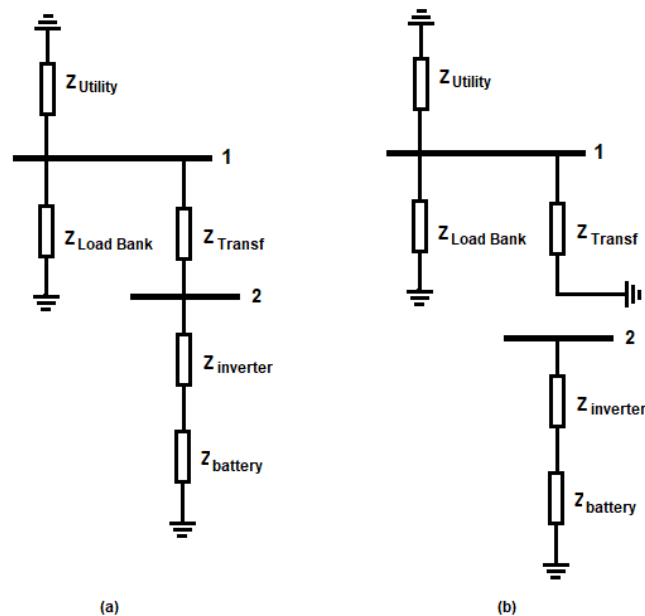


Figure 21- (a) Positive and negative-sequence systems; (b) Zero-sequence system.

Defining the schemas in their symmetrical components, it is possible to obtain the matrix of the admittances and consequently the matrix of the nodal impedances. For the positive and negative-sequence systems

Table 9- Equivalent impedances.

Branch $i - k$	$Z_{i-k p.u.}$	$y_{i-k p.u.}$
1 - 2	$j0.042$	$-j23.809$
Node k	$Z_{kk p.u.}$	$y_{kk p.u.}$
1	2.143×10^{-2} $+ j1.482 \times 10^{-2}$	$31.564 - j21.835$
2	$0.114 - j0.266$	$1.363 - j3.171$

From the equivalent impedances of the nodes and the connecting branches, can be obtained the matrix of the admittances

$$[Y]^{+,-} = \begin{bmatrix} 31.563 - 45.099 & j23.809 \\ j23.809 & 1.363 - j26.981 \end{bmatrix} \quad (4.30)$$

Where

$$Y_{ik} = -y_{i-k} \quad (i \neq k) \quad (4.31)$$

$$Y_{kk} = y_{kk} + \sum_{i \neq k} y_{i-k} \quad (i = k) \quad (4.32)$$

Being that

$$[Z] = [Y]^{-1} \quad (4.33)$$

$$[Z]^{+,-} = \begin{bmatrix} 1.981 \times 10^{-2} + j1.466 \times 10^{-2} & 1.808 \times 10^{-2} + j1.202 \times 10^{-2} \\ 1.808 \times 10^{-2} + j1.202 \times 10^{-2} & 1.832 \times 10^{-2} + j4.695 \times 10^{-2} \end{bmatrix} \quad (4.34)$$

For zero-sequence system

Table 10- Equivalent impedances.

Node k	$Z_{kk p.u.}$	$y_{kk p.u.}$
1	$1.025 \times 10^{-2} + j1.482 \times 10^{-2}$	$31.567 - j45.639$
2	$0.114 - j0.266$	$1.363 - j3.171$

From the previous table, the matrix of the admittances is

$$[Y]^0 = \begin{bmatrix} 31.567 - j45.639 & 0 \\ 0 & 1.363 - j3.171 \end{bmatrix} \quad (4.35)$$

Consequently

$$[Z] = [Y]^{-1} \quad (4.36)$$

$$[Z]^0 = \begin{bmatrix} 1.025 \times 10^{-2} + j1.482 \times 10^{-2} & 0 \\ 0 & 0.114 - j0.266 \end{bmatrix} \quad (4.37)$$

After obtaining all the values of the equivalent impedances referring to the symmetrical components of the system, it is possible to calculate the SCC for different types of faults.

Line-to-ground short-circuit

For the MG under analysis, it is considered a SC in bus 1, being possible to calculate the SCC by applying the Equation.3.47

$$I_1'' = \frac{3 \cdot V^f}{Z_{kk(1)} + Z_{kk(2)} + Z_{kk(0)} + 3 \cdot Z_{sc}} \quad (4.38)$$

Substituting the unknown variables for the values obtained previously

$$I_1'' = \frac{3}{2 \times (1.981 \times 10^{-2} + j1.466 \times 10^{-2}) + (1.025 \times 10^{-2} + j1.482 \times 10^{-2})} = 33.731 - j29.856 \text{ p.u.} \quad (4.39)$$

In order to calculate the magnitude of the SCC, it is necessary to take into account the base current of the bus. In this way, the SCC for the example described above is given by

$$I_{short-circuit} = |I_1''| * I_{Base400V} = 16255 \text{ A} \quad (4.40)$$

Line-to-line short-circuit

By applying equation 3.54 and considering a contact between phases b and c, the SCC can be calculated

$$I_1'' = \frac{-j\sqrt{3}V^f}{Z_{kk(1)} + Z_{kk(2)} + Z_{sc}} \quad (4.41)$$

Using the corresponding equivalent impedance values

$$I_1'' = \frac{-j\sqrt{3}}{2 \times (1.981 \times 10^{-2} + j1.466 \times 10^{-2})} = -20.904 - j28.247 \text{ pu} \quad (4.42)$$

The magnitude of the SCC is then calculated by

$$I_{short-circuit} = |I_1''| * I_{Base400V} = 12680 \text{ A} \quad (4.43)$$

Line-to-line short-circuit with ground connection

The last case to be studied will be the line-to-line SC between phases b and c, with ground contact. The value of the SCC is obtained through equations 3.61 and 3.62

$$I_{(0)} = -\frac{Z_{kk(2)}}{Z_{kk(2)} + Z_{kk(0)} + 3 \cdot Z_{sc}} \cdot I_{(1)} \quad (4.44)$$

(=)

$$I_{(0)} = - \frac{Z_{kk(2)} \cdot \underline{V}^f}{Z_{kk(1)} \cdot Z_{kk(2)} + Z_{kk(1)} \cdot (Z_{kk(0)} + 3 \cdot Z_{sc}) + Z_{kk(2)} \cdot (Z_{kk(0)} + 3 \cdot Z_{sc})}$$

$$(\Rightarrow)$$

$$I_{(0)} = 11.237 - j12.349 \text{ p.u.}$$

From the above equations, it is then possible to calculate the SCC

$$I_1'' = I_{(1)} + I_{(2)} (\Rightarrow) I_1'' = 3 \cdot I_{(0)} \quad (4.45)$$

$$(\Rightarrow)$$

$$I_1'' = 3 \times (11.237 - j12.349) = 33.709 - j34.046 \text{ p.u.}$$

The magnitude of the SCC is then given by

$$I_{short-circuit} = |I_1''| * I_{Base400V} = 18073 \text{ A} \quad (4.46)$$

Typically, the SCC is more severe for symmetrical faults. However, for the analysed case, it is verified that the earth faults present higher values of SCCs. This is due to the contribution of the zero-sequence component of the circuit impedance.

4.1.2.2. Microgrid connected to the Medium Voltage Grid

Applying the same principle to the study of MV grid-connected MG, it was decomposed into its symmetrical components.

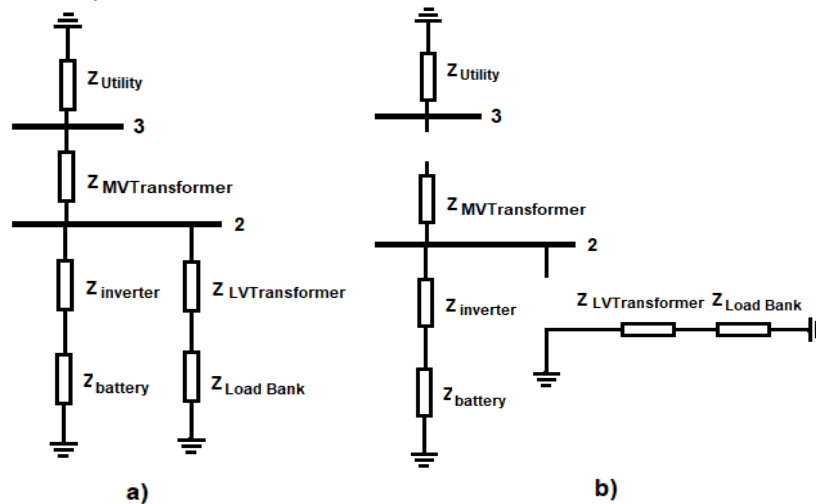


Figure 22- (a) Positive and negative-sequence systems; (b) Zero-sequence system.

To use the same methodology, it is necessary to construct the equivalent matrices of the system for the positive, negative and zero-sequence components.

Table 11- Positive and negative-sequence equivalent impedances.

Branch $i - k$	$Z_{i-k p.u.}$	$Y_{i-k p.u.}$
2 - 3	$j0.04$	$-j25$
Node k	$Z_{kk p.u.}$	$Y_{kk p.u.}$
2	$0.108 + j0.266$	$2.506 - j4.118$
3	$5.036 \times 10^{-4} + j2.451 \times 10^{-3}$	$80.321 - j391.216$

Table 12- Zero-sequence equivalent impedances.

Node k	$Z_{kk p.u.}$	$Y_{kk p.u.}$
2	$0.114 + j0.226$	$1.362 - j3.171$
3	$5.036 \times 10^{-4} + j2.451 \times 10^{-3}$	$80.321 - j391.216$

Since

$$[Z] = [Y]^{-1} \quad (4.47)$$

$$[Z]^{+,-} = \begin{bmatrix} 3.601 \times 10^{-4} + j3.578 \times 10^{-2} & 6.084 \times 10^{-4} + j2.032 \times 10^{-3} \\ 6.084 \times 10^{-4} + j2.032 \times 10^{-3} & 5.049 \times 10^{-4} + j2.427 \times 10^{-3} \end{bmatrix} \quad (4.48)$$

$$[Z]^0 = \begin{bmatrix} 0.114 + j0.226 & 0 \\ 0 & 5.036 \times 10^{-4} + j2.451 \times 10^{-3} \end{bmatrix} \quad (4.49)$$

As for the symmetrical SC analysis, a fault was considered in bus 2. In order to avoid repetition of information, since the calculation method is homologous to that presented in the previous case, the results of the calculation of the different types of fault were condensed in the table below

Table 13- Current magnitude

Type of fault	$I_{short-circuit} (A)$
Line-to-ground	4279
Line-to-line	11036
Line-to-line with ground connection	2546

The results obtained in the previous table show the impact of the zero-sequence component of the system on the SCC and the relevance of the transformer winding configuration.

4.1.2.3. Islanded mode of operation

The last case for analytical study of asymmetrical SCs will be the operation of the MG in isolated mode. In the same way as the previous cases were analysed, the system will be decomposed into its symmetrical components.

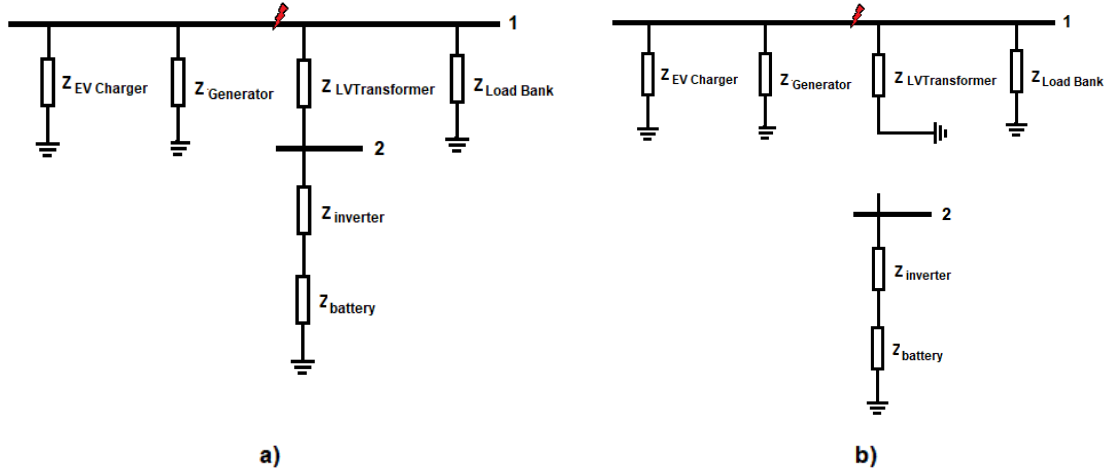


Figure 23- (a) Positive and negative-sequence systems; (b) Zero-sequence system.

From the schemes presented above, the equivalent matrices of the systems are

Table 14- Positive and negative-sequence equivalent impedances.

Branch $i - k$	$Z_{i-k p.u.}$	$Y_{i-k p.u.}$
1 - 2	$j0.042$	$-j23.809$
Node k	$Z_{kk p.u.}$	$Y_{kk p.u.}$
1	$1.261 \times 10^{-2} + j8.913 \times 10^{-2}$	$1.556 - j10.999$
2	$0.114 + j0.264$	$1.362 - j3.210$

Table 15- Zero-sequence equivalent impedances.

Node k	$Z_{kk p.u.}$	$Y_{kk p.u.}$
1	$1.282 \times 10^{-3} + j2.867 \times 10^{-2}$	$1.556 - j34.809$
2	$0.114 + j0.264$	$1.362 - j3.210$

Since

$$[Z] = [Y]^{-1} \quad (4.50)$$

$$[Z]^{+,-} = \begin{bmatrix} 1.308 \times 10^{-2} + j6.958 \times 10^{-2} & 1.458 \times 10^{-2} + j6.058 \times 10^{-2} \\ 1.458 \times 10^{-2} + j6.058 \times 10^{-2} & 1.736 \times 10^{-2} + j8.952 \times 10^{-2} \end{bmatrix} \quad (4.51)$$

$$[Z]^0 = \begin{bmatrix} 1.282 \times 10^{-3} + j2.867 \times 10^{-2} & 0 \\ 0 & 0.112 + j0.264 \end{bmatrix} \quad (4.52)$$

The results of the SCC calculation for different types of fault were condensed in the table below

Table 16- Current magnitude

Type of fault	$I_{short-circuit}$ (A)
Line-to-ground	6365
Line-to-line	4414
Line-to-line with ground connection	6473

Analysing the previous values, the relevance of the zero-sequence component of the MG for SC analysis is evident, since the attenuation of the fault current and the type of connection of the neutral conductor of the transformer can compromise the operation of the protection systems in the sense that it influences the value of the SC current due to its contribution to the zero-sequence impedance.

4.2. MATLAB/Simulink Simulation Platform

The study of electrical power systems most often requires more intuitive interfaces for analysis of power distribution networks. Typically, computational tools are used to allow replicating real systems with accuracy and to obtain precise results. In this sense, the designed solution would be a simple interface application that would enable to calculate the SC currents at all points of a MG.

Therefore, it was necessary that the program used for this purpose offered the functionality of creating a high-quality intuitive interface and at the same time allowed to use its mathematical tools for the resolution of the SC currents. The solution found was *MATLAB*, which, with the Simulink Guide User Interface, allows the construction of intuitive interfaces and excellent operability, and at the same time it is a program that allows the development of algorithms to obtain reliable results after analysis of the SC currents. The interface construction has a great degree of freedom that allows the programmer to create exactly what he wants and develop options for help and assistance to the user. Its application also allows the insertion of any renewable based network, for any network topology.

In order to carry out an analysis in the time domain, as well as to enable the performance of suitable tests for the operation of an electric power conversion system, a *MATLAB/Simulink* model was developed with similar characteristics to the previously presented MG. The implemented network was modelled in depth up to the level of the substations, representing all the Distributed Energy Resources (DER), existing connections between power plants and substations, energy transport network and transformers related to power distribution.

4.3. Chapter Summary

Through the linearization of electrical energy systems, it is possible to apply the classical SC study. This has increased relevance given the need to properly protect electrical equipment during fault scenarios. The presented SC model allows to gauge the magnitude of SC currents for a Converter-Based Distributed Generation (CBDG) MG in different operating scenarios.

- Section 4.1. presents the methodology used to calculate SC currents and consequently the results obtained during the connection of the MG to the LV and MV distribution networks and during the isolated mode.
- Section 4.2. of this chapter introduces the tool for dynamic MG modelling and its relevance in SC studies.

Chapter 5

The Democrat Case Study

This chapter aims to present a dynamic analysis of a Microgrid (MG) in the three operation scenarios described previously, based on a simulator. The results of the previous chapter will be confirmed, and the accuracy of the created models will be verified.

Given that most of the Low Voltage (LV) networks during their design have not been dimensioned or structured to integrate Distributed Energy Resources (DER) on a large scale, the challenges to its operation are becoming more and more crucial. There is, therefore, the need to coordinate new sources of consumption and sources of renewable generation, which will not only prevent increases in consumption peaks, which lead to investment needs in the reinforcement of electrical infrastructures, as well as allow these loads to be fed from renewable energy.

The DEMOCRAT project aims at demonstrating an integrated and innovative MG concept, applied to LV networks, as a suitable solution for efficiently managing their DER, working simultaneously as a flexible asset of the distribution networks [76]. Considering that this management is performed close to the majority of the end users, its effects are spread to the voltage levels above, improving substantially the overall system's operation leveraging the transition of the electrical power systems to the Smart Grid (SG) paradigm, enabling, among others, the increasing of the networks capacity to host new DER, to increase the penetration levels of renewable energy in the energy mix and the improvement of the quality of service and energy.

The integrated MG concept proposed by DEMOCRAT is based on the use of a set of innovative functionalities applicable to LV networks, of public or private nature, which have assets that can be controlled in a way that optimizes, either from a technical or economic point of view, the use of electric energy.

This project is the result of an integration process of a set of individual solutions and technologies, allowing the development of an innovative MG solution for wide-scale application for electrical power systems. The scalability of DEMOCRAT results from the fact that it is not only a solution for LV networks operated by regulated entities, namely Distribution System Operators (DSOs) but also for customers, such as industrial hubs [11].

In this chapter the computational application used for fault analysis in the MG context will be presented. There will be exposed the objectives to achieve by the application and the results obtained in three different operation scenarios: Medium Voltage (MV) grid connection, LV grid connection and islanded mode of operation. Initially, the models created in the simulator will be validated and, later, fault scenarios will be analysed.

5.1. Microgrid Data and Model Assumptions

The MG comprises several technological solutions, such a lithium-ion based Battery Energy Storage System (BESS), connected to the grid by a power inverter, controllable loads, electric vehicle charging stations and a synchronous generator. This project has as main objectives the operation in isolated mode, feeding a set of real installation loads, fulfilling the limits associated to the parameters of quality of energy, namely frequency and voltage nominal values; the activation of the storage system in island mode in the black-start scenario.

The DEMOCRAT project intends to create the conditions for MGs to be seen as an asset capable of locally managing disruptions while at the same time providing great flexibility in the overall management of the system. It has communication infrastructures that aim to provide the networks of means that allow to coordinate the diverse and heterogeneous assets in order to guarantee high standards of safety and efficiency.

The MATLAB/Simulink modelling involves the connection of Democrat project to MV and LV distribution networks and its isolated operation, although they operate in distinct scenarios, since they work independently from each other. These models require real technical data of the system components.

The MG, based on a real system, consists of a BESS of 218 kW/218kWh, a 250 kVA inverter, a load bank of 250 kVA, a LV/LV power transformer for LV distribution coupling and galvanic isolation a LV/MV power transformer for MV distribution connection, a 50 kVA electric vehicle charger, a 300 kVA diesel generator and their respective protection devices. Both MG's upstream networks were represented as voltage sources, connected to each of the distribution-side substations. The described elements were modelled, taking into account the existing Simulink blocks, initially validating the normal operation of the MG and, later, simulating the symmetrical and asymmetrical faults, observing the behaviour of the same MG. It is intended to verify the contribution of the various elements to the Short-Circuit (SC) current and, if in the critical case of isolated mode of operation, it can be fed in such a way to exceed the upper current threshold imposed by the protection system. After the fault, it is required that the system compensates the disturbances and maintains system's stability.

5.2. Microgrid Description

The constituent elements of this project and the main characteristics of its modelling are described in this section.

Battery Energy Storage System

DEMOCRAT comprises a high voltage battery storage system based on lithium-ion phosphate battery, used to support reliable power for various types of equipment and systems. The system is composed of multiple batteries connected in series to expand capacity for longer power support.

Table 17- BESS parameters

Parameter	
Cell Technology	LI-ion
Battery System Capacity (kWh)	218
Battery System Voltage (V_{DC})	736
Battery System Capacity (Ah)	296
Battery Module Quantity (pcs)	46
Battery System Charge/Discharge Current (Normal) (A)	148
Battery System Charge/Discharge Current (Maximum) (A)	296
Efficiency (%)	96

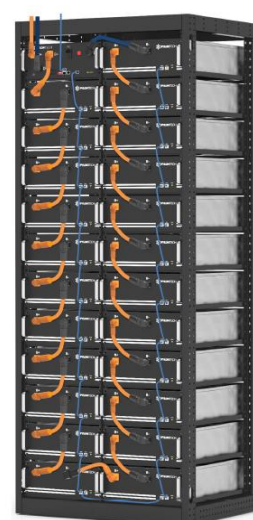


Figure 24- Battery Rack.

Power Inverter

As far as power electronics are concerned, bidirectional inverters are required for on-grid applications in various power segments and, more recently, the operation of the MG forces its operation in off-grid mode.

In the on-grid mode, the main function of the inverter is to control the power associated with the battery in its charge and discharge mode, by means of a reference value defined by the system management controller, and to provide a set of services related to the network support, or optimization of its exploitation.

During off-grid mode, the inverter will be responsible for generating and maintaining a stable voltage and frequency references according to the nominal parameters associated with the quality of service. This operation in island mode is more demanding due to the low inertia of the system forcing a bigger effort from the converter-based dispersed generation to ensure network stability, where its control will have a significant impact on microgrid's performance.

Table 18- Inverter Parameters.

Input	
Minimum Voltage (V)	480
Maximum Voltage (V)	880
Maximum Current (A)	542
Output	
Rated Power (kVA)	250
Rated Voltage (V)	315
Rated Current (A)	458
Efficiency (%)	98.4



Figure 25- Power Inverter

Load Bank

Residential and industrial hubs are represented as a three-phase controllable load bank consisting in two major components: a resistive load and a reactive load. Resistive load is provided by groups of tubular resistor elements switched in groups by contactors while the reactive load is provided by inductances of various values to match each resistive element group.

Table 19- Load Bank Parameters.

Parameter	
Rated Power (kVA)	250
Power Factor	0.8
Rated Voltage (V)	400
Frequency (Hz)	50

Distribution Transformers

Concerning power conversion, the MG includes two three-phase transformers: a step-up transformer for interconnection to the MV network and a decoupling transformer to connect to the LV distribution network. The interconnection to the LV or MV networks is mutually exclusive, depending on the use case in demonstration. The installation also includes MV equipment with protection by circuit breaker and measurement sensors, as well as LV equipment, with similar functions.

Table 20- Transformer Parameters.

MV/LV Transformer	
Rated Power (kVA)	250
Primary Voltage (V)	15000
Secondary Voltage (V)	315
Vector Group	Dy11
Short-Circuit Voltage (%)	4
LV/LV Transformer	
Rated Power (kVA)	250
Primary Voltage (V)	315
Secondary Voltage (V)	400
Vector Group	Dyn11
Short-Circuit Voltage (%)	4.2



Figure 26- Power Transformer

Electric Vehicle Charger

The paradigm shift towards greener and more sustainable solutions has affected the mobility sector. In this way, the DEMOCRAT project comprises a management model for electric charging, incorporating charging stations for electric vehicles.

Table 21- EV Charger Parameters.

AC Nominal Input for the DC Output	
Rated Power (kVA)	50
Power Factor	0.98
Rated Voltage (V_{AC})	400
Rated Voltage (V_{DC})	50 to 500
Rated Current (A_{AC})	73
Rated Voltage (A_{DC})	0 to 120
Frequency (Hz)	50



Figure 27- Electric Vehicle Charger

Diesel Generator

A generator model is presented, aiming at power sharing with the BESS during emergency scenarios, as well as reducing costs associated with the loss of battery life. This model coordinates the BESS with a diesel generator, while ensuring the stability of the MG.

Table 22- Generator Parameters.

AC Nominal Input for the DC Output	
Rated Power (kVA)	300
Power Factor	0.8
Rated Voltage (V)	400
Rated Current (A)	432
Frequency (Hz)	50



Figure 28- Diesel Generator

Protection Devices

In the event of a fault, it is crucial that protective devices act safely by creating an electrical insulation from the power system, and efficiently, cancelling the fault as soon as possible to minimize damage to electrical equipment and prevention of injuries, whilst leaving as much of the network as possible still in operation. The MG that the Democrat intends to demonstrate has protection systems based on circuit-breakers.

Table 23- Circuit-Breaker Parameters.

Parameters		
Rated short-circuit breaking capacity (kA)	50	150
Rated Current (A)	630	630
Overload Trip (A)	315-630	315-630
Rated Voltage (V)	400-415	400-415
Frequency (Hz)	50	



Figure 29- Circuit Breaker

5.3. Microgrid Fault Analysis

To further illustrate the behaviour of the proposed MG under specific scenarios, the previously presented elements were modelled according to their previously mentioned parameters in the MATLAB/Simulink simulation platform, and the behaviour of the MG was studied in three different case studies: LV grid connection, MV grid connection and islanded mode.

5.3.1. Case 1: Microgrid Connected to the Low Voltage Grid

The first scenario refers to the LV grid connection where the integration of the storage system connected by an inverter to feed a three-phase load was analysed, and later the analysis of a fault, as shown in the following figure.

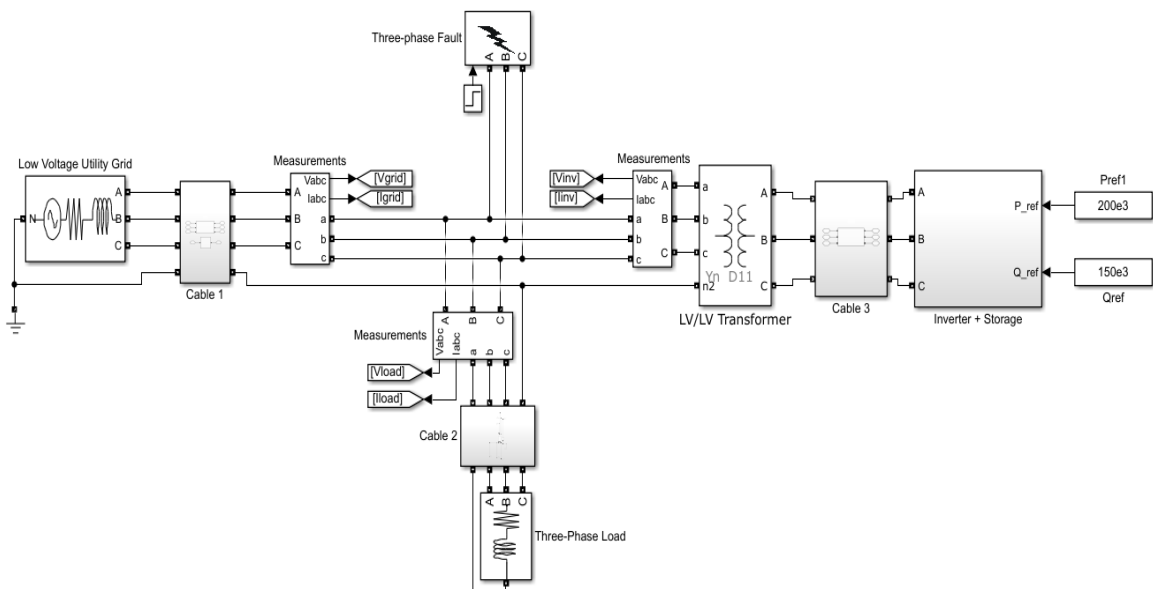


Figure 30-Simulink Model of a Low Voltage Microgrid.

It was studied the behaviour of the integration of the battery system in the network and evaluated the distribution of power supplied to the load. The inverter is activated at 0.3 seconds, and from this moment on, it is verified the attenuation of the current on the distribution network side and the respective increase of the current injection by the inverter in order to feed the load in a shared way. This establishes a balance between the contribution of the distribution network and the energy storage system, although the voltage has increased slightly. The results of this transition are presented in the following figures

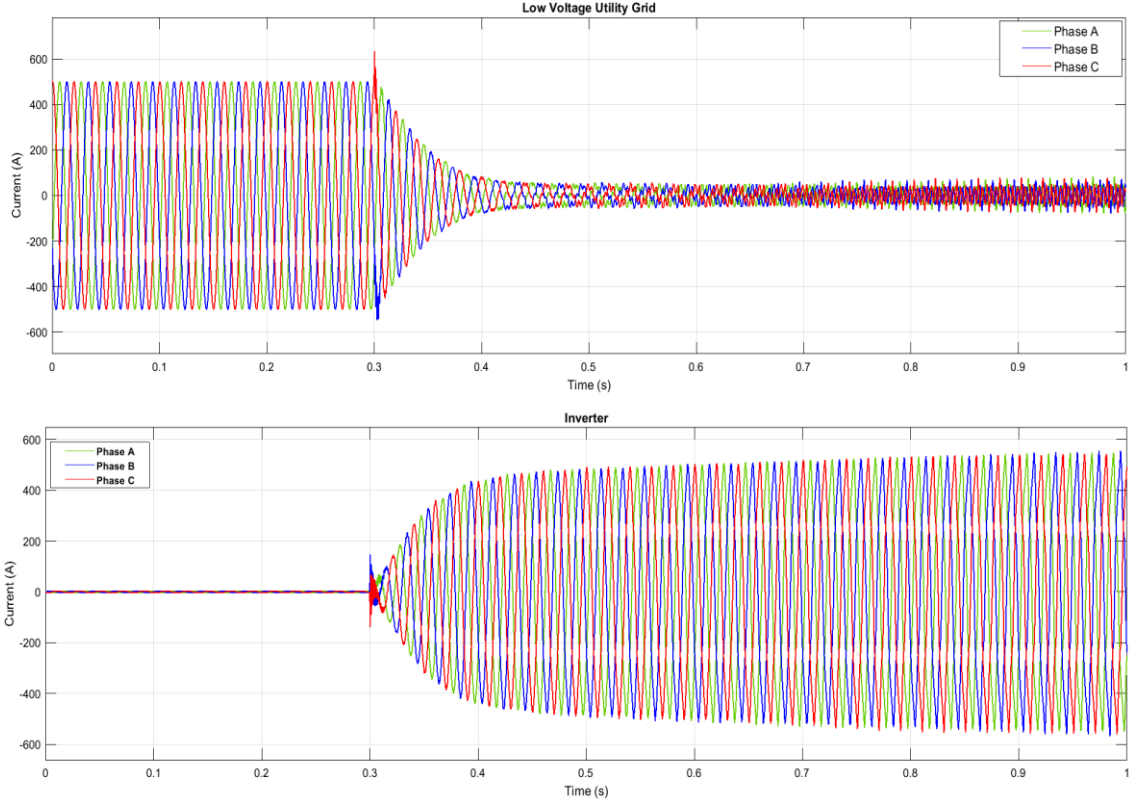


Figure 54-Current waveforms in the LV utility grid and in the inverter, respectively.

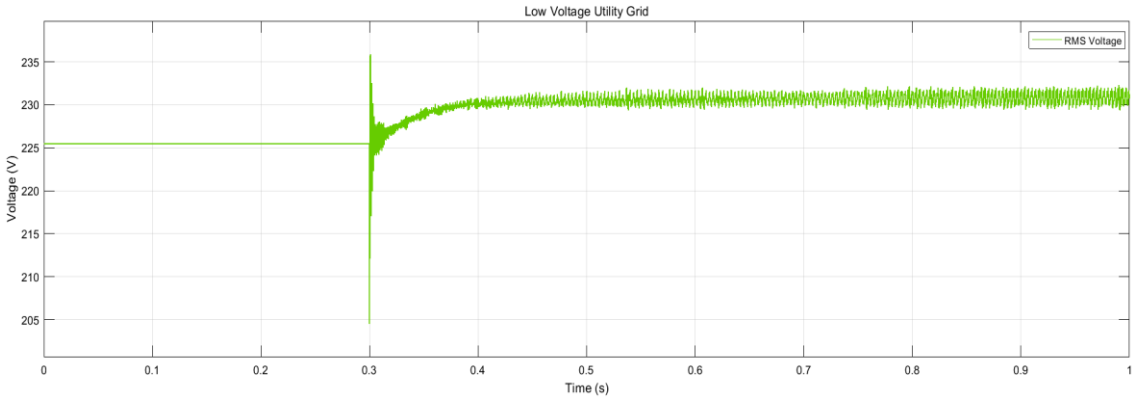


Figure 55- Utility grid RMS voltage waveform.

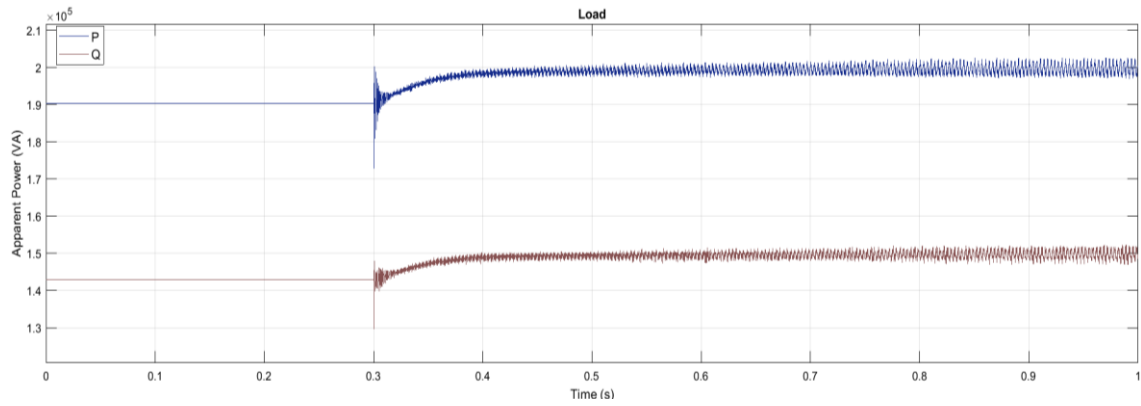


Figure 56- Active and reactive power waveforms.

After the analysis of this integration, the behaviour of the MG during different types of SC is studied for a SC occurred in the 400V network section.

5.3.1.1. Three-Phase Short-Circuit

The first type of SC analysed has been symmetrical three-phase. The results obtained will be presented in the following figures

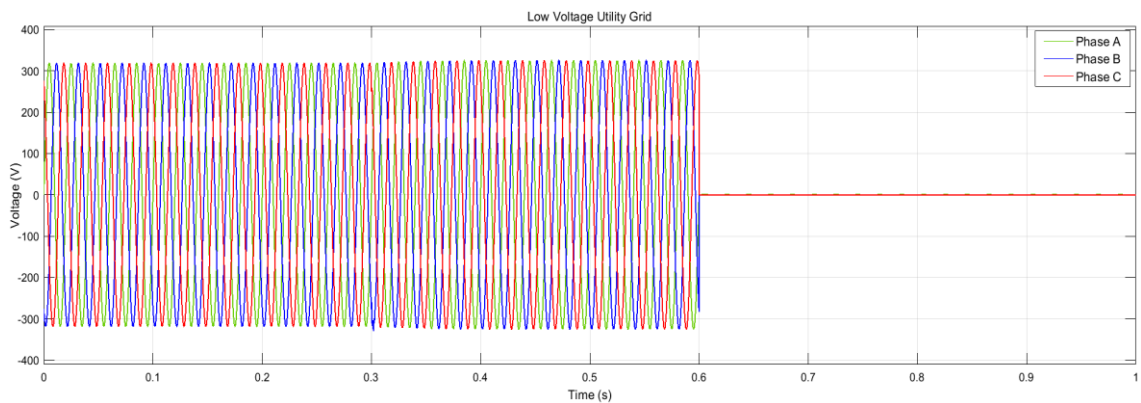


Figure 57-Utility grid voltage waveforms for symmetrical short-circuit- Case1.

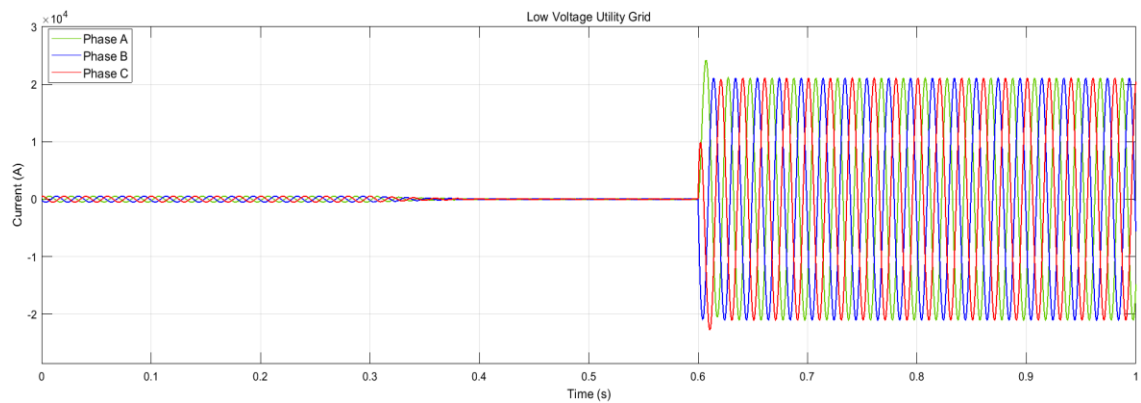


Figure 58-Utility grid current waveforms for symmetrical short-circuit - Case1.

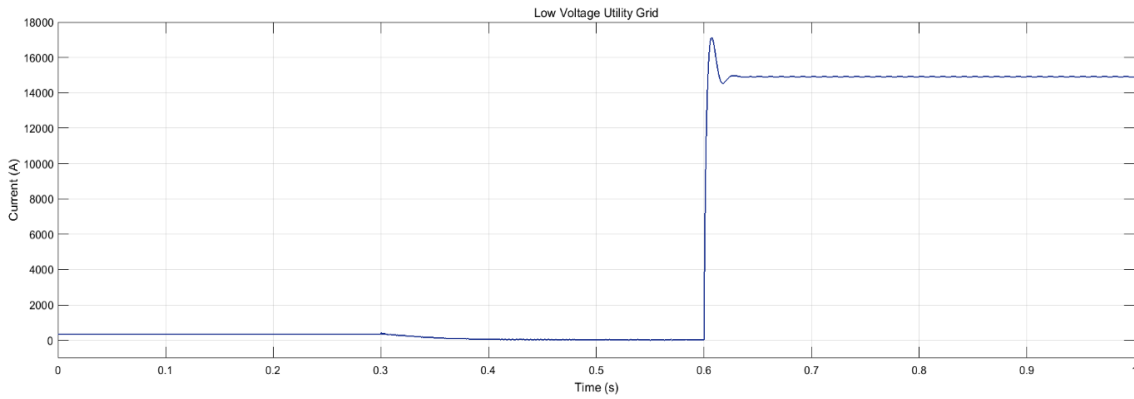


Figure 59- RMS Values of the Short-Circuit Current for symmetrical short-circuit - Case1.

Figures 57, 58 and 59 shown above represent the fault behaviour for symmetrical three-phase SC. In figure 57 it is possible to observe a sinusoidal behaviour of the voltage waveforms in the three distinct phases. In this behaviour is identified a slight increase at 0.3 seconds resulting from the activation of the storage system, and, as expected, when the SC occurs at 0.6 seconds, the voltages become null.

In figure 58 are represented the fault currents in the respective three phases already mentioned. The transient behaviour is visible immediately after the SC and, posteriorly, the current stabilises when it reaches the steady state.

In figure 59 the same behaviour of figure 58 is observed, and the magnitude of the SC current during the steady state is then represented, having a value of 14910 A.

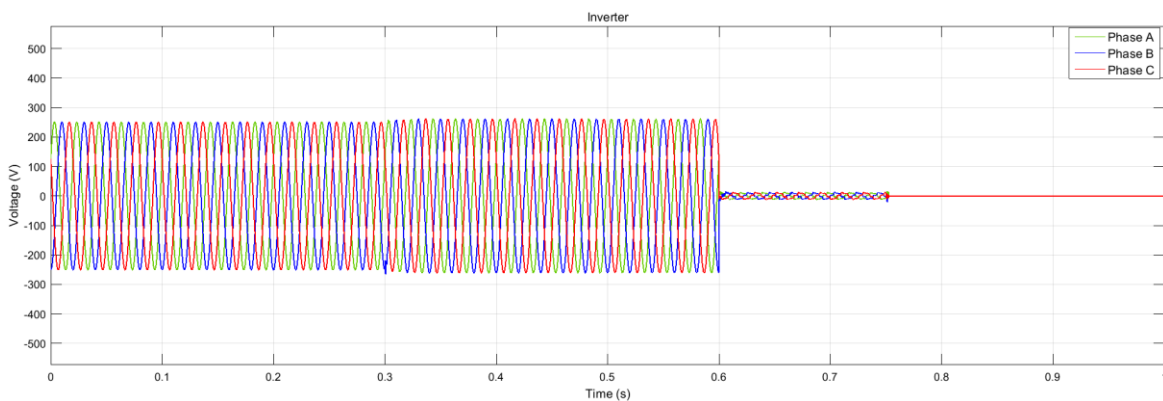


Figure 60- Inverter voltage waveforms for symmetrical short-circuit - Case1.

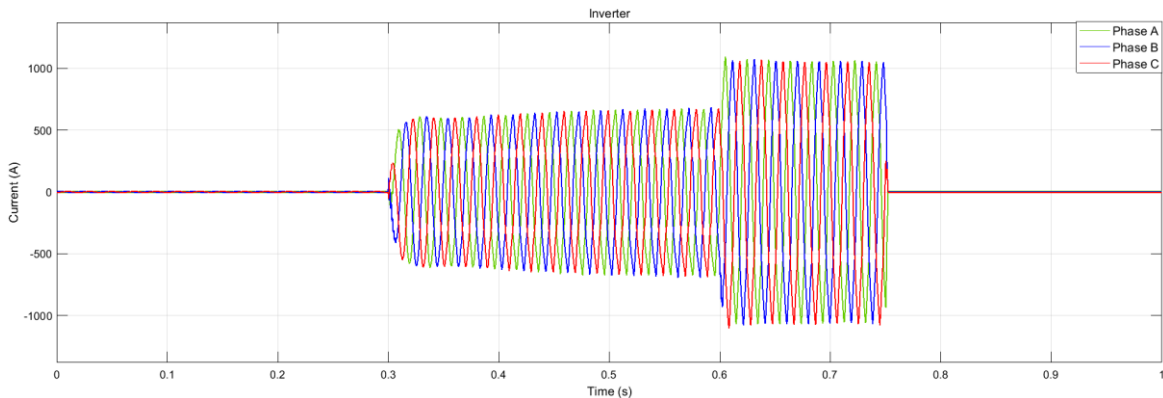


Figure 61- Inverter Current Waveforms for symmetrical short-circuit - Case1.

Figure 60 and figure 61 represent the voltage and current of the inverter in the fault scenario. In the first one (figure 60), there is a voltage drop at 0.6 seconds, precisely when the SC occurs. From there and up to about 0.75 seconds, the voltage maintains the residual value. After this situation, the inverter is out of service because the control of the inverter is not designed to withstand such large voltage unbalances in the three phases. In the second (figure 61), the current injection by the storage system at the moments subsequent to the fault is observed, which is about twice the nominal current of the inverter.

From the last figure, it is concluded that the load is initially fed by the network, and then by the inverter until the moment of the fault. Due to the magnitude of the SC current and the voltage drop, the load is disconnected after the fault.

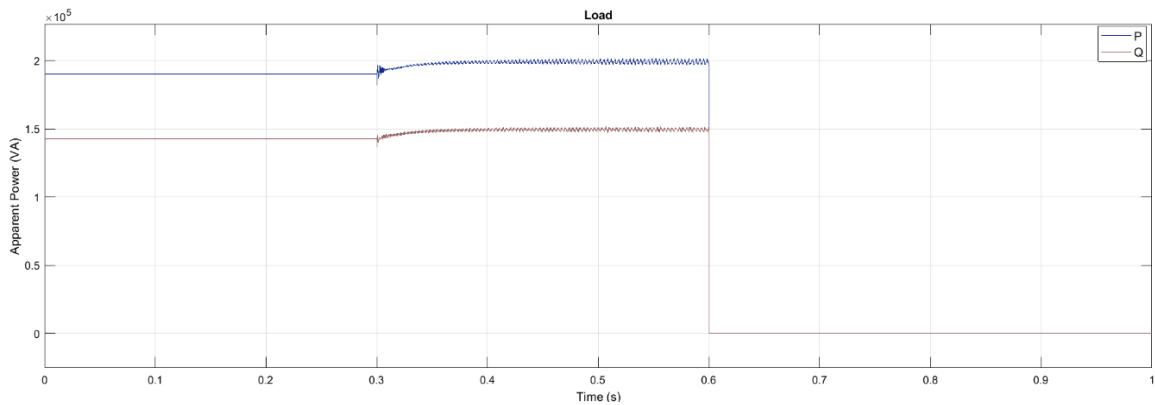


Figure 62- Active and reactive power waveforms for symmetrical short-circuit - Case1.

5.3.1.2. Line-to-Line Short-Circuit

It was also analysed the behaviour of the MG for the occurrence of a phase-to-phase SC and, as expected, a decrease of voltage magnitude was observed in the phases where the fault occurred (Phase A and Phase B). Also, the voltage in the sane phase, visible in Figure 63, keeps its nominal value. In relation to the currents in the bolted lines, there is a symmetrical behaviour of its waveforms whose effective value is 12850 A.

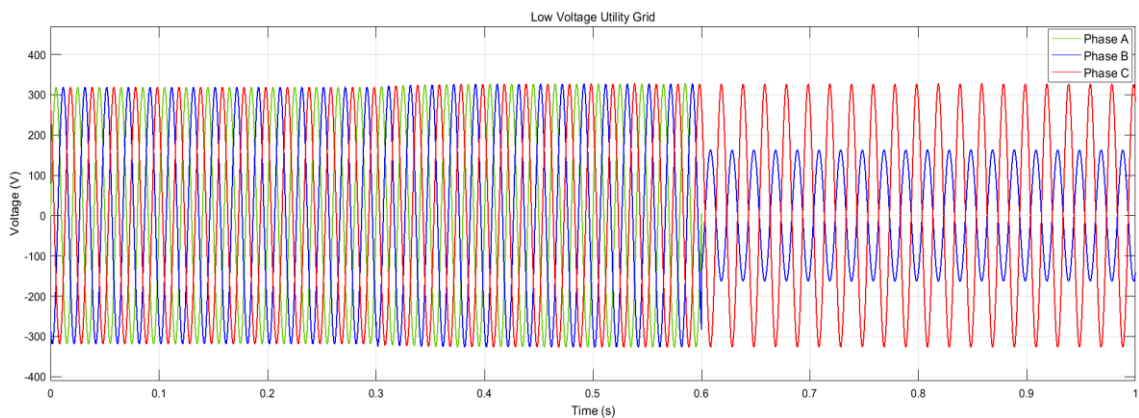


Figure 63- Utility grid voltage waveforms for line-to-line short-circuit - Case1.

80 The Democrat Case Study

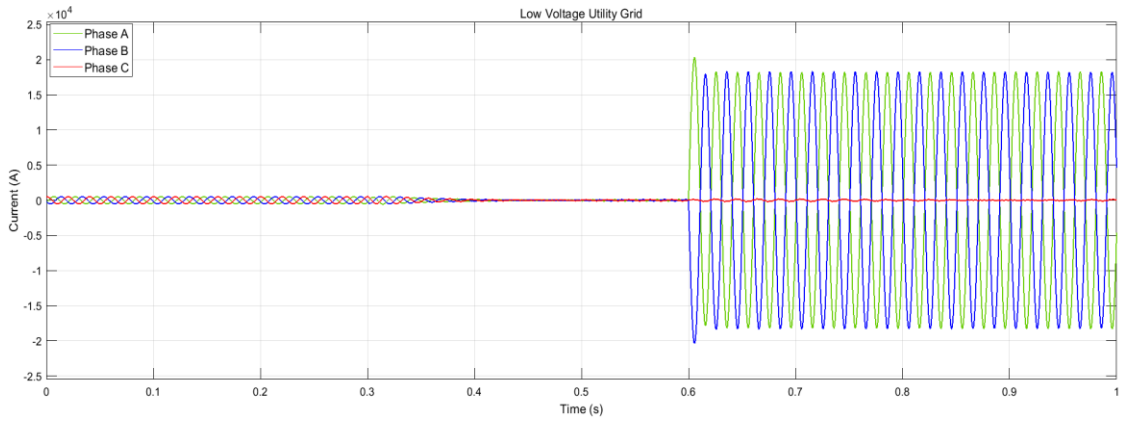


Figure 64- Utility grid current waveforms for line-to-line short-circuit - Case1.

The behaviour of the inverter for this type of SC was different from the three-phase SC, which was maintained in service after the fault by injecting its nominal current in the healthy phase and practically twice that current in the faulted phases, as a consequence of the voltage decrease in inverter phases A and B. For this SC scenario, the inverter keeps in operation, because its control allows an imbalance of phase-to-phase voltages of about 80%.

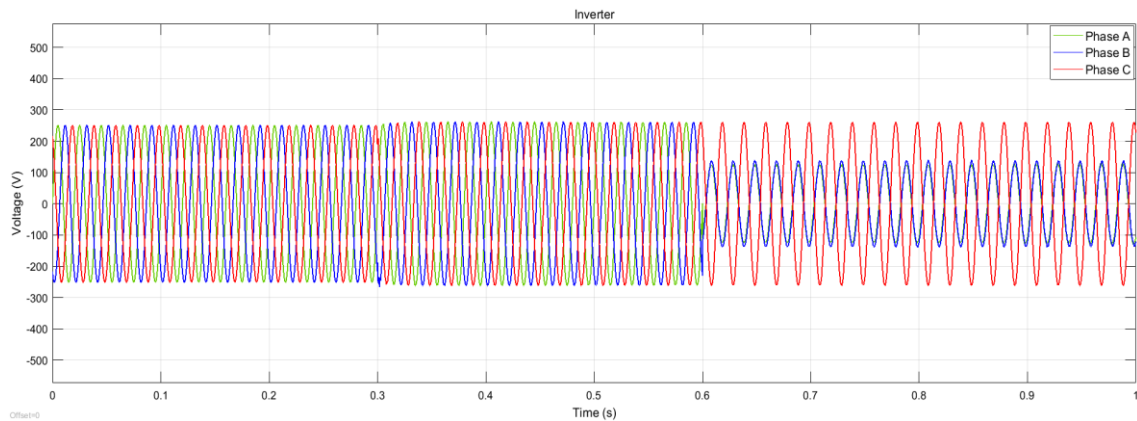


Figure 65- Inverter voltage waveforms for line-to-line short-circuit - Case1.

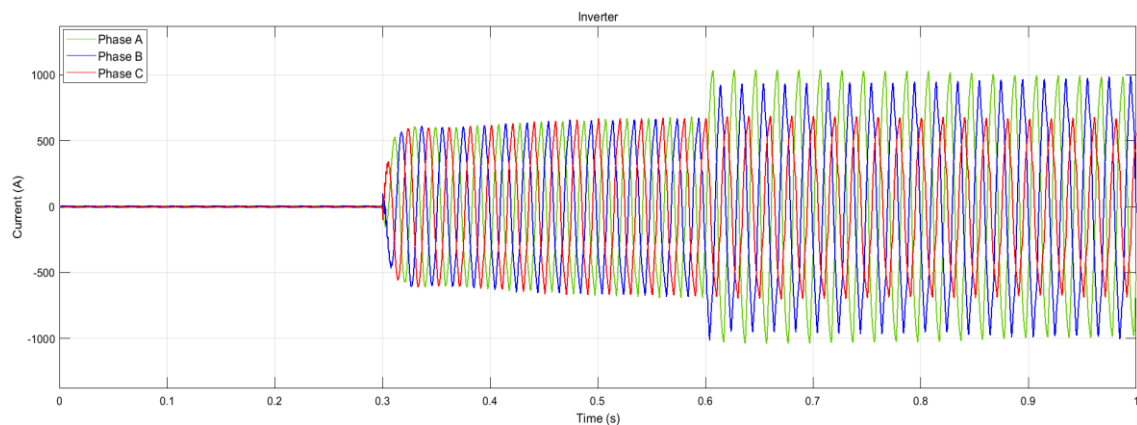


Figure 66- Inverter current waveforms for line-to-line short-circuit - Case1.

The following figure represents the supply of the load before and during the fault, it being verified that after 0.6 seconds, the active power is very unstable due to the persistence of the fault in the system.

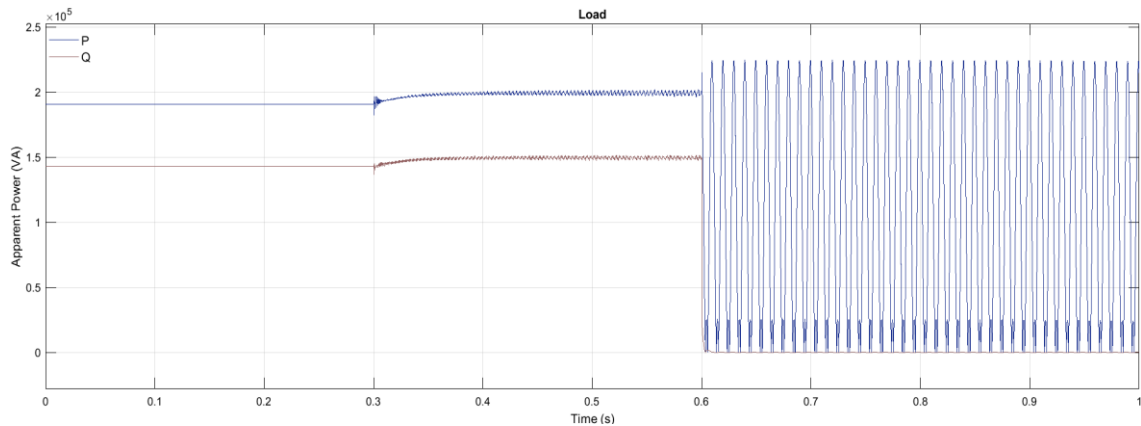


Figure 67- Active and reactive power of the load for line-to-line short-circuit - Case1.

5.3.1.3. Line-to-Ground Short-Circuit

The third type of SC to be analysed refers to a contact with low impedance between phase A and the ground. After the occurrence of the defect, the voltage in this phase becomes zero while in phases B and C it remains at its nominal value, although an increase due to phase unbalance is expected.

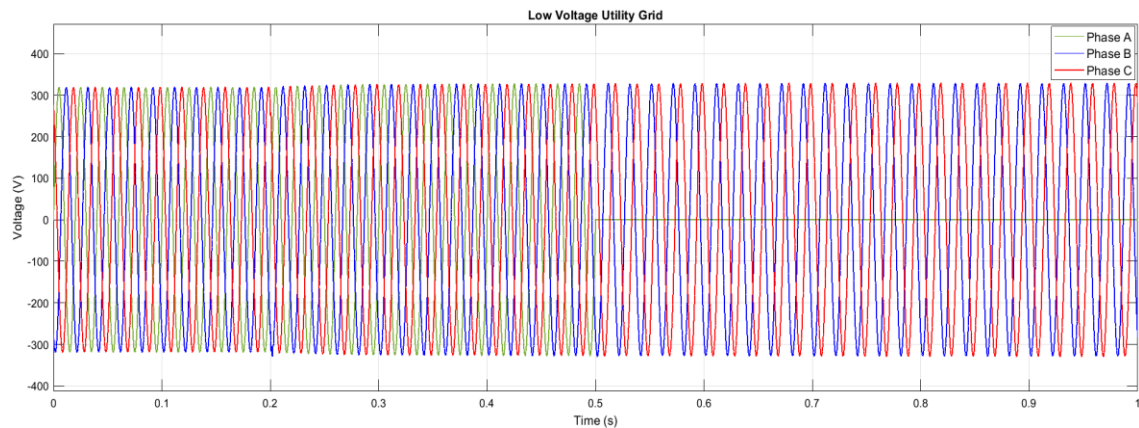


Figure 68- Utility grid voltage waveforms for line-to-ground short-circuit - Case1.

The following figure illustrates the behaviour of current waves after the fault. The current in the contact phase with the ground is maximum and equal to the SC current, having an effective value 15050 A. The other two waveforms represent a defective behaviour of the inverter model, which, by including a transformer in its internal model, affects the operation of the simulator by injecting currents five times higher than the current of the inverter.

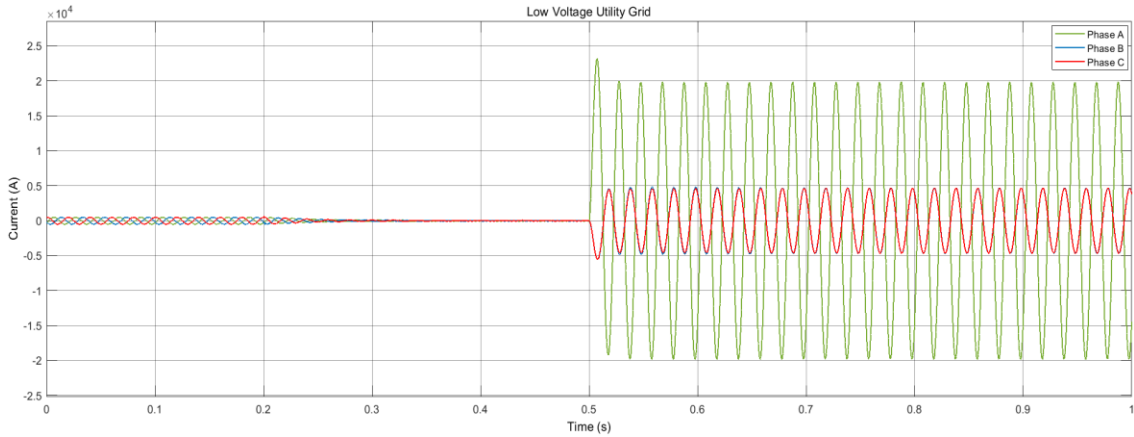


Figure 69- Utility grid current waveforms for line-to-ground short-circuit - Case1.

Unlike the SCs studied so far, the inverter has a very distinct behaviour for a line-to-ground fault. Although the fault occurs in phase A, there is an internal imbalance in the voltage waveforms, which causes the current to be injected into the phases where the voltage drop occurred. As in the previous case, the inverter stays in service, although it behaves differently than expected.

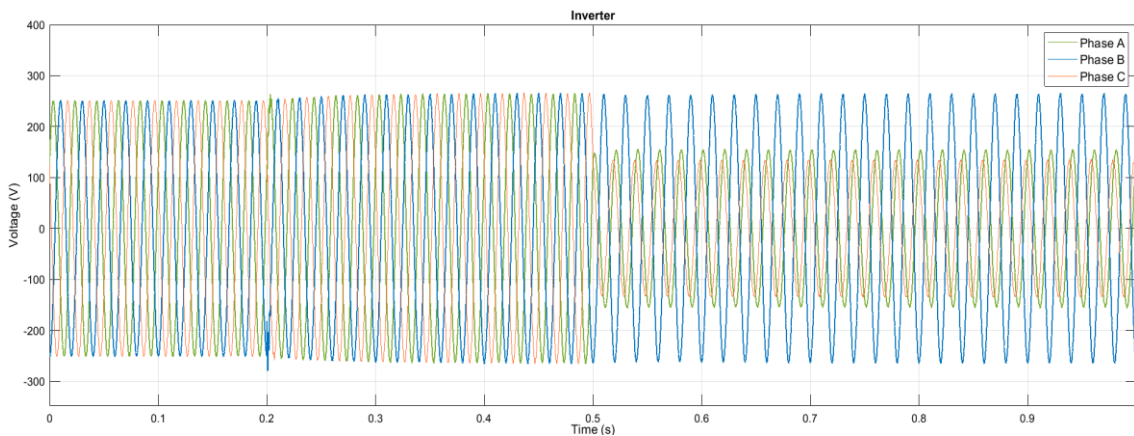


Figure 70- Inverter voltage waveforms for line-to-ground short-circuit - Case1.

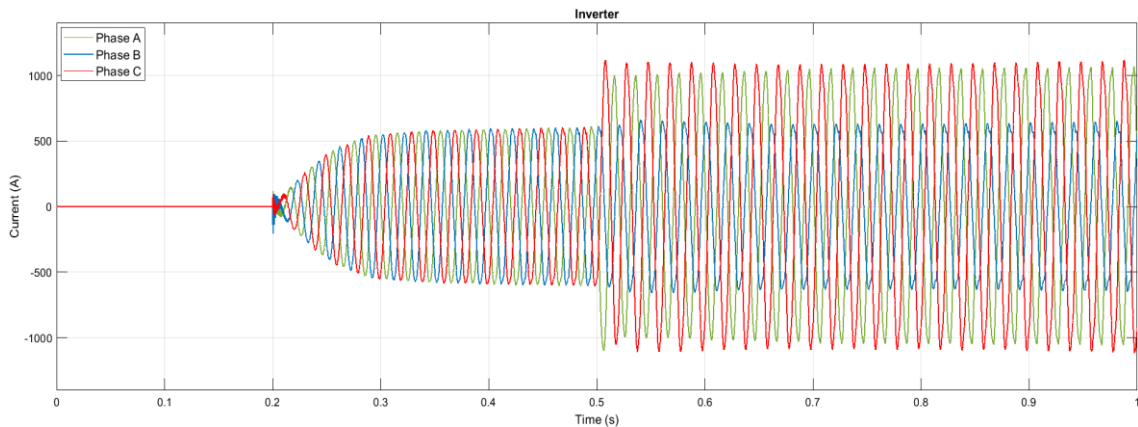


Figure 71- Inverter current waveforms for line-to-ground short-circuit - Case1.

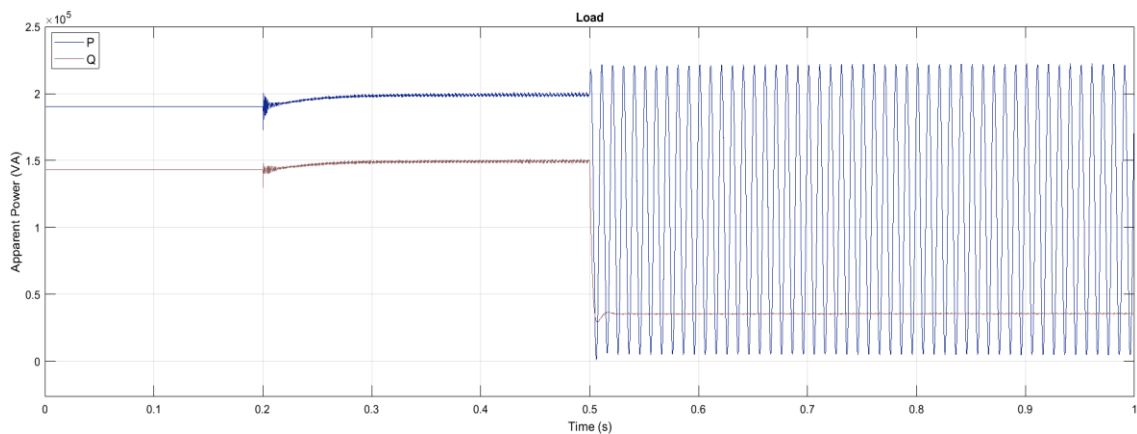


Figure 72-Active and reactive power of the load for line-to-ground short-circuit - Case1.

The waveform of the active power maintains the same oscillatory behaviour due to the permanence of the fault and it is verified that the supply of some reactive energy is maintained.

5.3.1.4. Line-to-Line Short-Circuit with Ground Connection

Finally, the line-to-line SC with ground connection was analysed. Since the contact between phases A and B has occurred, it is expected, that the voltage waveforms become zero. However, in the same phase there is a voltage drop referring to the connection of the inverter, although the voltage should be higher than its nominal value due to the imbalance caused in the phases.

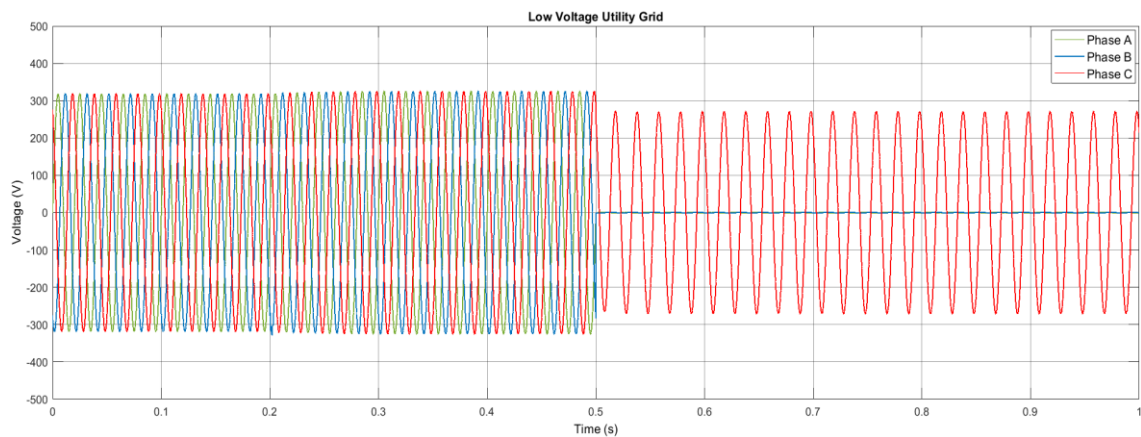


Figure 73- Utility grid voltage waveforms for line-to-line-to-ground short-circuit - Case1.

Therefore, the current in the bolted lines has increased, the effective value of the SC current being 15030 A. The current in the same phase has increased considerably due to the voltage drop and the current injection by the inverter.

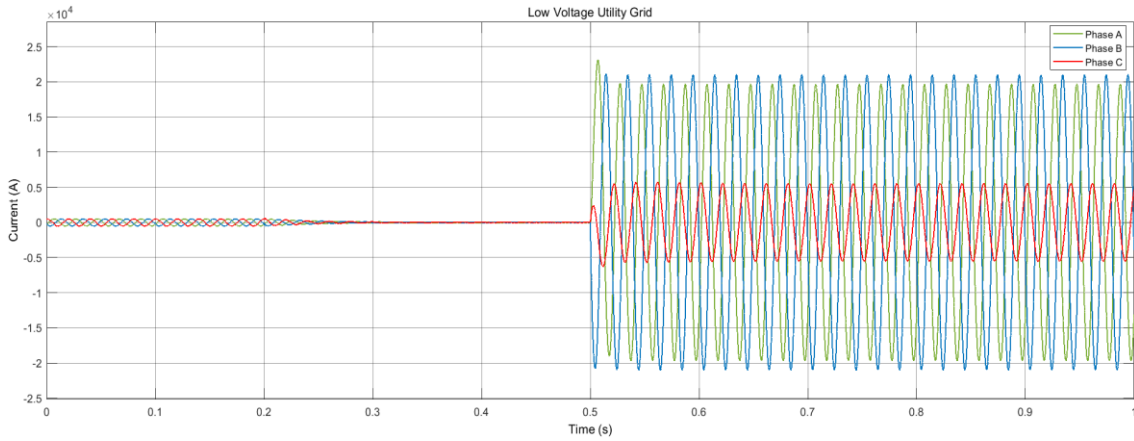


Figure 74- Utility grid current waveforms for line-to-line-to-ground short-circuit - Case1.

As in the previous SC, the inverter had a peculiar behaviour, with a substantial voltage drop and a voltage unbalance after the fault. This was translated into current injection in all phases, being in phase A, a value greater than twice the nominal current of the inverter.

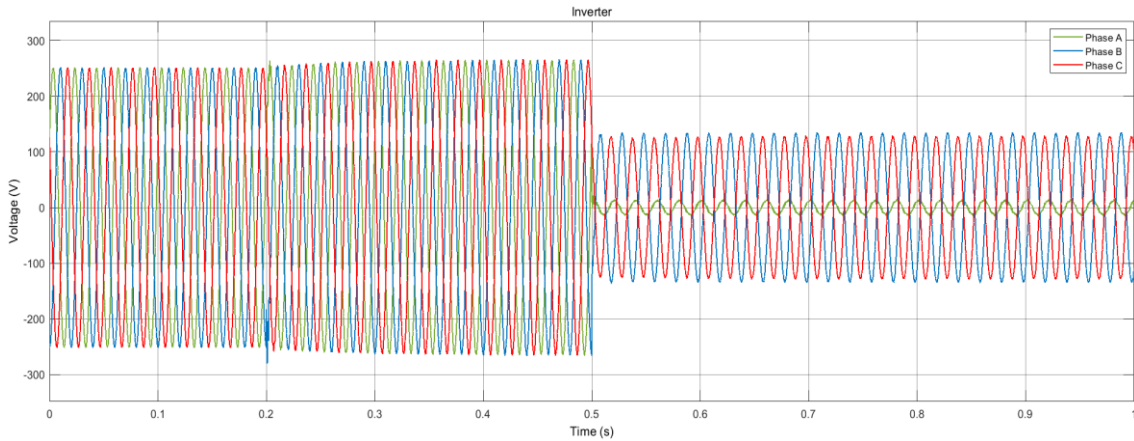


Figure 75- Inverter voltage waveforms for line-to-line-to-ground short-circuit - Case1.

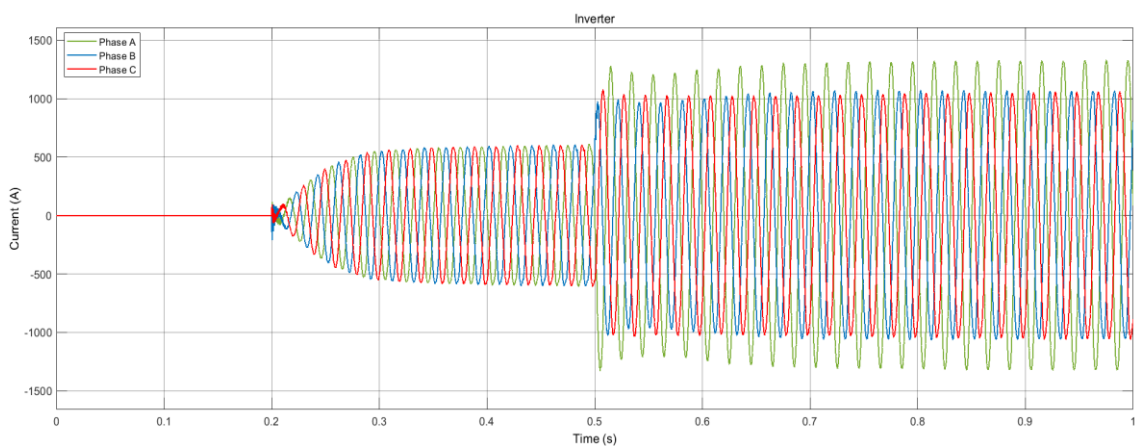


Figure 76- Inverter current waveforms for line-to-line-to-ground short-circuit - Case1.

After the fault, the waveform of the power in the load has a similar behaviour to the other SCs.

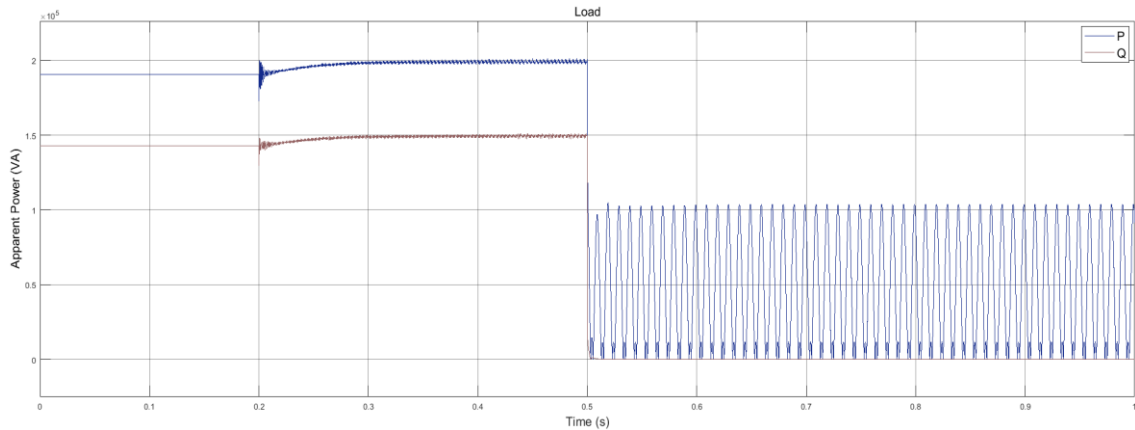


Figure 77- Active and reactive power waveforms of the load for line-to-line-to-ground short-circuit - Case1.

In summary, the SC current values obtained through the simulation in MATLAB/Simulink and their relative error are shown in the table below, compared to the values calculated in the previous chapter.

Table 24- Short-Circuit Currents- Case 1.

Type of Short-Circuit	Calculated	Simulated	Relative Error (%)
Three-phase	14645	14910	1.81
Phase-to-Ground	16255	15050	7.41
Phase-to-Phase	12680	12850	0.79
Phase-to-Phase-to-Ground	18073	15030	16.84

It is verified that the model created is partially valid, although it has some flaws with respect to the modelling of the SCs that involves ground connection.

As far as the protection systems are concerned, it is verified that the circuit-breakers would operate correctly, in about 0.01 seconds, since the value of the SC current exceeds its minimum limit of operation. This way, the fault is isolated and the electrical equipment and people, protected.

5.3.2. Case 2: Microgrid Connected to the Medium Voltage Grid

The following case study refers to the MV grid connection with the integration of the storage system connected by an inverter to feed a three-phase load. As in the previous case study, a fault analysis was carried out, as shown in the following figure. The normal behaviour of the system will not be presented since is similar to the previous case

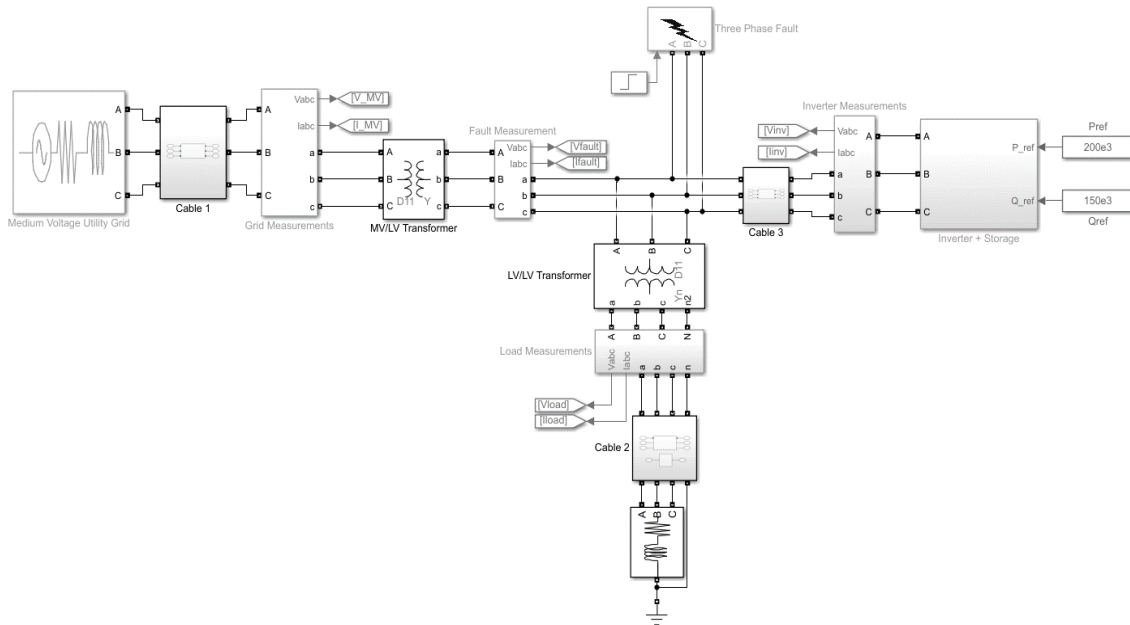


Figure 78- Simulink model of a Low Voltage Microgrid Connected to the Medium Voltage Utility Grid.

5.3.2.1. Three-Phase Short-Circuit

The first analysis for this type of connection was the symmetrical SC in the 315V network section. The results of the simulation of this fault are presented in the following figures.

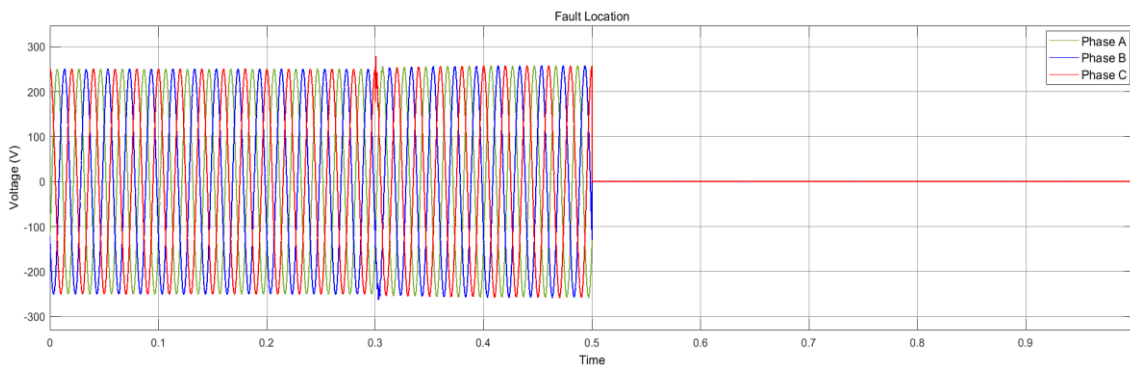


Figure 79- Fault Location voltage waveforms for symmetrical short-circuit- Case2.

In the previous figure, the beginning of the operation of the battery and inverter system is visible at 0.3 seconds, with a slight increase in voltage. At 0.5 seconds, when the fault occurs, the voltages in the three phases are zero, as expected.

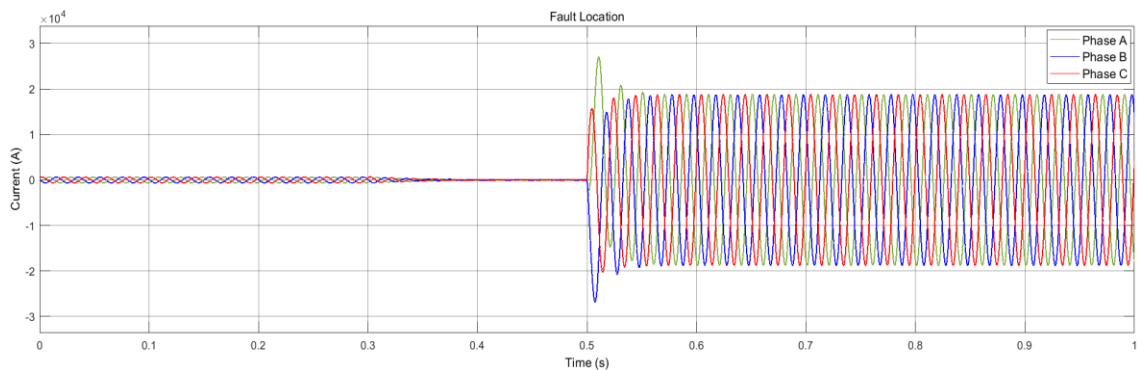


Figure 80- Fault location current waveforms for symmetrical short-circuit- Case2.

At 0.3 seconds there is an attenuation of the current coming from the network, having a power sharing between the network and the storage system in the load supply. When the SC occurs, there is a small asymmetry in the waveforms of the current during the transient period, stabilising in the stationary period. In this period, the magnitude of the current in the three phases stabilises as can be seen in the following figure, with the effective value of 13290A.

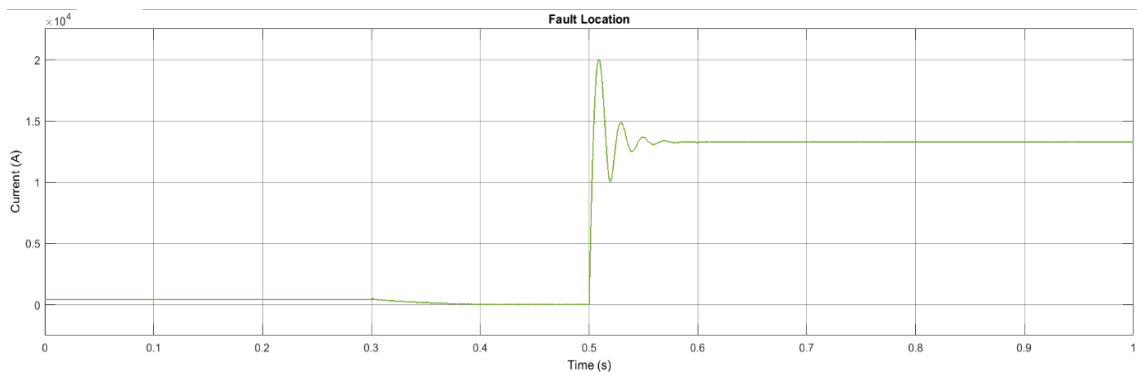


Figure 81- RMS values of the short-circuit current for symmetrical short-circuit- Case2.

During the transient period, there is an oscillation of the current waveform, stabilising at the end of 5 cycles. This is due to the inductive character of the distribution network.

88 The Democrat Case Study

The inverter has a normal behaviour, cancelling the voltage in the three phases after the occurrence of the SC and supplying the SC current with about twice its nominal current.

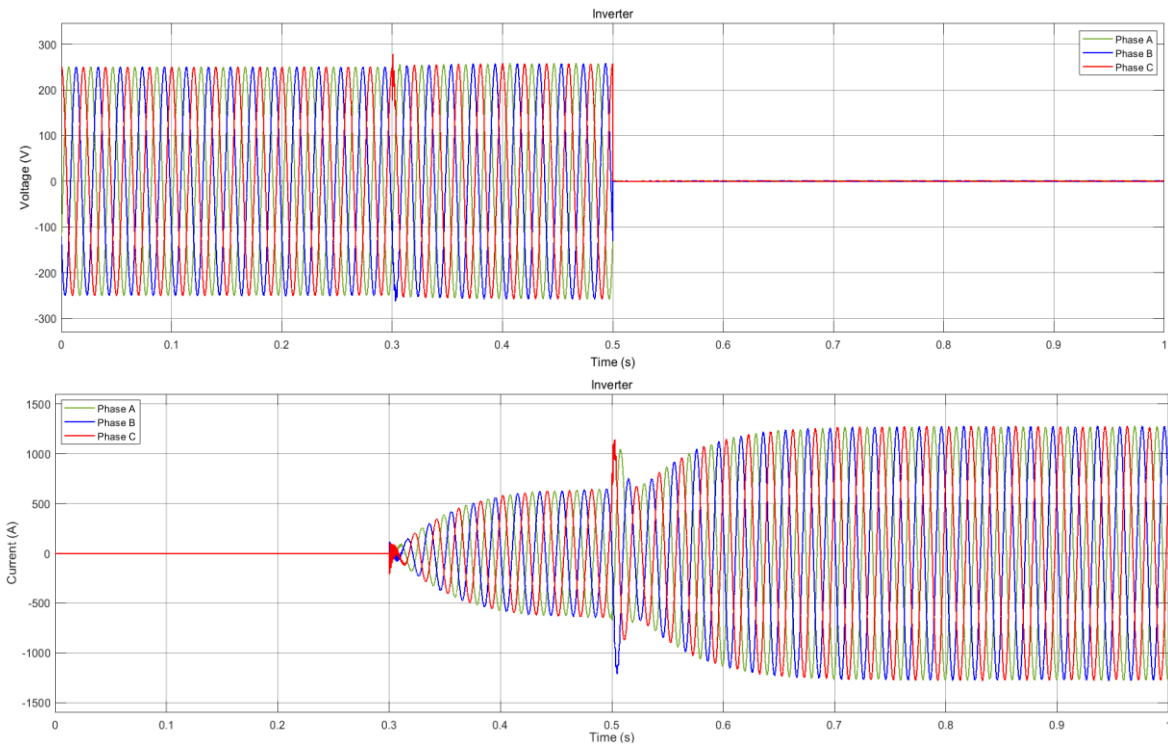


Figure 82- Inverter voltage and current waveforms for symmetrical short-circuit, respectively - Case 2.

After the fault, the load is no longer fed and there is no active and reactive power flow.

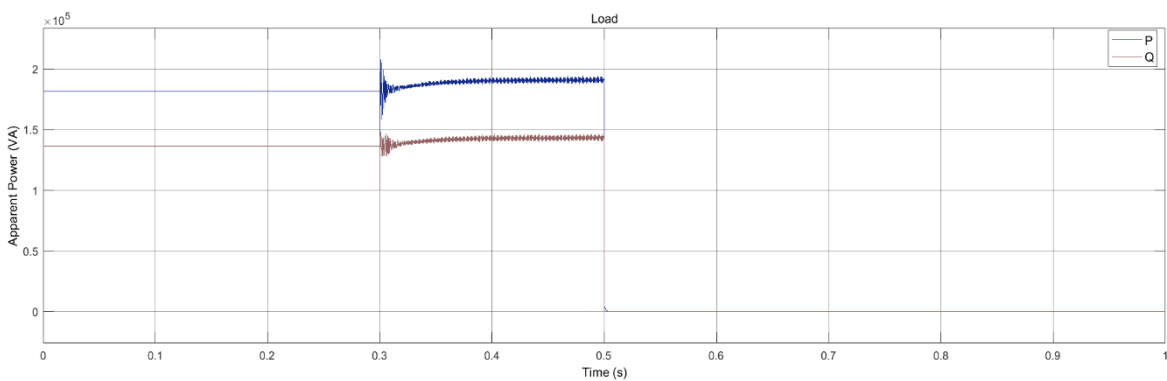


Figure 83- RMS values of active and reactive power for symmetrical short-circuit- Case1.

5.3.2.2. Line-to-Line Short-Circuit

The behaviour of the system during a contact between two phases (A and B) is just as expected, with voltage attenuation in the fault for 0.5 p.u. and stabilisation of the remaining voltage in 1 p.u.

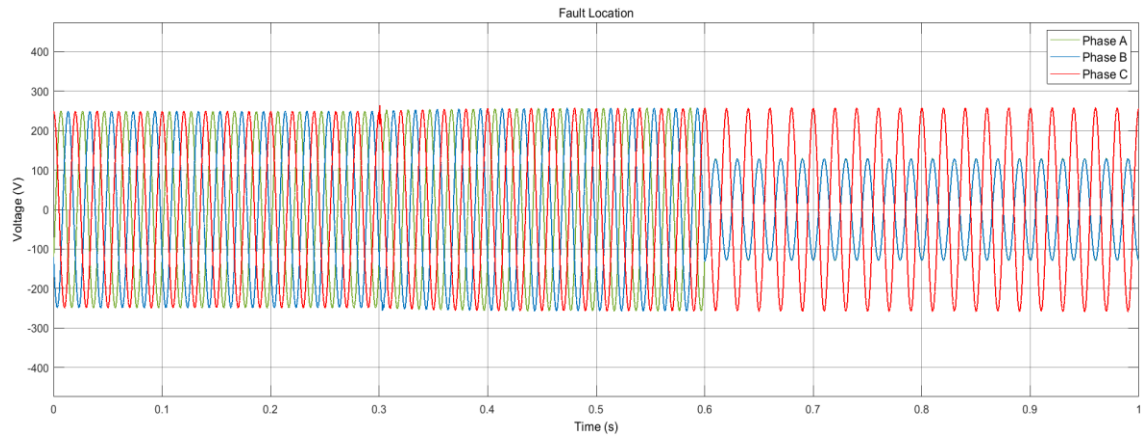


Figure 84- Fault Location voltage waveforms for line-to-line short-circuit - Case2.

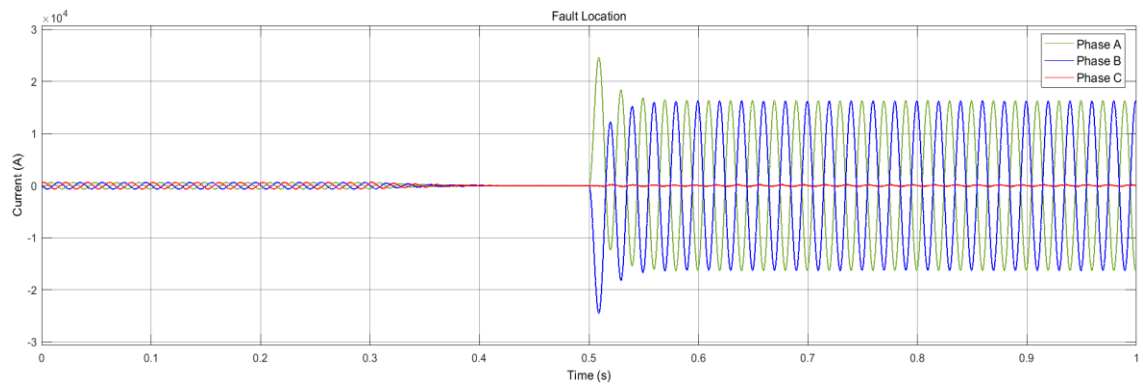


Figure 85- Fault location current waveforms for line-to-line short-circuit - Case2.

The currents are symmetrical in phases A and B, corresponding to the SC current. These currents have an effective value of 11510A.

Since the voltage measurement at the fault location is the same as the voltage measurement at the inverter output, only the current injected by the inverter must be taken into account. In this way, it is verified that this is double the nominal current of the inverter in the faulted phases and equal to the nominal current in the sane phase.

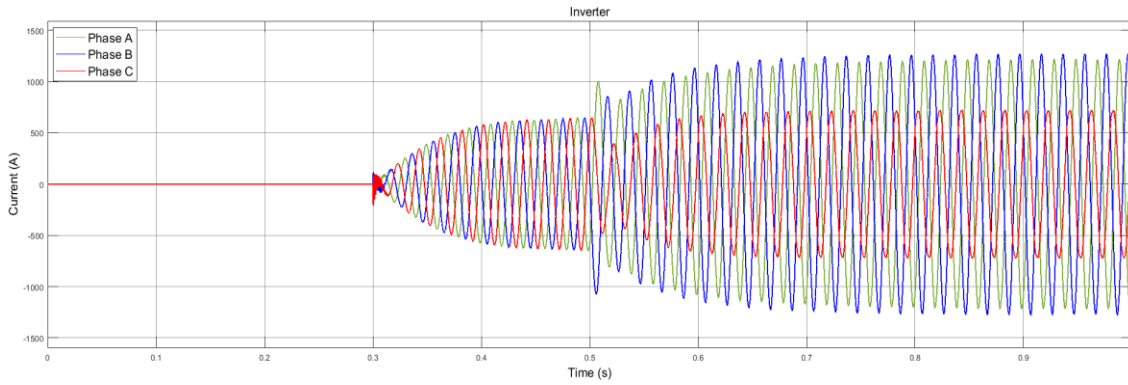


Figure 86- Inverter current waveforms for line-to-line short-circuit - Case2.

As in the previous case study, the active power in the load becomes oscillatory due to the remaining fault current, while the reactive power in the load becomes zero.

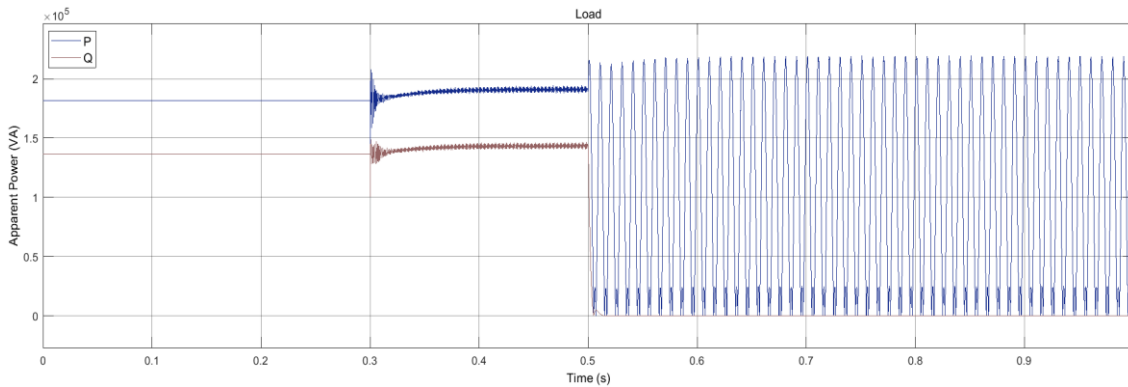


Figure 87- RMS values of active and reactive power of the load for line-to-line short-circuit - Case2.

5.3.2.3. Line-to-Ground Short-Circuit

After a line-to-ground fault, as expected, the voltage in the phase that had contact with the ground (Phase A) becomes zero, while the voltage in the others remains close to the nominal. In both sane phases, the voltage should rise slightly to compensate for imbalance. This behaviour can be seen in the following figure.

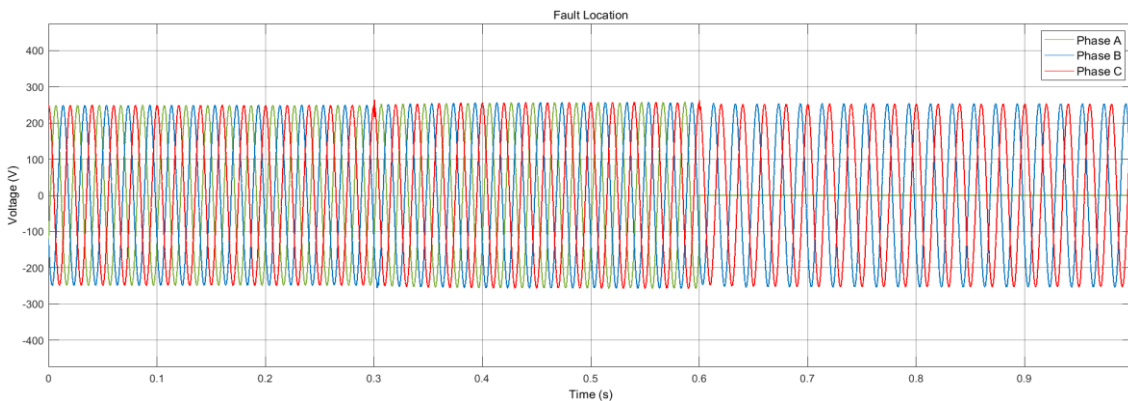


Figure 88- Fault Location voltage waveforms for line-to-ground short-circuit - Case2.

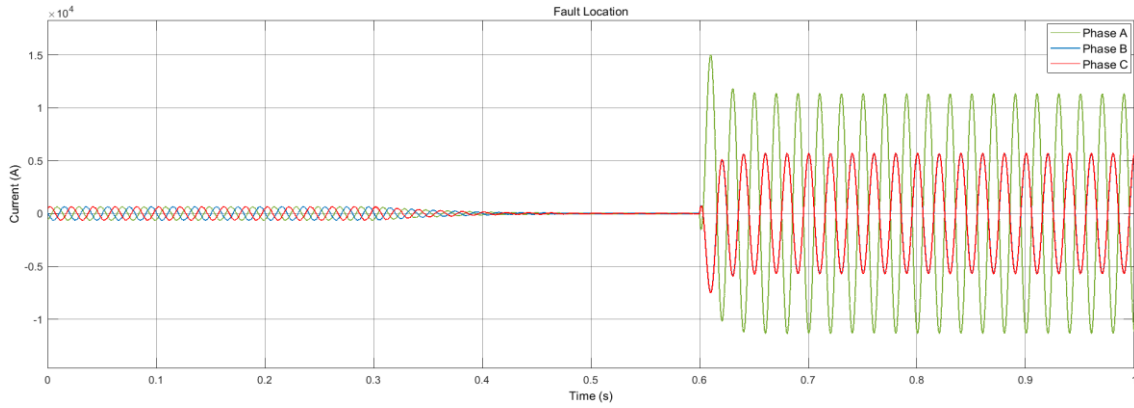


Figure 89- Fault location current waveforms for line-to-ground short-circuit - Case2.

Regarding the post-fault current, it rises in the faulted phase, corresponding to the SC current, with an effective value of 8615A, and in the others it presents a value different from the nominal value, due to the current injection by the inverter. This current should be about twice as high as the nominal current of the inverter, but it is explained by the existence of a transformer in the inverter model that affects the behaviour of the simulator. Due to the configuration of this transformer and the corresponding voltage levels, the injection and current in the network should be only approximately 30% above the current of the inverter.

After the fault, the active power values are oscillatory due to the persistence of the SC currents in the system and a constant supply of reactive power is verified.

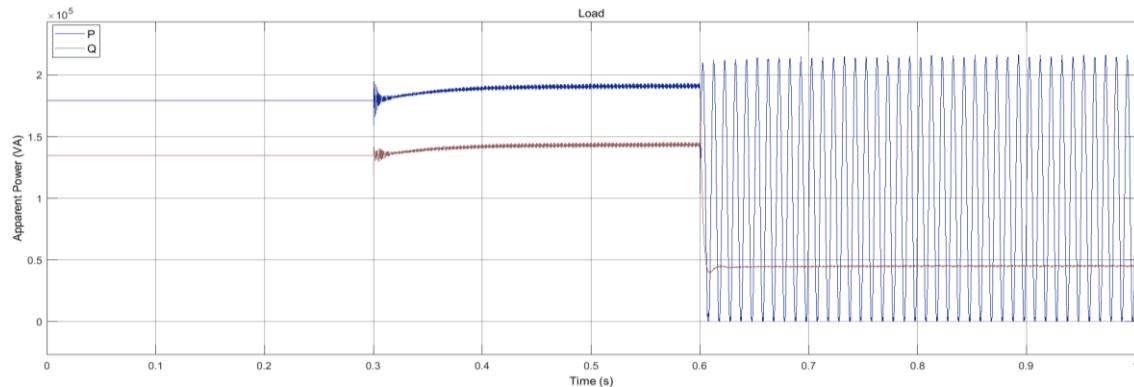


Figure 90- RMS values of active and reactive power of the load for line-to-ground short-circuit - Case2.

5.3.2.4. Line-to-Line Short-Circuit with Ground Connection

At last, the line-to-line SC with ground connection was analysed, revealing the same behaviour observed in the connection to the LV distribution network. After the contact between phases A and B, it is expected, that the voltage waveforms reach zero and in the same phase there is a voltage drop referring to the connection of the inverter, although the voltage should be higher than its nominal value due to the imbalance caused in the phases.

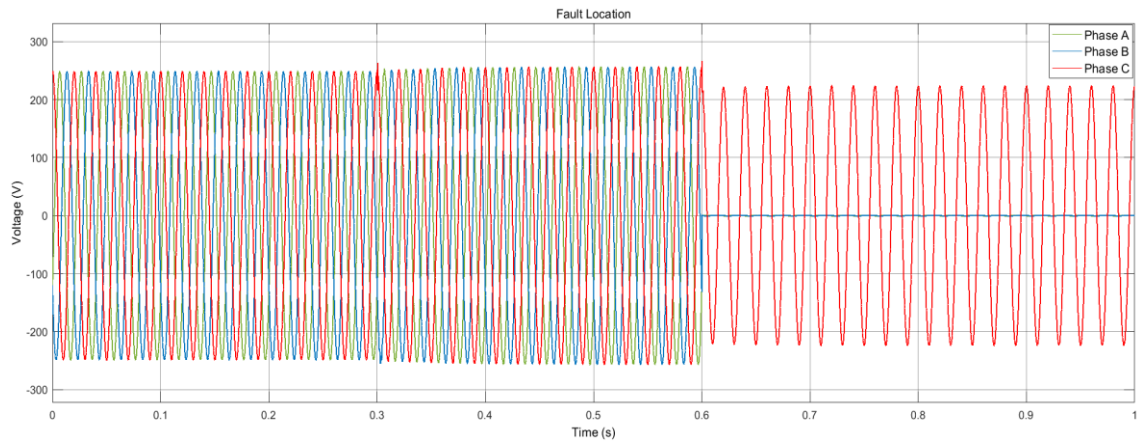


Figure 91-Fault location voltage waveforms for line-to-line-to-ground short-circuit - Case2.

Therefore, the current in the bolted lines has increased, with the effective value of the SC current being 11640 A. The current in the same phase has increased considerably due to the voltage drop and the current injection by the inverter.

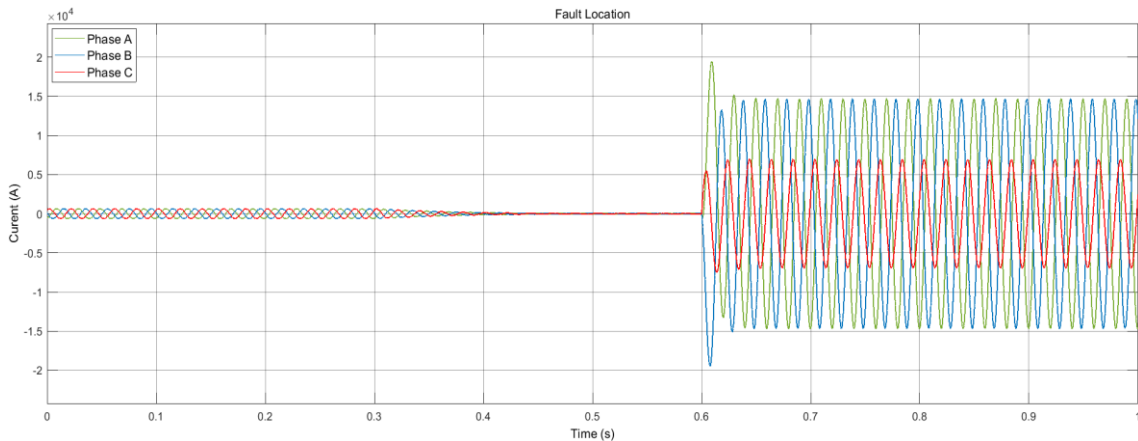


Figure 92- Fault Location current waveforms for line-to-line-to-ground short-circuit - Case2.

As in previous types of SC, the behaviour of the current in the load causes oscillation of the active power waveform and reactive power flow to the load becomes null.

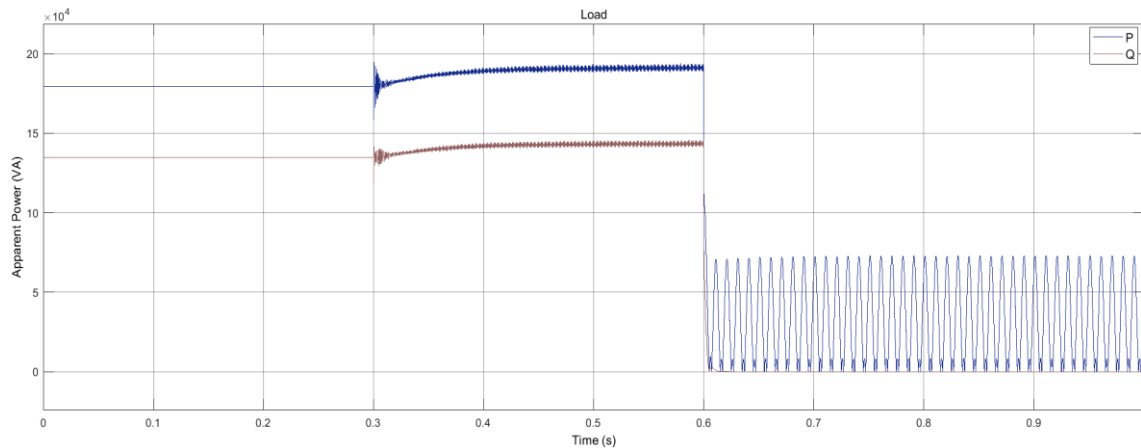


Figure 93- RMS values of active and reactive of the load for line-to-line-to-ground short-circuit - Case2.

As in the previous case study, the SC current values obtained through the MATLAB/Simulink simulation and their relative error are shown in the table below, compared to the values calculated in the previous chapter.

Table 25- Short-Circuit Currents - Case 2.

Type of Short-Circuit	Calculated	Simulated	Relative Error (%)
Three-phase	12743	13290	4.29
Phase-to-Ground	4279	8615	—
Phase-to-Phase	11036	11510	4.30
Phase-to-Phase-to-Ground	2516	10360	—

It is verified that the model created is valid for load balancing and for SC analysis without ground connection, presenting some flaws with respect to the modelling of SCs with ground connection.

As far as the protection systems are concerned, it is verified that the circuit-breakers would operate correctly, in about 0.01 seconds, since the magnitude of the SC current exceeds its minimum limit of operation. This way, the fault is isolated and the electrical equipment and people, protected.

5.3.3. Case 3: Microgrid Connected to an Islanded Grid

The last scenario refers to the behaviour of Democrat during an isolated mode of operation. The model regards the integration of the storage system connected by an inverter to feed a three-phase load and an electrical vehicle charging station. The system is supported by a diesel generator, operating for load support. This system can be seen in the in the following figure.

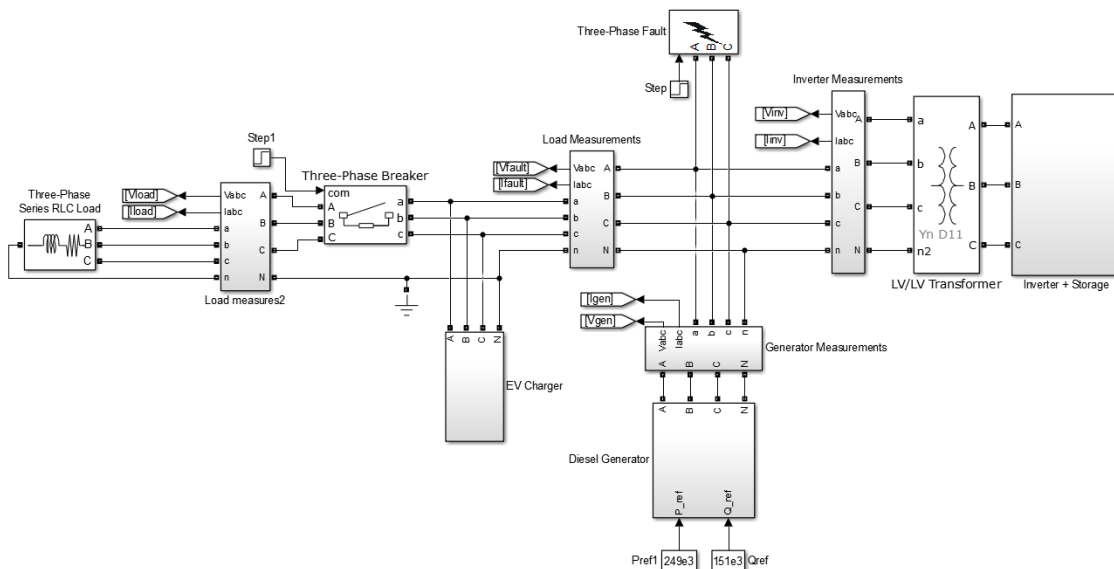


Figure 94- Islanded Microgrid.

Since the inverter model used in the simulations of the Democrat project connected to the distribution networks followed the voltage references of the network for its operation, it was necessary to adapt the inverter model to become a grid formation unit, since there is no voltage reference. In this way, this unit assumes control of the voltage and frequency of the MG, responding quickly to the imbalances between generation and consumption. The operation of the following MG is shown in the following figures.

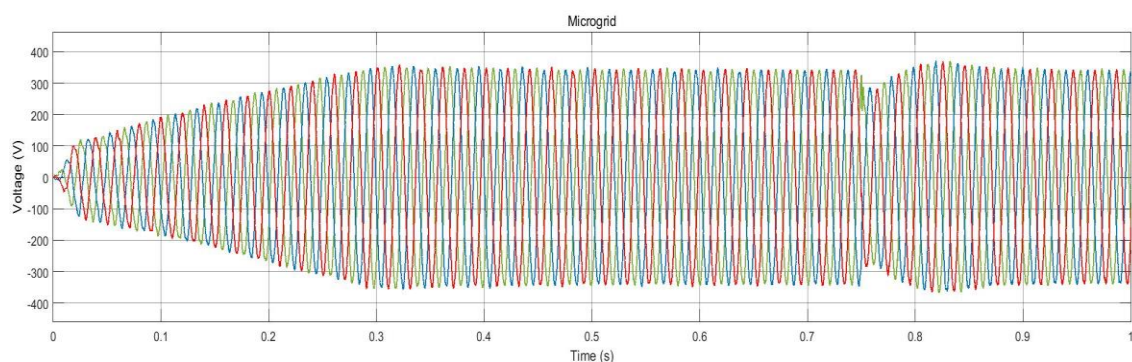


Figure 95- Microgrid voltage waveforms- Case 3.

The previous figure shows the formation of the grid by the inverter in the first 0.3 seconds, feeding the electric vehicle charger, considered as a load. The voltage values stabilise after this moment and at 0.75 seconds there is a voltage drop related to the drive of the load bank, and the voltage is quickly recovered by the inverter.

Figure 96 represent the actuation of the generator and the inverter after the introduction of the load bank. When the system senses the voltage drop, it quickly and efficiently activates the generating units and it is verified the current sharing by the two elements for powering the electric vehicle charger and the load.

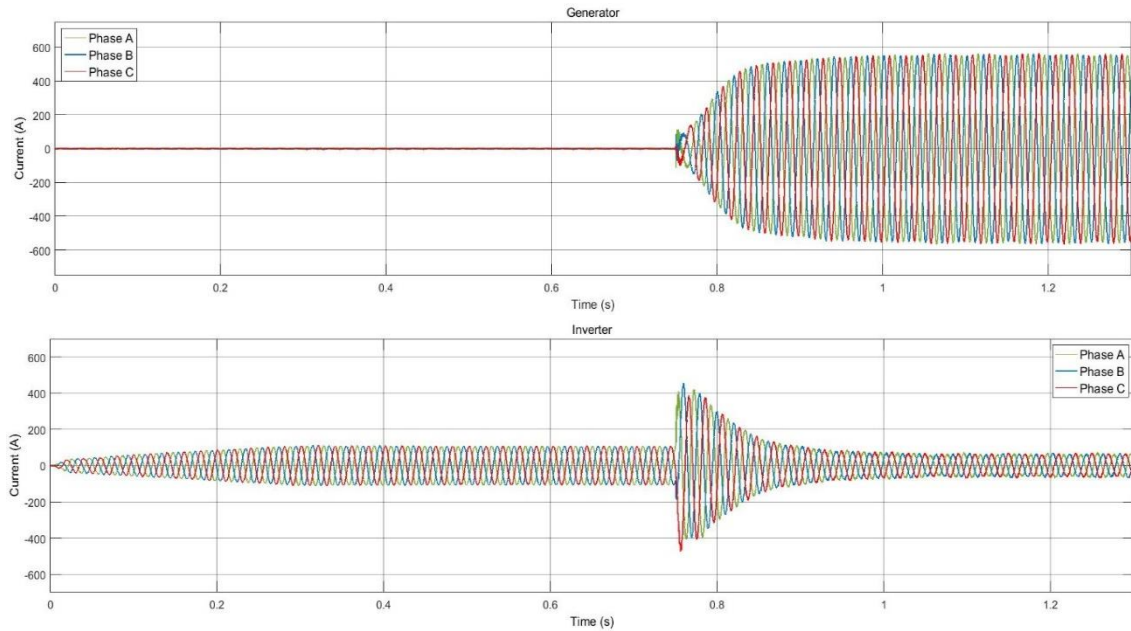


Figure 96- Current waveforms of the Generator and Inverter, respectively- Case 3.

The following figures present the active and reactive power provided by the generating units. Figure 96.a shows the power supplied to the electric vehicle charger and figure 96.b shows the power supplied to the system load bank.

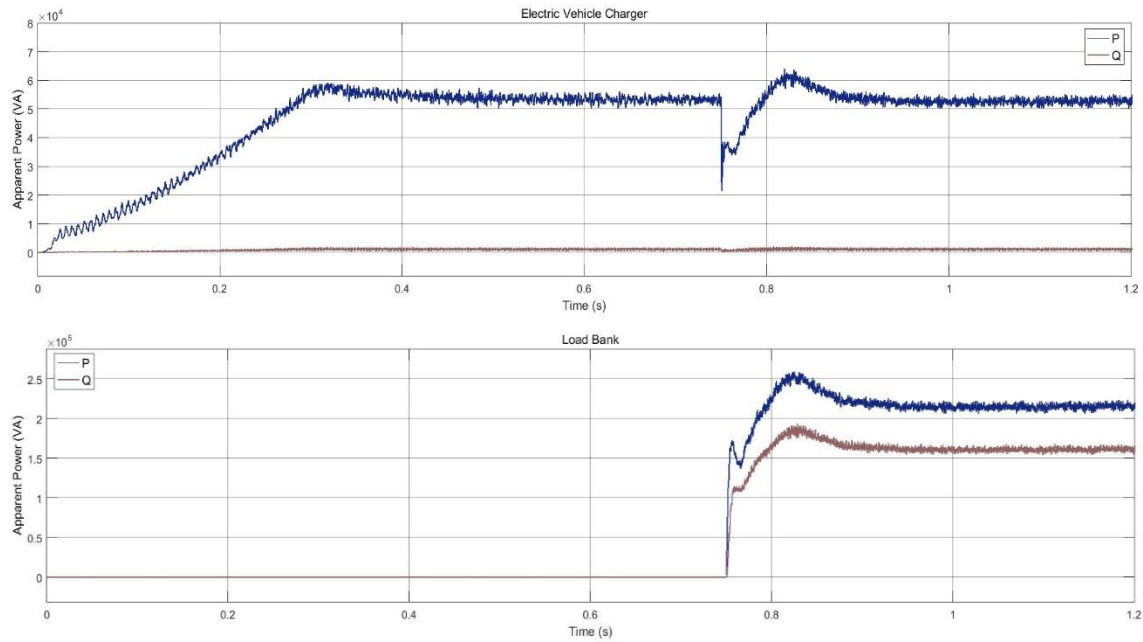


Figure 97- RMS values of active and reactive of the EV Charger and Load bank, respectively- Case 3.

After demonstrating the correct functioning of the MG, different types of SCs were simulated, as in previous case studies.

5.3.3.1. Three-Phase Short-Circuit

The first analysis for this type of connection was the symmetrical SC in the 400V network section. The results of the simulation of this fault are presented in the following figures.

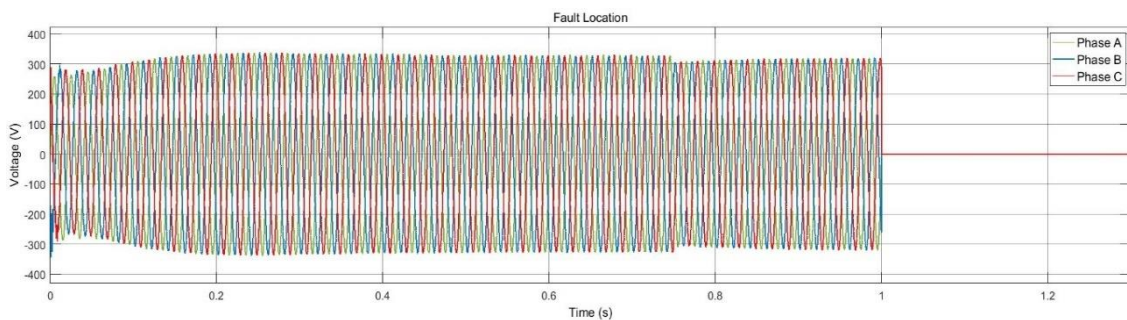


Figure 98- Fault Location voltage waveforms for symmetrical short-circuit- Case3.

The previous figure shows the voltage behaviour before and during the fault. A slight voltage drop is visible at 0.75 seconds referring to the connection of the load bank although it is recovered by the system. At 1 second, the symmetrical SC occurs, and there are voltage drops to zero on the bolted lines.

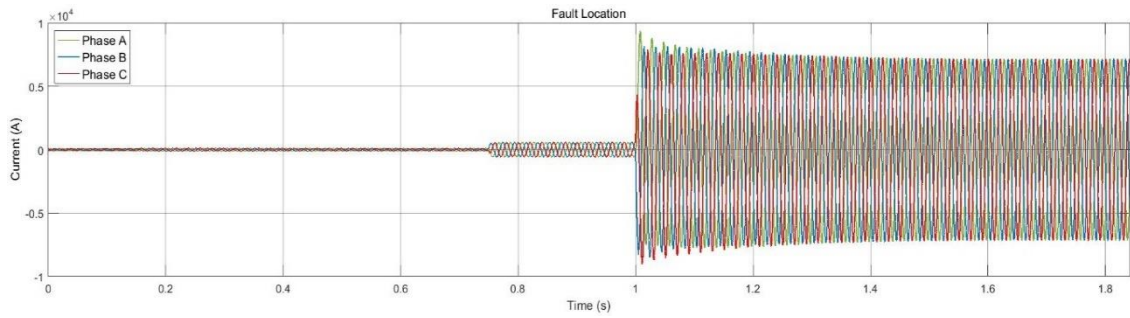


Figure 99- Fault location current waveforms for symmetrical short-circuit- Case3.

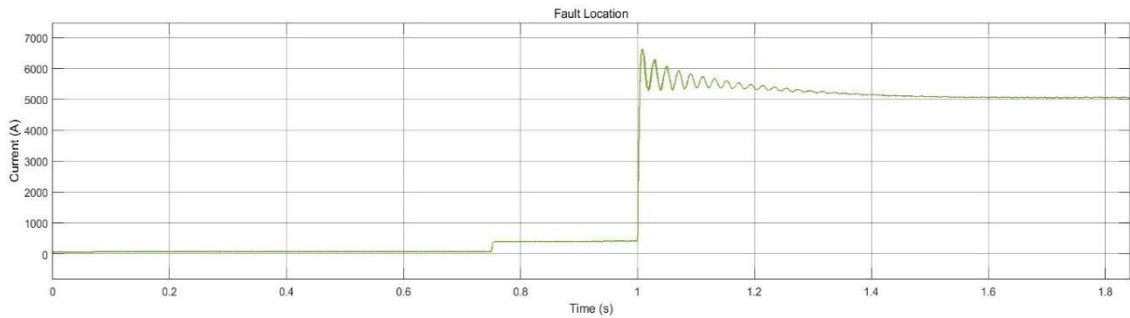


Figure 100- RMS values of the short-circuit current for symmetrical short-circuit- Case3.

Figures 99 and 100 show the current waveforms during the operation of the MG, with a slight increase in current due to the introduction of the load and after the SC, the current waves in the three phases stabilise to the same value. There is a short transient period, for 0.2 seconds, stabilising the value of the currents after about 10 cycles in 5128A.

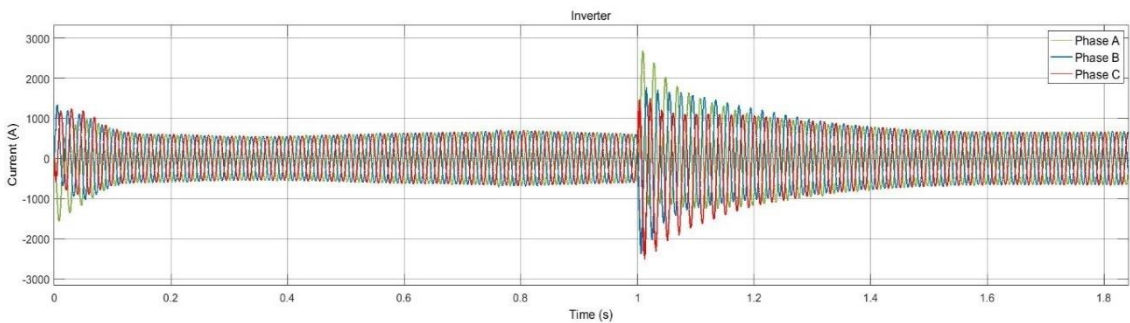


Figure 101- Inverter current waveforms for symmetrical short-circuit- Case 3.

The inverter has a normal behaviour, injecting, after the SC, a current slightly above its nominal current.

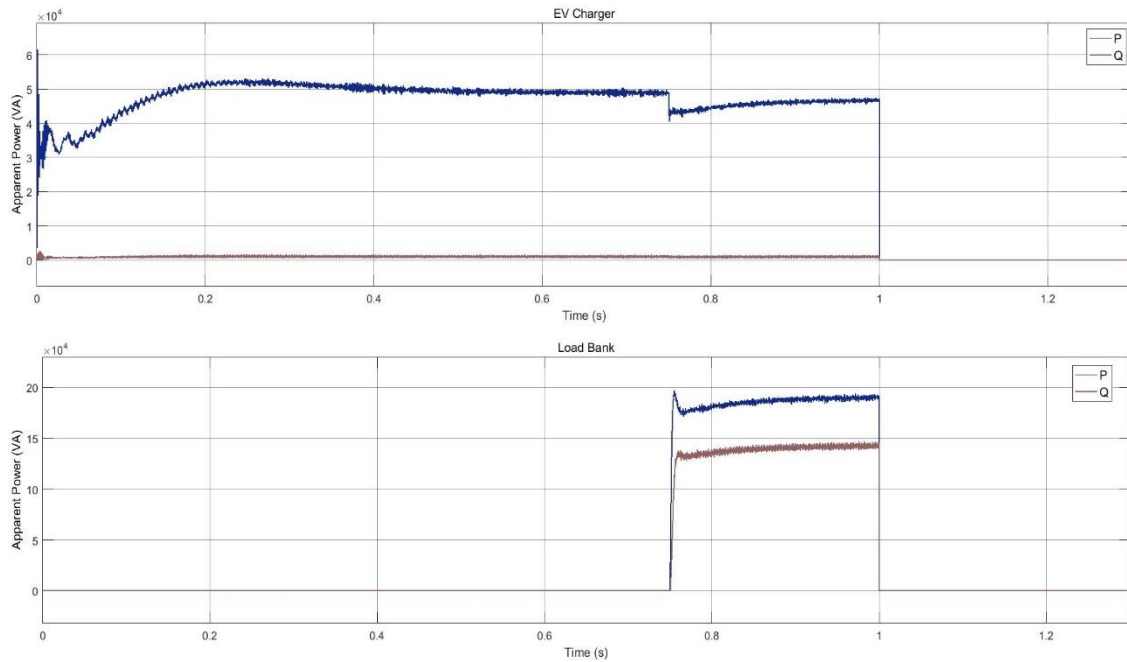


Figure 102- RMS values of active and reactive power of the EV Charger and Load bank for symmetrical short-circuit, respectively- Case 3.

The previous figure shows the correct supply of the loads until the occurrence of the SC, which is interrupted after that moment.

5.3.3.2. Line-to-Line Short-Circuit

The second type of SC analysed was the fault that involves the contact between phases A and B of the network. As expected, there is a voltage drop in the defective phases, with the post-fault voltage being about 0.5 p.u. and a small rise in voltage in the same phase, then stabilising to its nominal value.

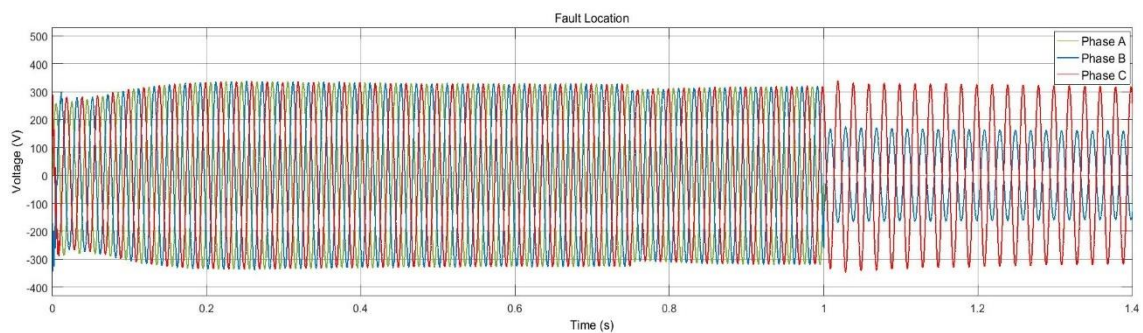


Figure 103- Fault Location voltage waveforms for line-to-line short-circuit - Case3.

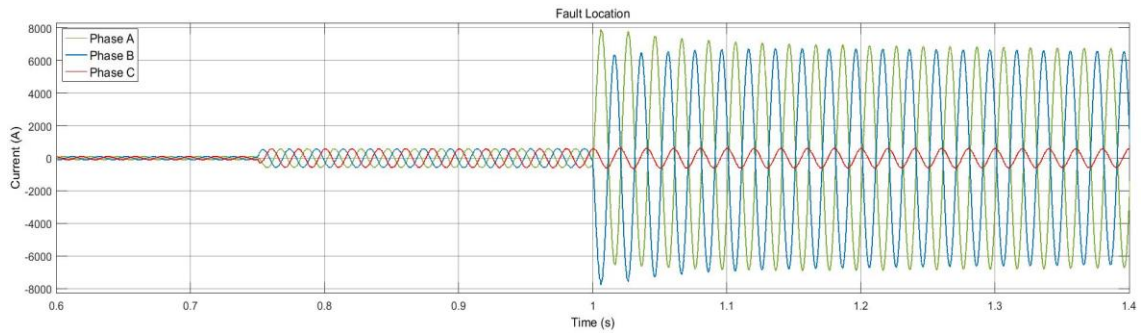


Figure 104-Fault location current waveforms for line-to-line short-circuit - Case3.

The currents are symmetrical in phases A and B, corresponding to the SC current. After the transient period, these currents stabilise to an effective value of 4497A.

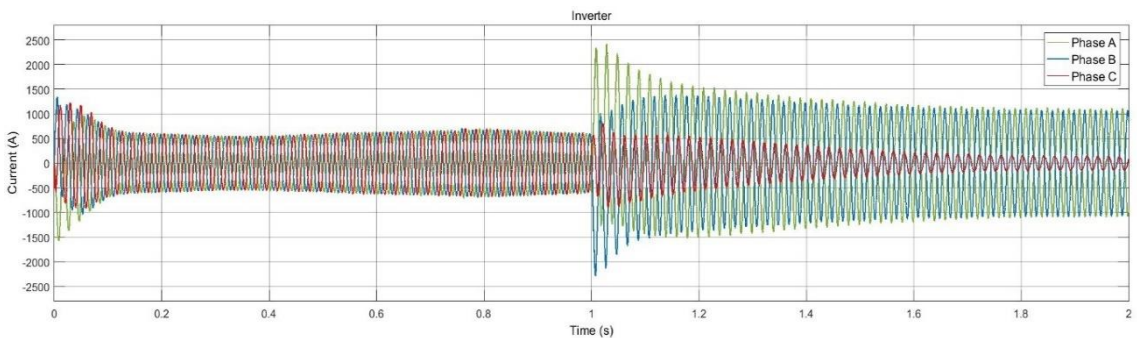


Figure 105- Inverter current waveforms for line-to-line short-circuit - Case3.

There is a normal behaviour of the inverter, contributing with about twice its rated current to the SC current.

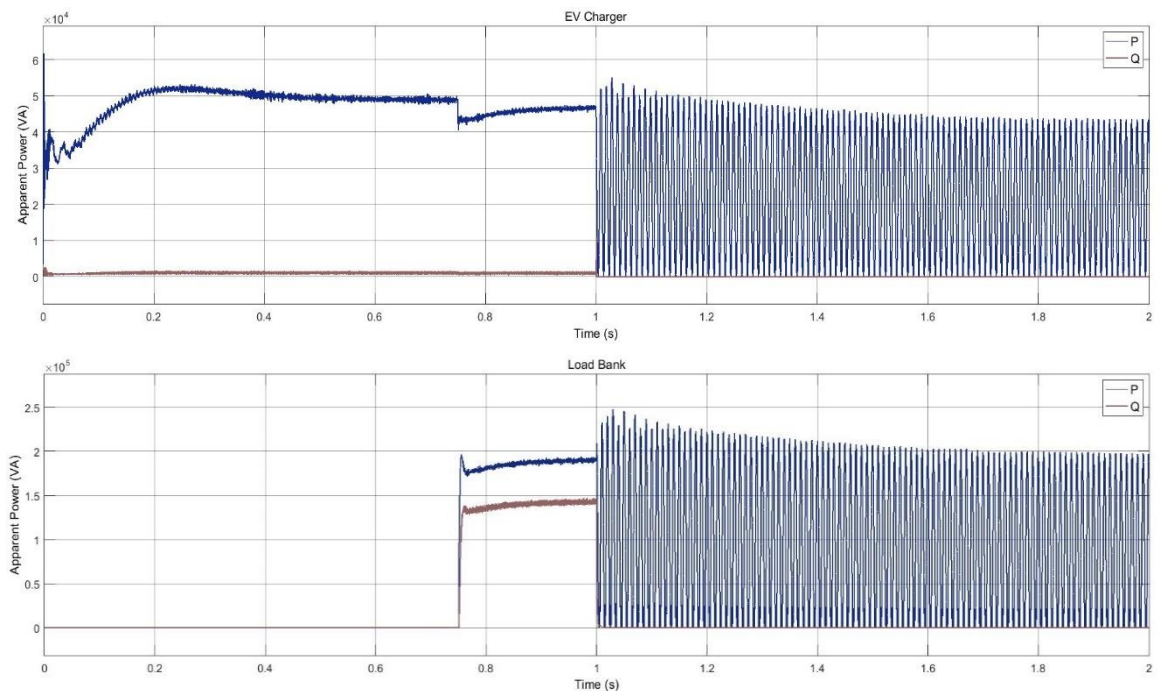


Figure 106- RMS values of active and reactive power of the EV Charger and Load bank for a line-to-line short-circuit, respectively- Case 3.

For asymmetrical faults, as verified in previous case studies, the waveforms of the active powers in the system load have an oscillatory behaviour due to the permanence of the fault in the system.

5.3.3.3. Line-to-Ground Short-Circuit

After a line-to-ground fault, the voltage in the faulted phase (Phase A) becomes zero, while the voltage in the others remains close to the nominal values. In both sane phases, the voltage should rise slightly to compensate the imbalance. This behaviour can be seen in the following figure.

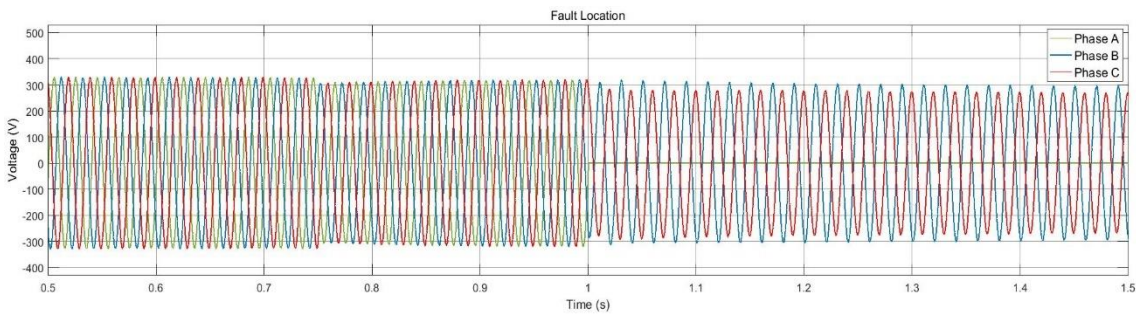


Figure 107- Fault Location voltage waveforms for line-to-ground short-circuit - Case3.

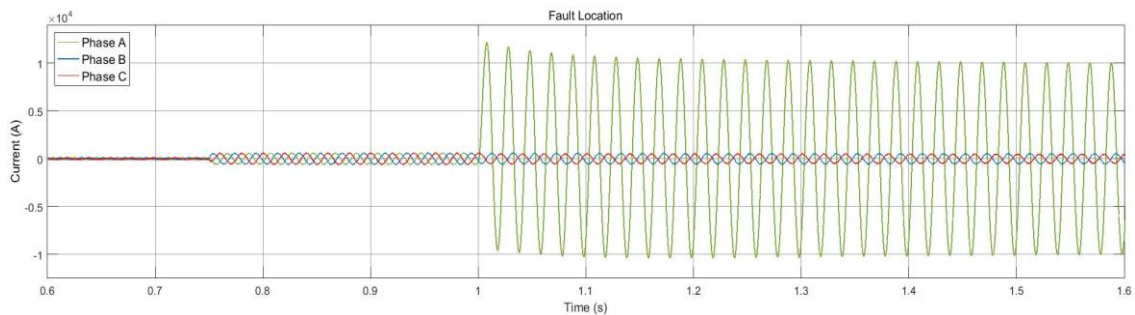


Figure 108- Fault location current waveforms for line-to-ground short-circuit - Case3.

Regarding the post-fault current, it rises in the faulted phase, corresponding to the SC current, with an effective value of 7017A, and in the others it presents a similar value to its nominal. These currents have the correct behaviour for this type of SC, although some elements of the system contribute irregularly to the SC current, as will be presented next.

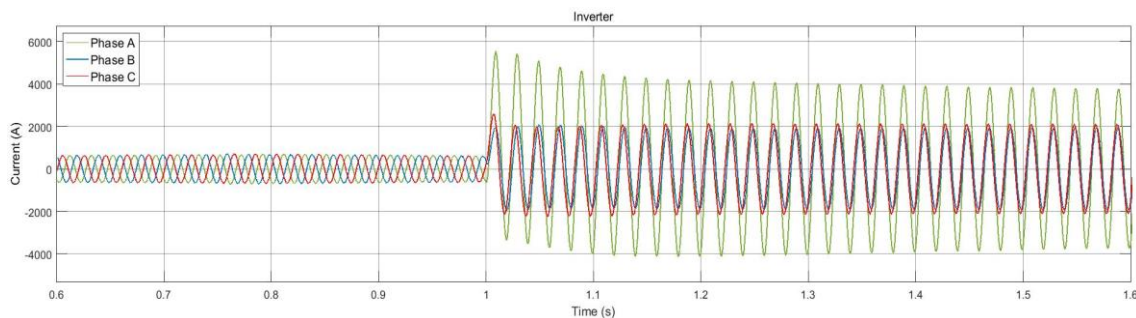


Figure 109- Inverter current waveforms for line-to-ground short-circuit - Case3.

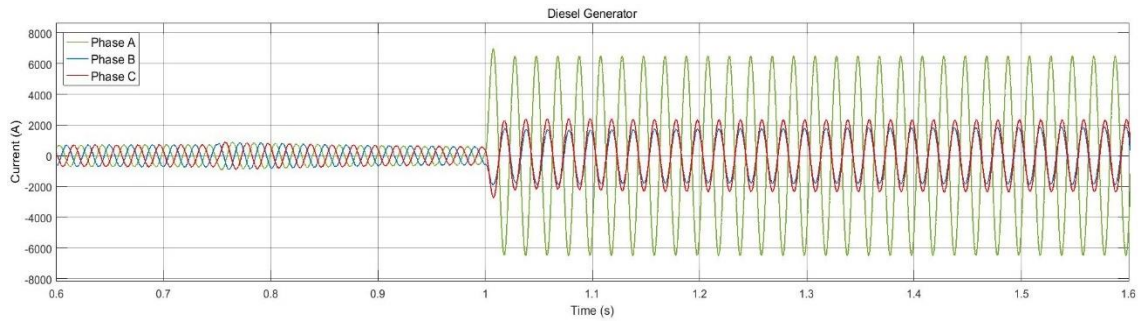


Figure 110- Diesel generator current waveforms for line-to-ground short-circuit - Case3.

Figures 109 and 110 show the injection of high fault currents in the same phases of the system, although at the fault location, the current value is the expected one. At this point in the system, current waveforms correspond to the sum of the currents injected by the two elements, and the current injected by the inverter is influenced by the behaviour of the transformer in an earth fault scenario. However, these currents have phase shifts, which translates into an apparently correct behaviour at the fault location. These behaviours can be seen in the following figure.

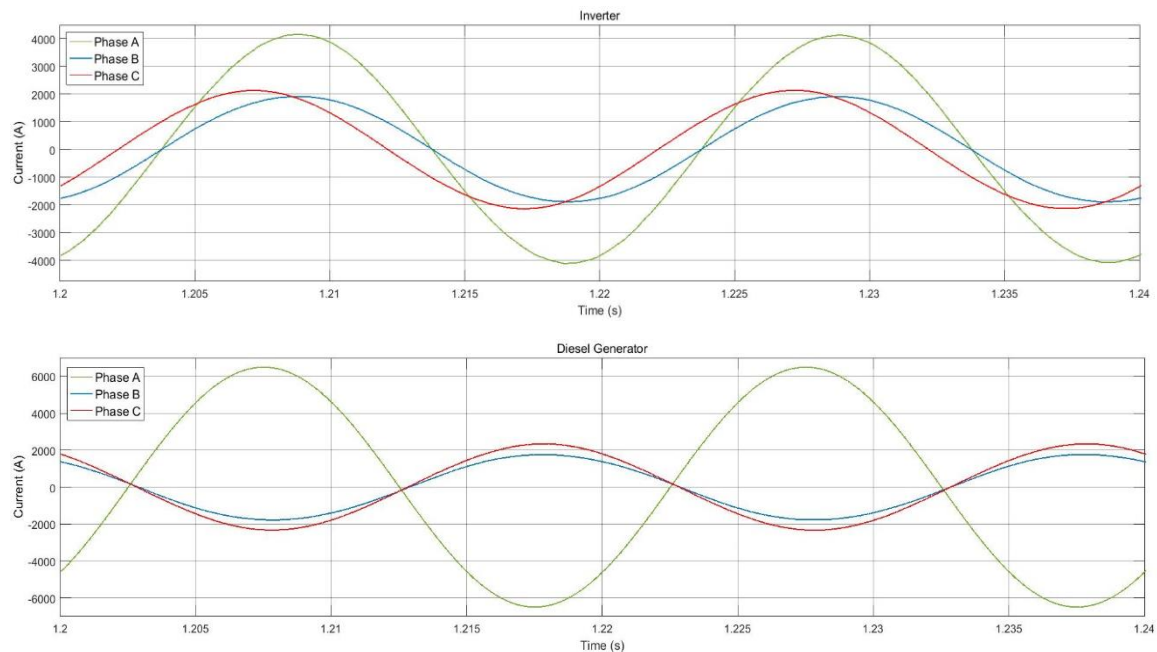


Figure 111- Current waveforms and respective phase shifts for the inverter and generator.

After the fault, the active power values are oscillatory due to the persistence of the SC currents both for the load bank and the electric vehicle charger while there was some remaining reactive power in the load bank.

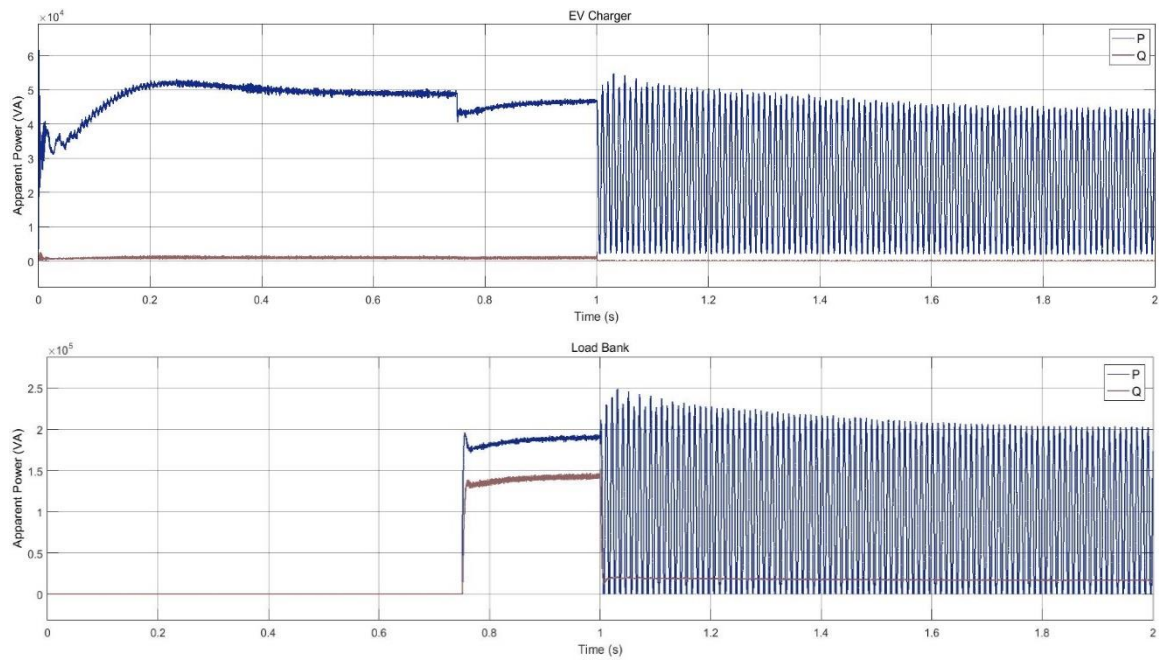


Figure 112- RMS values of active and reactive power of the EV charger and load bank for line-to-ground short-circuit - Case3.

5.3.3.4. Line-to-Line Short-Circuit with Ground Connection

Finally, the line-to-line SC with ground connection was analysed, revealing a similar behaviour observed in previous case studies. After the contact between phases A and B, it is expected, that the voltage waveforms reach zero and in the same phase there is a substantial voltage drop referring to the fault and the connection of the inverter, although the voltage should be slightly higher than its nominal value due to the imbalance caused in the lines.

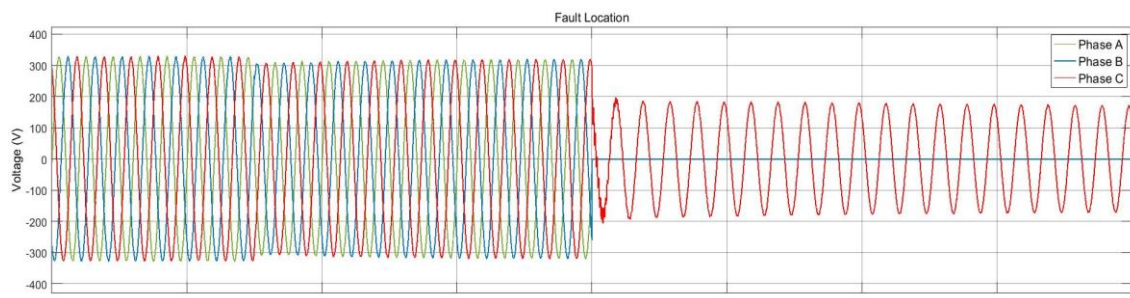


Figure 113- -Fault location voltage waveforms for line-to-line-to-ground short-circuit - Case3.

Therefore, the current in the bolted lines has increased, with the effective value of the SC current being 6943 A. The current in the same phase stayed within its nominal values. However,

this behaviour was due to the phase shifting of the fault currents injected by the inverter and the diesel generator, as explained in the previous SC study.

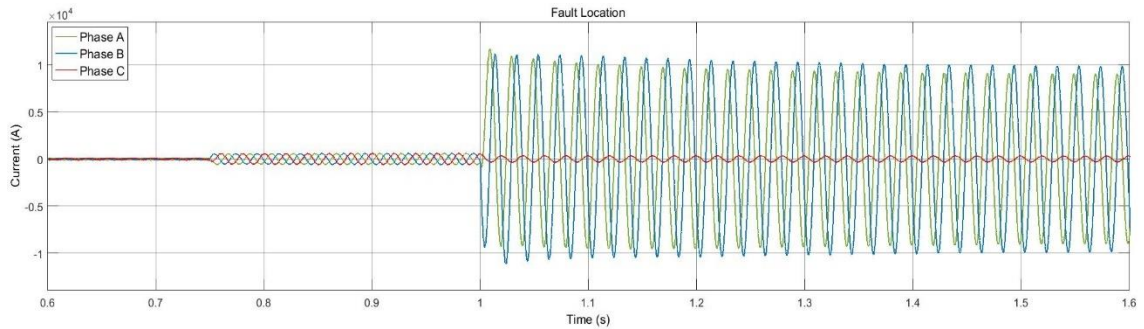


Figure 114- Fault Location current waveforms for line-to-line-to-ground short-circuit - Case3.

As in previous type of SC, the behaviour of the current in the load causes fluctuations in the active power waveform, and reactive power flow to the load becomes null both for the electric vehicle charger and the load bank.

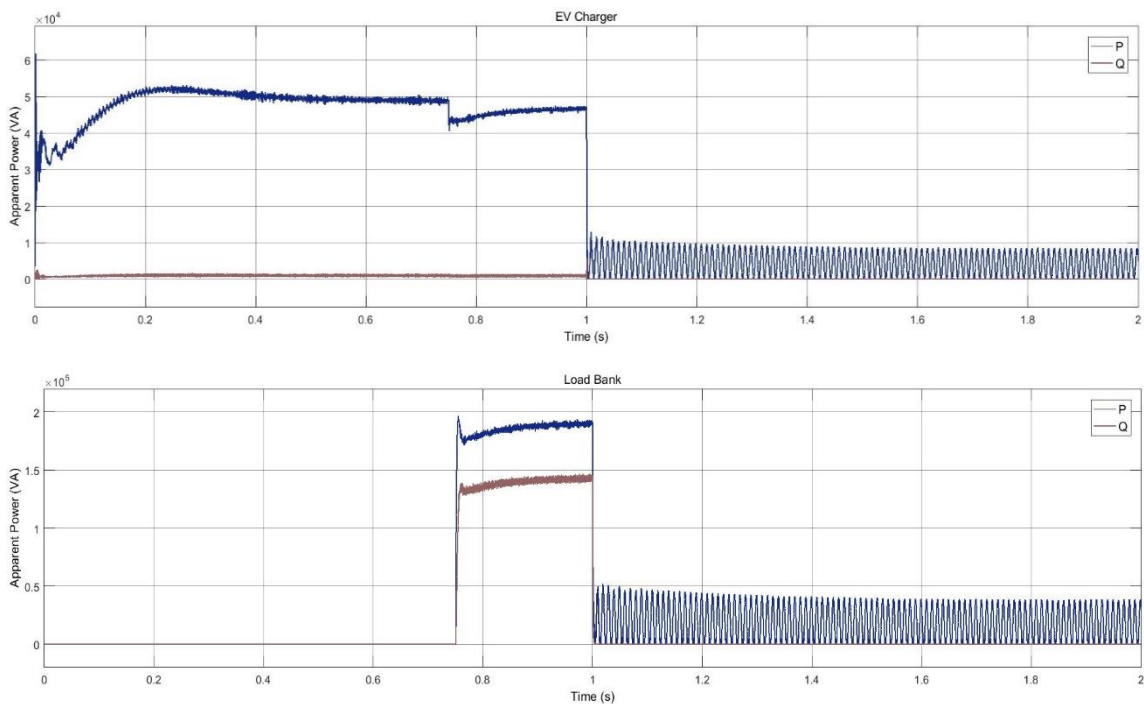


Figure 115- RMS values of active and reactive power of the load bank and EV charger for line-to-line-to-ground short-circuit - Case3.

The SC current values obtained through the MATLAB/Simulink simulation and their relative error are shown in the table below

Table 26- Short-Circuit Currents - Case 3.

Type of Short-Circuit	Calculated	Simulated	Relative Error (%)
Three-phase	5056	5128	1.42
Phase-to-Ground	6365	7017	10.24
Phase-to-Phase	4414	4497	1.88
Phase-to-Phase-to-Ground	6473	6943	6.81

The model for isolated SC analysis is reasonably accurate and can be considered valid, although as in the interconnections of this system to the distribution networks, it presents flaws with respect to ground faults.

Although isolated networks may have challenging behaviours in what concerns the protection systems, the analysis of this MG proved the effective performance of the existing circuit breakers and consequent suppression of the fault.

5.4. Chapter Summary

The DEMOCRAT project reveals itself innovative in terms of the MG concept. It provides a viable power supply solution in coordination with the distribution networks or in its stand-alone operation, being able to efficiently feed system loads. Due to the characteristics of power systems in isolated mode, namely in the capacity of current injection by the static elements in fault scenarios, it is important to ensure the proper functioning of the protection systems.

- Section 5.1. presents the purpose of this system in the power supply, and the relevance of the study of protection systems in fault scenarios.
- Section 5.2. of this chapter gives a detailed description of the constituents of the DEMOCRAT project and their characteristics.
- Section 5.3. demonstrates the operation of the system in three different case studies through computational simulations. The case studies refer to the connection of the system to LV and MV distribution networks and its operation in isolated mode. An extensive analysis of different SC scenarios is presented, in order to prove the results obtained in the previous chapter.

Chapter 6

Conclusions and Future Work

6.1. Conclusions

This dissertation analyses the inclusion of Battery Energy Storage Systems (BESSs) in Microgrids (MGs), focusing on the analysis of the behaviour of the MG in the occurrence of different types of electrical faults and, consequently, the adequacy of existing protection systems.

A MATLAB/Simulink simulation was performed, analysing the behaviour of the MG and its elements in time domain. The purpose of this analysis was due to the need of studying the impact of different types of Short-Circuits (SCs) at different points of Low Voltage (LV) MGs, when they are interconnected with the main distribution network and in isolated mode, confirming the suitability and evaluating behavioural requirements of the existing protections.

Typical protection systems may not provide reliable protection for inverter interfaced units, because there is limited fault current since most inverters, in fault scenarios, may only inject their nominal current. These fault currents would require a complete redesign, including huge investment costs, of all existing protection systems at the lower voltage levels of the grid, as these protection systems rely on the magnitude of the fault currents. Having a controllable fault current level allows power electronics to optimally regulate and limit Distributed Energy Resources (DER) fault current at the connection point.

Due to the relevance and pertinence of this subject, a numerical and dynamic SC analysis was carried out in the MG context to study the impact of the electrical faults in the protection systems in a real MG.

According to the numerical results obtained, the application of the Democrat project in the LV and Medium Voltage (MV) distribution networks does not jeopardise the viability of the protection systems. As the networks are robust and solid, they have sufficient SC capacity to generate enough fault currents to exceed the minimum threshold imposed by circuit breakers. However, its operation isolated from the network could be jeopardised by the low inertia of the MG, since it may not have enough SC power, due to the predominance of Converter-Based Distributed Generation (CBDG).

Both numerical results and the simulation results in MATLAB/Simulink prove the correct performance of the protections in case of symmetrical and asymmetrical SCs. The theoretical

analysis of SC currents is in concordance with the experimental results presented by the simulator in cases of SCs that do not involve ground connection. In order for the protections to be correctly triggered, it is necessary that the maximum current injected by the inverter reaches the minimum limit imposed by the circuit breakers. It is important to take into account that this minimum limit refers to the SC condition and not to the overload condition, being imperative that the circuit breakers can differentiate them. If this condition does not occur, the SC current will remain in the system and may damage the electrical equipment connected to the network and even endanger personnel.

The simulation proves that the operation of the inverter without backup system for load supply has the ability to inject enough SC currents, tripping the protections. In practice, power converters are provided with protections that limit this current injection due to the electrical parameters of their semiconductor components. It is verified that the operating times of the circuit breakers implemented in the MG will act according to that corresponding current, fulfilling the minimum acting times that refers to the limits imposed by the circuit-breakers curves of operation.

Regarding the simulation model, it revealed some limitations during the study of ground faults due to the internal model of the transformers used, and therefore, some results presented errors in the effective values of the SC current, especially in the MV grid connection. During the simulations, a sensitivity analysis was performed to detect the errors, where several configurations and types of transformers were tested, as well as different generation sources. Besides that, due to approximations and linearization of the system components during theoretical calculations, relative errors were higher than expected. Such consideration is justified by the conservative hypotheses that the IEC 60909 standard uses to determine the SC currents. Also, the models of the inverters presented some limitations, showing a correct behaviour during normal operation conditions of the MG, but an unexpected behaviour during some types of asymmetrical faults, due to its control.

In conclusion, fault detection and analysis are a crucial subject in the study of electrical energy systems, being necessary to select or design suitable switchgear equipment, relays, circuit breakers and other protection devices. Finally, with the accomplishment of this work, the importance of such study became evident, since the need to adapt the electric power systems is crucial for its correct functioning.

6.2. Future Work

The work carried out during the dissertation is at an early stage in the modelling of MGs, focusing on the models of CBDG and also on inverter models, for fault scenario studies. As presented, the inverter models used have irregular behaviours in situations of accentuated imbalances, imposing new challenges in the control of these elements.

In order to continue developing MG-based simulations, it is necessary to improve its operation to minimize errors found in its modelling and also study the transition from on-grid mode to isolated mode and the reconnection to the grid, besides the ability of the system to withstand these transitions, respecting the limits associated with power quality parameters. Testing of actual inverter fault characteristics is needed to develop information that could be used in modelling and fault analysis programs, namely inverter-based DER fault current-ride-through capability on distribution system protection schemes.

Other points of interest would be the study of the behaviour of the MG for system restoration after a fault condition and the modelling of adaptive protections for transition of connection to the distribution network to isolated mode of operation. Other renewable sources and multiple loads in the system may be included in these analysis for coordination studies and performance of the protection systems, based on selectivity and classification of priority loads.

Finally, another suggestion is to determine the LV ride-through capability of inverter-based DER and defining how protective relay coordination will be affected during such events.

References

- [1] C. Haisheng, N. Thang, Y. Wei, T. Chunqing and L. Y. D. Yongliang, "Progress in electrical energy storage system: a critical review," in *Progress in Natural Science*, 2009, pp. 291-312.
- [2] C. Moreira, "Microgrid Islanding Operation," Porto, 2016.
- [3] I. Miranda, "Integration of Battery Energy Storage Systems in the planning and operation of distribution networks," Porto, 2017.
- [4] I. Miranda, "Otimização do Planeamento de Sistemas de Armazenamento Distribuído de Energia em Redes com Elevada Produção Dispersa," Porto, 2012.
- [5] I. Miranda, N. Silva and H. Leite, "Distribution Storage System Optimal Sizing and Techno-economic Robustness," Porto, 2012.
- [6] A. Banswar, N. Sharma, Y. Sood and R. Shrivastava, "Renewable energy sources as a new participant in ancillary service markets," Elsevier, India, 2017.
- [7] F. Cebulla, T. Naegler and M. Pohl, "Electrical energy storage in highly renewable European energy systems: Capacity requirements, spatial distribution, and storage dispatch," Elsevier, Germany, 2017.
- [8] K. Zame, C. Brehm, A. Nitica, C. Richard and G. Schweitzer, "Smart grid and energy storage: Policy recommendations," Newark, 2017.
- [9] I. Colak, "Introduction to Smart Grid," in *2016 International Smart Grid Workshop and Certificate Program*, Istanbul, 2016.
- [10] C. K. Das, O. Bass, G. Kothapalli, T. S. Mahmoud and D. Habibi, "Overview of energy storage systems in distribution networks: Placement, sizing, operation, and power quality," Elsevier, 2018.
- [11] Efacec Energia, SA, "DEMOCRAT- DEMOnstrator of a miCro grid integRAting sTorage," Portugal 2020, Maia, 2017.
- [12] J. Peças Lopes, N. Hatziargyriou, M. J., P. Djapic and N. Jenkins, "Integrating distributed generation into electric power systems: A review of drivers, challenges and opportunities," Elsevier, 2006.

- [13] International Electrotechnical Commission, "Electrical Energy Storage," International Electrotechnical Commission, Geneva, 2011.
- [14] C. Moreira, "Identification and Development of Microgrids Emergency Control Procedures," Porto, 2008.
- [15] M. S. Guney and Y. Tepe, "Classification and assessment of energy storage systems," Elsevier, Giresun, 2017.
- [16] A. Madureira, L. Seca and J. Peças Lopes, "Coordinated voltage control in distribution systems under the smart grid concept," in *CIREN 2012 Workshop: Integration of Renewables into the Distribution Grid*, Lisbon, 2012.
- [17] J. Gouveia, C. Gouveia, J. Rodrigues, R. Bessa, A. Madureira, R. Pinto, C. Moreira and J. Peças Lopes, "MicroGrid Energy Balance Management for Emergency Operation," IEEE, Porto, 2017.
- [18] I. Miranda, H. Leite and N. Silva, "Coordination of multifunctional distributed energy storage systems in distribution," *IET Journal*, 8 August 2015.
- [19] H. C. Hesse, M. Schimpe, D. Kucevic and A. Jossen, "Lithium-Ion Battery Storage for the Grid—A Review of Stationary Battery Storage System Design Tailored for Applications in Modern Power Grids," *Energies*, 11 December 2017.
- [20] C. Caruana, A. Sattar, A. Al-Durra and S. Muyeen, "Real-time testing of energy storage systems in renewable energy applications," Elsevier, 2015.
- [21] A. Gallo, J. Simões-Moreira, H. Costa, M. Santos and E. Moutinho dos Santos, "Energy storage in the energy transition context: A technology review," Elsevier, São Paulo, 2016.
- [22] D. M. Hart, W. B. Bonvillian and N. Austin, "Energy Storage for the Grid: Policy Options for Sustaining Innovation," MIT Energy Initiative, Cambridge, 2018.
- [23] European Association for Storage of Energy, "Thermal Energy Storage," EASE, Brussels, 2013.
- [24] H. Akbari, M. C. Browne, A. Ortega, M. J. Huang, N. J. Hewitt, B. Norton and S. J. McCormack, "Efficient energy storage technologies for photovoltaic systems," Elsevier, Dublin, 2018.
- [25] European Association for Storage of Energy, "Electrical Energy Storage," EASE, Brussels, 2013.

- [26] I. Miranda, N. Silva and A. Maia Bernardo, "Assessment of the potential of Battery Energy Storage Systems in current European markets designs," Porto, 2012.
- [27] S. Sabihuddin, A. E. Kiprakis and M. Markus, "A Numerical and Graphical Review of Energy Storage Technologies," *Energies*, 29 December 2014.
- [28] D. J. Bradwell, H. Kim, A. H. Sirk and D. R. Sadoway, "Magnesium-Antimony Liquid Metal Battery for Stationary Energy Storage," American Chemical Society, Cambridge, 2012.
- [29] Ambri, "Liquid Metal Battery Cell Technology," Ambri Inc., Marlborough, 2014.
- [30] F. Mumtaz and I. S. Bayram, "Planning, Operation, and Protection of Microgrids: An Overview," in *3rd International Conference on Energy and Environment Research*, Barcelona, 2016.
- [31] T. L. Vandoom, B. Meersman, J. D. M. De Kooning and L. Vandeveld, "Transition From Islanded to Grid-Connected Mode of Microgrids With Voltage-Based Droop Control," *IEEE TRANSACTIONS ON POWER SYSTEMS*, 18 October 2012.
- [32] N. Jayawarna, C. Jones, M. Barnes and N. Jenkins, "Operating MicroGrid Energy Storage Control during Network Faults," Manchester, 2007.
- [33] A. Hatata, E.-H. Abd-Raboh and B. E. Sedhom, "A Review of Anti-islanding Protection Methods for Renewable Distributed Generation Systems," *Journal of Electrical Engineering*, vol. 16, no. 1, pp. 235-247, 2016.
- [34] P. A. Kumar, J. Shankar and Y. Nagaraju, "Portection Issues in Microgrid," *International Journal of Applied Control, Electrical and Electronics Engineering*, vol. 1, no. 1, 1 May 2013.
- [35] I. J. Balanguer, Q. Lei, S. Yang, U. Supatti and F. Z. Peng, "Control for Grid-Connected and Intentional Islanding Operations of Distributed Power Generation," *IEEE TRANSACTIONS ON INDUSTRIAL ELECTRONICS*, vol. 58, no. 1, 10 December 2010.
- [36] C.-T. Lee, R.-P. Jiang and P.-T. Cheng, "A Grid Synchronization Method for Droop-Controlled Distributed Energy Resource Converters," *IEEE TRANSACTIONS ON INDUSTRY APPLICATIONS*, vol. 49, no. 2, 15 March 2013.
- [37] V. Santos, "Continuidade de Serviço nas Redes de Distribuição de Energia Elétrica," ISEC, Coimbra, 2012.
- [38] J. E. Hill, S. D. A. Fletcher, P. J. Norman and S. J. Galloway, "Protection System For an Electric Power Network". United States of America Patent 13/359,010, 9 August 2012.

- [39] S. Katyara, L. Staszewski, H. A. Musavi and F. Soomro, "Short Circuit Capacity: A Key to Design Reliable Protection Scheme for Power System with Distributed Generation," *International Journal of Mechanical Engineering and Robotics Research*, vol. 6, no. 2, March 2017.
- [40] A. Johnson and P. Simango, "RfG - Fast Fault Current Injection," National Grid, 2017.
- [41] J. Keller and B. Kroposki, "Understanding Fault Characteristics of Inverter-Based Distributed Energy Resources," U.S. Department of Energy, Golden, 2010.
- [42] W. Kramer, S. Chakraborty, B. Kroposki and H. Thomas, "Advanced Power Electronic Interfaces for Distributed Energy Systems," U.S. Department of Energy, Golden, CO, 2008.
- [43] A. Janssen, M. v. Riet and A.-y. Justin, "Fault current contribution from state of the art DG's and its limitation," in *International Conference on Power Systems*, Delft, 2011.
- [44] N. Belda, C. Plet, C. Spallarossa and T. Kazuyori, "HVDC Network Fault Analysis," PROMOTioN - Progress on Meshed HVDC Offshore Transmission Networks, 2016.
- [45] T. N. Boutsika and S. A. Papathanassiou, "Short-circuit calculations in networks with distributed generation," *Electric Power Systems Research*, vol. 78, pp. 1181-1191, 2008.
- [46] S. Garnas, "Short Circuit Current Contribution from Converters," Trondheim, 2017.
- [47] R. Nelson and H. Ma, "Short-Circuit Contributions of Full-Converter Wind Turbines," in *2012 IEEE/PES Transmission & Distribution Conference and Exposition*, Orlando, 2012.
- [48] S. Chakraborty, M. G. Simões and W. E. Kramer, *Power Electronics for Renewable and Distributed Energy Systems*, London: Springer, 2013, pp. 2-7.
- [49] T. Wijnhoven, "Evaluation of Fault Current Contribution Strategies by Converter Based Distributed Generation," Catholic University of Leuven, Flanders, 2015.
- [50] R. Teodorescu, M. Liserre and P. Rodríguez, *Grid Converters for Photovoltaic and Wind Power Systems*, West Sussex: John Wiley & Sons, Ltd, 2011, pp. 31-41.
- [51] J. Dirksen, "LVRT - Low Voltage Ride-Through," *DEWI Magazin*, no. 43, pp. 56-60, August 2013.
- [52] D. Popovic and I. Wallace, "International Review of Fault Ride-Through for Conventional Generators," KEMA Limited, London, 2010.
- [53] N. Roy and H. Pota, "Distribution Grid Codes: Opportunities and Challenges," in *2013 IEEE Grenoble Conference*, Grenoble, 2013.

- [54] S. Mohod and M. Aware, " Power Quality and Grid Code Issues in Wind Energy Conversion System, An Update on Power Quality," IntechOpen, 2013.
- [55] European Committee for Electrotechnical Standardization, "Standard EN 50160: Voltage Characteristics of Public Distribution System," CENELEC, Brussels, 1999.
- [56] International Electrotechnical Commission, "Short-circuit currents in three-phase a.c. systems," International Electrotechnical Commission, Geneva, 2001.
- [57] T. Jacobson, "Complex impedance method for AC circuits," College Park, 2002.
- [58] C. A. Gross and S. P. Meliopoulos, "Per-Unit Scaling in Electric Power Systems," in *IEEE/PES 1991 Summer Meeting*, San Diego, 1991.
- [59] C. Moreira, *Análise de Curto-Circuitos Simétricos*, Porto, 2017.
- [60] Siemens AG, "High-voltage cable systems," Erlangen, 2016.
- [61] A. Sinha, "Transmission Line Modeling," Kharagpur, 2004.
- [62] Siemens AG, "Transformer insights," Siemens AG 2018, Dispo, 2018.
- [63] A. K. Sinha, "Transformer Model," Kharagpur, 2004.
- [64] K. O. Oureilidis and C. S. Demoulias, "An enhanced role for an energy storage system in a microgrid with converter interfaced sources," *The Journal of Engineering*, no. 11, p. 618-625, 2014.
- [65] Y. Pan, W. Ren, S. Ray, R. Walling and Reichard, "Impact of Inverter Interfaced Distributed Generation on Overcurrent Protection in Distribution Systems," in *2011 IEEE Power Engineering and Automation Conference*, Wuhan, 2011.
- [66] V. Gevorgian and E. Muljadi, "Wind Power Plant Short-Circuit Current Contribution for Different Fault and Wind Turbine Topologies," in *The 9th Annual International Workshop on Large-Scale Integration of Wind Power into Power Systems as well as on Transmission Networks for Offshore Wind Power Plants*, Québec, 2010.
- [67] X. Pei, Z. Chen, S. Wang and Y. Kang, "Overcurrent Protection for Inverter-Based Distributed Generation System," in *2015 IEEE Energy Conversion Congress and Exposition*, Montreal, 2015.
- [68] V. Miranda, "Curto Circuitos e Outros Incidentes Assimétricos," Porto, 2014.

- [69] IEEE, IEEE Recommended Practice for Calculating Short-Circuit Currents in Industrial and Commercial Power Systems, New York: The Institute of Electrical and Electronics Engineers, Inc., 2006, pp. 13-34.
- [70] A. Berizzi, S. Massuco, A. Silvestri and D. Zaninelli, "Short- Circuit Current Calculation: A Comparison between Methods of IEC and ANSI Standards Using Dynamic Simulation as Reference," *IEEE Transactions on Industry Applications*, vol. 30, no. 4, August 1994.
- [71] B. Metz-Noblat, F. Dumas and C. Poulain, "Calculation of short-circuit," Schneider Electric, Grenoble, 2005.
- [72] Open Electrical, "Anatomy of a Short Circuit," 12 February 2017. [Online]. Available: https://wiki.openelectrical.org/index.php?title=Anatomy_of_a_Short_Circuit. [Accessed 28 November 2018].
- [73] C. Moreira, *Análise de Curto-Circuitos Assimétricos*, Porto, 2017.
- [74] W. D. Stevenson, Elements of power system analysis, 1st ed., F. E. Terman, Ed., London: McGraw-Hill Publishing Company Ltd-, 1955.
- [75] B. Weedy, B. Cory, N. Jenkins, J. Ekanayake and G. Strbac, Electric Power Systems, 5th ed., John Wiley & Sons Ltd, 2012, p. 514.
- [76] M. Ribeiro, I. Miranda, L. Marques and A. Bernardo, "Democrat: Demonstrator of a Micro-Grid Integrating Storage," in *CIREN Workshop*, Ljubljana, 2018.